MODELLING NUTRIENT RECOVERY AND DYNAMICS OF PURPLE NON-SULPHUR BACTERIA IN MIXED-CULTURE RACEWAY REACTORS.

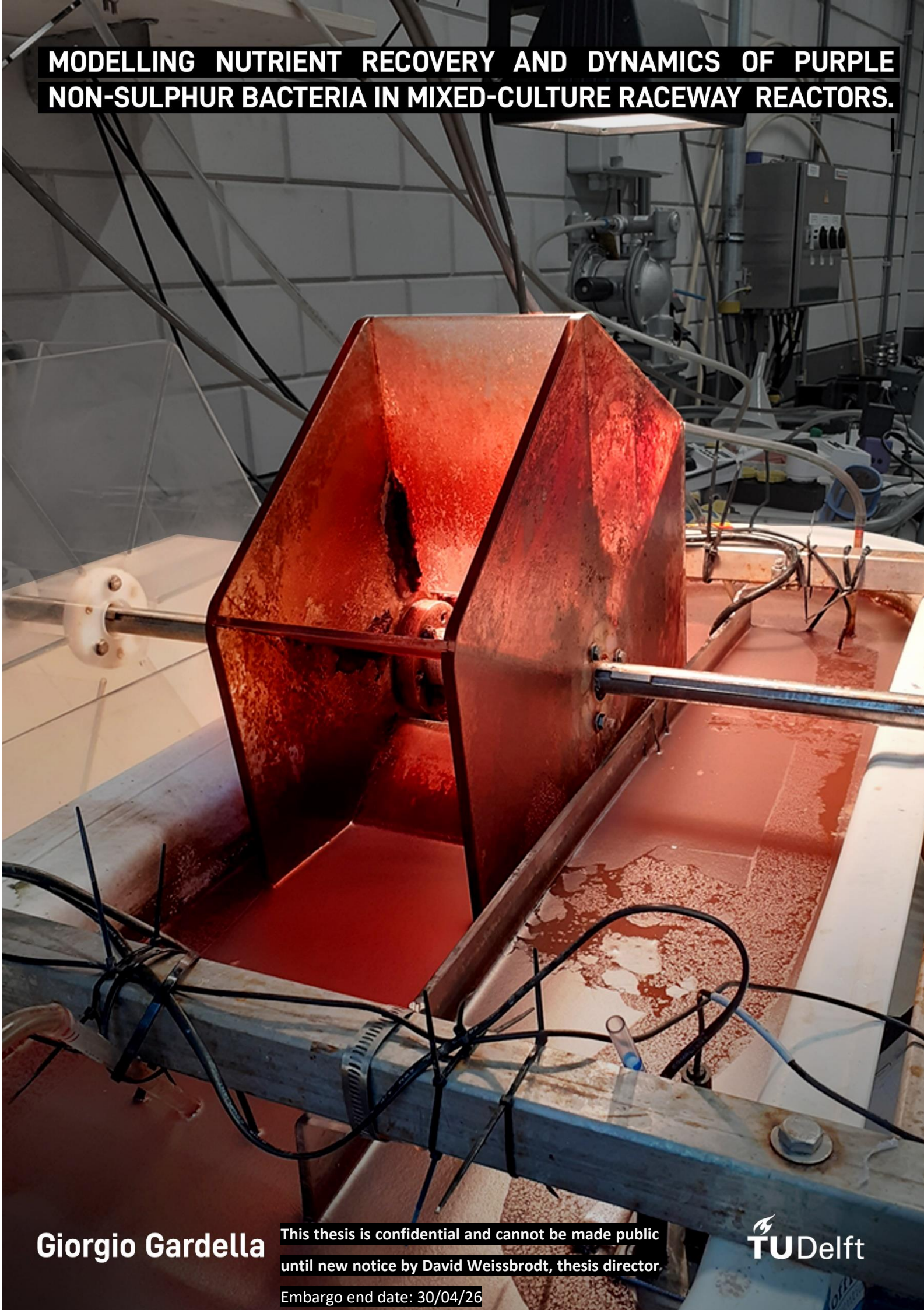

Giorgio Gardella

TU Delft

Modelling nutrient recovery and dynamics of purple non-sulphur bacteria in mixed-culture raceway reactors

Master Thesis submitted to Delft University of Technology

In partial fulfilment of the requirements for the degree of

Master of Science

in Civil Engineering and Geosciences

by

Giorgio Gardella

Student number: 4777905

To be defended on April 30th 2021

Graduation committee

David Weissbrodt, Assistant professor TU Delft, Environmental Biotechnology (Responsible thesis supervisor and Chair of the graduation committee)

Abbas Alloul, Postdoctoral Researcher, TU Delft, Environmental Biotechnology and UAntwerp, Bioscience Engineering (co-supervisor)

Ralph Lindeboom, Assistant professor ,TU Delft, Sanitary Engineering

Edo Abraham, Assistant professor, TU Delft, Water Resources

This thesis is confidential and cannot be made public until new notice by David Weissbrodt, thesis director Embargo end date: 30/04/26

Acknowledgment

I sincerely express my gratitude to my supervisors David Weissbrodt, Ralph Lindeboom and Edo Abraham for their help and guidance throughout this special year. I owe a special thanks to Abbas Alloul who introduced me to the world of purple bacteria, and, since our first meeting, always showed his enthusiasm and support for my project. Despite the hard times we all have been living through during this pandemic, they have been steadfast in their support, strengthening my determination to succeed and achieve my goals.

I cannot fail to express my gratitude to the SEMiLLA Group, and especially Radu Giurgiu: they gave me the opportunity to work directly on the field facing the daily practical problems of the wastewater treatment sector. As well, without the availability and assistance of Prior Isaac, Peter van Krieken and Annemay Garretsen at the Koningshoeven Abbey this project would not have been possible.

Thank you.

This thesis has requested me the perseverance of one, or even twelve, Labors of Heracles which I was able to accomplish only with the unconditional love of my parents, my sisters and my supergrannies. They are roots which breached the ground in the Netherlands.

This thesis is the end of a long journey, which started in September 2018 during which I have met many and wonderful friends. A very special thanks goes to Stefano, my 2-years housemate chez Vergar, to Arita, with whom I shared endless afternoons working on this project, and to Filippo, Luigi, Nicolò, Giulio, Valerio and Alessandro who became a Dutch adoptive family.

This Thesis is also the result of a totally unreasonable decision made in 2014 to become an environmental engineer which led me to discover incredibly dirty wastewaters. Nevertheless, I have met incredibly talented people and colleagues, among which I have to personally thank Davide, Luca, Matteo and Pietro who shared with me more than one special moment.

Finally, I would like to thank my closest friends back in Italy who were always able to find the right words to cheer me up and pull myself back together again, despite the distance which kept us apart during these years,. So a special thanks to all the members of “La Famiglia”, Martina, Giorgia, Sara and Adelaide.

Un sincero grazie a tutti

Giorgio

Abstract

Purple non-sulphur bacteria (PNSB) are phototrophic bacteria currently under study in the wastewater treatment sector due to their performant nutrient and resource recovery. Until recently, most of researches have focused on closed anaerobic photobioreactors resulting in high selectivity of PNSB and appealing hydrogen, microbial proteins, and carotenoids productivity. Unfortunately, these researches also showed that the implementation of this technology is hampered by its relatively high costs. As is the case for microalgae technology, raceway reactors could possibly overcome this problem thanks to their low investment and maintenance costs. However, a survey of the scientific literature shows that only few researches have investigated the application of PNSB technology with open raceway reactors and that the limited available mechanistic models do not consider the specific conditions which characterize these reactors. Therefore, this study aims to construct a mechanistic mathematical model which includes the mixotrophic metabolism of PNSB and could be used to predict the nutrient removal and recovery and PNSB relative abundance in the raceway reactor. The model was structured mainly considering the photoorganoheterotrophic and respiring chemoorganoheterotrophic growth of PNSB competing with standard (an)aerobic-respiring and fermenting chemoorganoheterophic bacteria under semi-aerobic conditions. The model was tuned with seven batch and sequencing batch reactor (SBR) laboratory experiments. It simulates the reactor performance (COD removal rate 480-780 mgCOD/L/d, yield 0.40– 0.65 $mgCOD_x/mgCOD_s$) and the relative PNSB abundance (10-60%) under different operational conditions (light, dissolved oxygen, surface area) with a relative error around ± 20%. This research proposes an one-at-the-time sensitivity analysis, analysing the impact of those variables (TSS, SRT, COD, light, and biotic competition) which could play an important role in real-case scenarios. From this analysis, it emerged that influent suspended solids (TSS>250 mgTSS/L), hourly variations of the natural light cycle intensity and drops of the available soluble substrate (COD<1000mgCOD/L) could strongly disturb the abundance of PNSB in the system (from 48% to 10%). An extension of the sludge retention time, from 2 to 5 days, was observed to favour the relative abundance of PNSB (from 48% to 60%) and to increase the TSS productivity (from 235 to 400 mgTSS/L/d). The model was intended as a first attempt to simulate the nutrient removal and the PNSB dynamic in a raceway reactor. It has the flexibility to study the impact of the crucial parameters evidenced from the literature review (light, oxygen, carbon source). However, several implementations will be needed in the future, mainly focusing on anoxic chemoheterotrophic growth and hydrolysis.

Contents

Glossary

Nomenclature

S_S	Complex soluble substrate (glucose)	X_S **[mgCOD/L]**	Organic particulate
S_{VFA} **[mgCOD/L]**	Volatile fatty acid substrate	X_{PB} **[mgCOD/L]**	Purple non-sulphur bacteria biomass
S_{AC} **[mgCOD/L]**	Acetate substrate	X_{HET} **[mgCOD/L]**	Standard chemoheterotrophic bacteria
S_I **[mgCOD/L]**	Inorganic inert soluble	X_{FR} **[mgCOD/L]**	Fermenting heterotrophic bacteria
S_{IN} **[mgN/L]**	Soluble total inorganic nitrogen	X_I **[mgCOD/L]**	Inorganic inert particulate
S_{IP} **[mgP/L]**	Soluble total inorganic phosphorus	S_{O2} **[mgO_2/L]**	Soluble oxygen
S_{HCO3} **[mol HCO_3/L]**	Bicarbonate/alkalinity	S_{CO2} **[mgCO_2/L]**	Soluble carbon dioxide
S_{H2}	Soluble Hydrogen	X_{MA}	Microalgae
K_S	Saturation constant for S_S	$S_{S,O2}$	Oxygen saturation constant
K_{VFA}	Saturation constant for S_{VFA}	$S_{S,CO2}$	CO_2 saturation constant
K_{AC}	Saturation constant for S_{AC}	S_H	pH
K_I	Saturation constant for Light	$K_{eq,1}$	Bicarbonate Chemical equilibrium
$K_{O2,ph}$	Inhibition constant of phototrophic growth for O_2	$k_{eq,1}$	Bicarbonate Dissociation constant
$K_{O2,ch,PB}$	Inhibition constant of chemotrophic growth (X_{PB}) for O_2		
$K_{O2,ch,HET}$	Inhibition constant of chemotrophic growth (X_{HET}) for O_2		
$f(S_i)$	Substrate preference factor		
$\nu_{i,i}$	Cybernetic metabolic factor		
k_{dec}	Decay constant		
k_{HYD}	Hydrolysis rate constant		
$k_{la,O2}$	Mass transfer coefficient for oxygen		
$S_{S,O2}$	Mass transfer coefficient for CO_2		

1 Introduction

Steffen et al. (2015) identified the unbalance in the nutrients cycle, mainly nitrogen and phosphorus, as one of the major threat for the humankind[1]. In this context, wastewater treatment plants (WTTPs) can be seen as an already existing production site to achieve an energy-nutrients-water nexus [2]. Anaerobic digestion processes can achieve a good energy recovery thanks to methane production performance, but they are not efficient in nutrient recovery and seldom reach quality effluents standards [3].

Within this context, the SARASWATI research project aims to improve and innovate India's wastewaters management and treatment. It is promoted by the Government of India, Department for Science and Technology and the European commission (FP7), under the joint program "EU-India Cooperation in Water Technology". Started in 2012, the SARASWATI project identified many of the critical issues of India's wastewater management, such as the very low average efficiency and the widespread failure in meeting discharge standards. At the same time, the project has been identifying and proposing the most relevant "best available technologies" (BATs) which should be further researched and developed. Today, the project has reached a second phase, called SARASWATI 2.0, and is concretely exploring the development of the proposed BATs, within the framework of the H2020 EU-India water co-operation agreement.

In India, anaerobic digestors are often not properly functioning, because of poor maintenance, design's errors and personnel inexperience[3]. For these reasons, production of methane, which is the main added value by-product of this treatment technology, is often very low and not optimized. Moreover, anaerobic digestion process is not efficient in terms of nutrient recovery and methane is starting to be considered a low valuable product compared to the most recent COD-based commodities such as polyhydroxyalkanoates [4]. Henceforth, one recent implementation within the anaerobic technology is the combination of an acidification step followed by a biological treatment by purple non-sulphur bacteria (PNSB) [5]. These peculiar microorganisms have been already studied and applied in industrial effluents and, only more recently, in domestic wastewater [6,7]. One of the main reasons to use these microorganisms lies in the fact that, as phototrophic bacteria, they can reach sufficient nutrient recovery [8]. Moreover, specifically for PNSB, valuable resources can be extracted such as hydrogen[9], carotenoids[10], bacteriochlorophyll, and microbial protein (SCP) [11]. To mention just one of these studies, Alloul et al. (2020) found that the European sewage might recover between 0.6-2.2 megatons of microbial proteins equivalent to 21-72% of the global fishmeal demand with the use of PNSB microorganisms [5].

Raceway reactors are defined as photobioreactors that make use of natural light for the cultivation of phototrophic organisms, from microalgae to PNSB. Compared to the standard closed photobioreactors, the main advantage of this system is the lower investment and maintenance costs, mainly related to the absence of artificial light, which is energetically unsustainable and economically unaffordable [12]. Despite its inherent inefficiency and limited productivity, at large scale, raceway reactors are largely used and, for instance, cover 95% of worldwide microalgae production [13].

In conclusions, in the recent years, the implementation of PNSB bacteria with raceway reactors has been growing as a possible new technology for the wastewater treatment sector. As a proof of this trend, a pilot-scale raceway reactor has been started up by the SEMiLLA Foundation in Amsterdam and, in the coming months, the SARASWATI project 2.0 will start up a raceway reactor in the Kolkata region.

1.1 Problem Definition: modelling gap for PNSB selection under semi-aerobic condition

Mathematical models are effective tools which can contribute the understanding and the design of WWTPs. They can simulate under various circumstances the performance of WTTPs in order to define optimal designs, control tools and best operational conditions [14]. Moreover they can help the development of some practical experiments which usually require longer effort and dedication.

In the scientific literature there are few complete mathematical models simulating the application of PNSB in wastewater treatment. Biohydrogen production with PNSB has been deeply investigated in the past 10 years, but this represents only one of the diverse metabolic pathways of these bacteria [15,16]. Puyol et al. (2017) developed the first general kinetic model with PNSB bacteria for domestic wastewater in anaerobic conditions [17]. However, this model did not include some important parameters, such as the oxygen presence or the metabolic flexibility of PNSB. Furthermore, the model simulates a closed anaerobic photobioreactor, in which important external conditions were kept stable (e.g. light). As of today, there is not any modelling study which investigated the application of PNSB in raceway reactors even though some experimental works focused on the growth of PNSB under similar conditions [18–21].

Because of this knowledge gap and the existing Saraswati project, there is the need to understand which parameters influence the stability of PNSB in raceway reactors. Some laboratory experiments are currently ongoing at Antwerp and Calcutta university, reproducing similar conditions to the Indian case (click here). Therefore, the development of a mechanistic model will help understanding the sensitivity of the most relevant parameters, giving some useful indications regarding wastewater

treatment process and identifying some operational control tools to achieve a greater abundance of PNSB and improving the reactor performance.

1.2 Research questions: can we model the dynamics of PNSB growth and nutrient removal in semi-aerobic mixed-culture raceway reactor?

As result of the challenges descripted above the formulation of Thesis objective can be stated as:

Develop a mechanistic model in order to evaluate the nutrient recovery and the influence of the most relevant parameters for the operability and control of PNSB in a raceway reactor.

With this overall objective it was decided to formulate the following research questions investigated:

1. *What are the main parameters influencing the growth of PNSB in a raceway reactor?*

To answer to this question, a critical literature review of the main parameters affecting PNSB kinetic will be implemented according to present scientific knowledge. Based on this research, the effects of light, oxygen and the biotic competition were selected as the most relevant variables. These variables will be implemented in the already existing model proposed by Puyol et al. (2017)[17], which therefore will have to be adjusted and structurally modified. As a final step, the model will be explained in detail in all its processes.

2. *Can the proposed model accurately represent experimental data?*

The model will be tuned and parameterized on batch and sequencing batch reactor laboratory experiments performed by Alloul et al. (2020) [18]. The results and errors of the simulations are reported and commented, individuating the strengths and weakness of the model structure.

3. *What factors should be considered to favour the growth of PNSB in a raceway reactor under more realistic practical conditions?*

Once the model was tuned with experimental data, a series of different scenarios were investigated with a one-at-the-time (OAT) sensitivity analysis studying the effects of most impacting variables with more realistic conditions than laboratory results. In order to optimise the abundance and production of PNSB, this investigation analysed the system response and new steady state to instantaneous and long terms variations.

1.3 Thesis structure

The Thesis is divided in the following sections:

2) **:** the purpose is to collect sufficient background information regarding PNSB and raceway reactor in order to answer the first research question. In particular, the parameters affecting the growth of PNSB under semi-aerobic conditions will be majorly investigated. Finally, it would be stressed out the most important factors that should be considered in order to develop a model able to simulate the growth of PNSB in raceway reactor.

3) **Material and Methods:** in this part the model structure and development is explained in detail for each process. Furthermore, the most relevant information regarding the tuning of the model and the structure of the sensitivity analysis are reported. Then, in order to answer the second question, the characteristics of the laboratory experiments on which the model was parametrized, are given. Finally, the structure and objective of the different scenarios in the sensitivity analysis are explained.

4) **Results:** in this section the results of the simulations are reported and compared with the experimental results, indicating the errors of the model. Then, the results of the scenarios from the sensitivity analysis, are shown and commented, indicating the effects on the reactor performance and the abundance of PNSB bacteria.

5) **Discussion:** once the main results are explained, the attention is shifted on the main findings and the critical aspects of the model and its simulations, indicating as well further implementations .

6) **Conclusion:** in this section the key findings are summarized and listed, answering at the three research questions and defining the most important amelioration of the model.

2 Critical literature review

The purpose of this section aims to give to the reader adequate background information for a general overview of the Thesis. Moreover, this section intends to answer the first research question identifying the most relevant parameters for the growth of PNSB in raceway reactors (page 3). At first, general information regarding PNSB and raceway reactor is reported (2.1 - 2.3). Then, the attention shifts on the main parameters affecting the growth of PNSB under semi-aerobic conditions and the design of raceway reactor (2.4 - 2.5). The literature review was already sifted in order to select those parameters that would have been implemented in the model. At last, among the available models in the literature, the one from Puyol et al. (2017)[17] was studied in detail and taken as reference for development of the proposed model (2.6).

2.1 What are PNSB bacteria ?

Purple non-sulphur bacteria are alpha- or betaproteobacteria that convert light energy into chemical energy by anoxygenic photosynthesis. The original differentiation between purple non-sulphur bacteria (PNSB) and purple sulphur bacteria (PSB) dates back to the thirties of XX century [22]. According to these studies PNSB could not grow in presence of sulphide. Further researches proved that such distinction should not be valid as PNSB can tolerate and oxidize certain level of sulphide, up to 0.05 mM/L [23]. However, PSB store the formed S^0 intracellularly, whereas PNSB excrete it outside the cell [24]. The group of purple non-sulphur bacteria is characterized by an important diversity. This variety is noticeable in greatly distinct morphology, internal membrane structure, carotenoid conformation, the assortment of diverse carbon sources, and electron donors, among other features [25].

Favourable ecological niches for purple non-sulphur bacteria are those anoxic parts of waters and microbial mats that receive sufficient light to allow phototrophic development. Henceforth, these bacteria are endemic in all kind of stagnant water bodies, as wastewater ponds, coastal lagoons, and in moist sediments like paddy fields [26]. They thrive with significant amounts of soluble organic matter, and light-exposed surfaces but rarely form coloured blooms like those of purple sulphur bacteria. In conclusion, the best conditions to proliferate in nature for PNSB are represented by illuminated, sulphide-deficient water bodies with high-strength organic matter and in a limited range of ORP (−93 to 23 mV) [27].

Since the 1950s, PSNB have been applied as an innovative technology to treat different industrial effluents. Brewery and dairy wastes, olive and soy-bean wastewaters, rubbery and pharmaceutical discharges are some of the examples in which photobioreactors were proposed as possible

applications [28–31]. More recently, the application of PNSB have been proposed as well in the domestic wastewater technology[32]. The elevated yield and the selectivity of growth are two main reasons supporting the cultivation of PNSB from which it is possible to recover valuable products such as single cell proteins, biopolymers, carotenoids, bacteriochlorophylls and hydrogen.

2.2 How do PNSB grow?

According to biochemistry, photophosphorylation, substrate-level phosphorylation, and oxidative phosphorylation are the energy production centres for PNSB, corresponding respectively to photosynthesis, fermentative and aerobic respiration form of metabolism [19]. In fact, purple non-sulphur bacteria are known for their versatile metabolism which have been studied and observed in different experiments.

Under anoxic and light conditions most common species of purple non-sulphur bacteria can grow with a photoorganoheterotrophic or photolithoautotrophic metabolism, typically preferring the first pathway[33]. Originally purple non-sulphur bacteria were cultivated under strictly anaerobic or anoxygenic conditions, but, later on, it was demonstrated that they can tolerate aerobic or semi-aerobic conditions[34]. Anoxygenic photosynthesis is possible thanks to the bacteriopheophytin couple, P870-P870e. In presence of sufficient infrared light, this compound is excited and activates an electron chain, allowing the synthesis of ATP[35]. The most common electron donors during anoxygenic photosynthesis are organic compounds or inorganic as H_2, and less likely Fe^{2+} and SO_4^{-2}. Depending on the oxidation state of the substrate, CO_2 is required – if present[36] – or produced during the metabolism [35]. Thanks to phototrophic metabolism, PNSB can reach biomass-substrate yield around 0.8-1.2 $gCOD_x/gCOD_s$[37]. The overall growth depends from different species, substrates and light conditions, but, in mixed cultures, it is ranged 0.8-1.7 d^{-1} [29].

Under absence or poor light conditions some species of PNSB can perform a chemotrophic metabolism[21]. They can switch to a respiring or fermentative chemoorgano-heterotrophic metabolism, and, less likely, respiring chemolithotrophic[33]. Oxygen presence has been extensively studied and its tolerance varies considerably among species. In general, oxygen inhibits the reaction centre of the anoxygenic photosynthesis, becoming a striking factor for some resources for which PNSB are cultivated (e.g. single-cell protein, H_2, bacteriochlorophyll)[38]. However, more recently, it has been proved that some species of PNSB can achieve a better organic and nutrients removal than in strictly anaerobic-light conditions[39].

Figure 1 and Figure 2 show a schematization of the metabolic pathways for PNSB bacteria. Figure 1 focuses on the phototrophic pathway, separating autotrophic and heterotrophic metabolism. It stresses out the distinct forms of phosphorylation which determines the organo or lithotrophic metabolism. Figure 2 shows the distinctive metabolic pathways under chemotrophic and phototrophic growth, here summarized as light anaerobic and dark-aerobic conditions. More details and accurate information about the specific steps in their metabolism can be found in the review on the carbon metabolism by Zannoni (1995)[23].

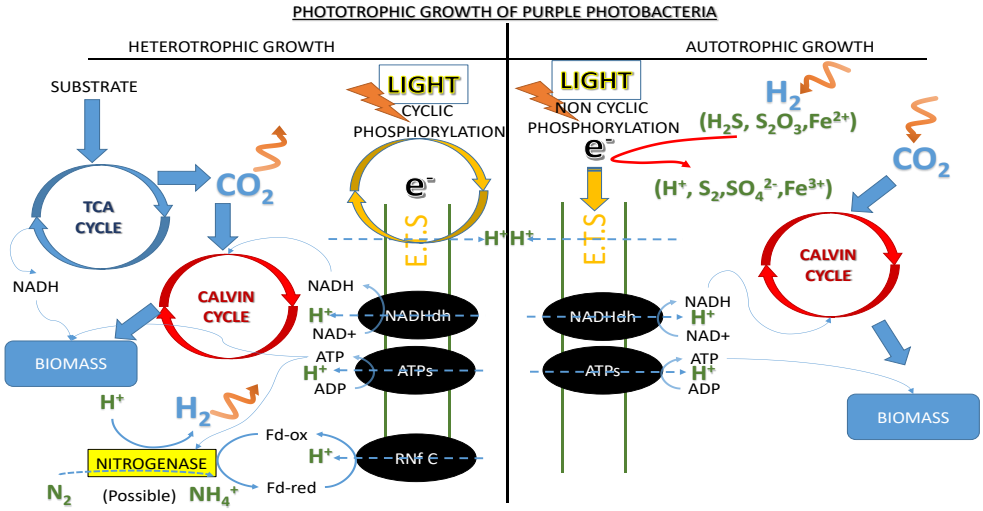

Figure 1 Schematic representation of PNSB phototrophic growth divided into heterotrophic and autotrophic growth (Puyol et al. 2017)[17]. Under photoheterotrophic growth, cyclic phosphorylation is performed, so electrons transport is a complete inner process. However, in case of electrons excess, nitrogenase activity is possible reduction reaction.

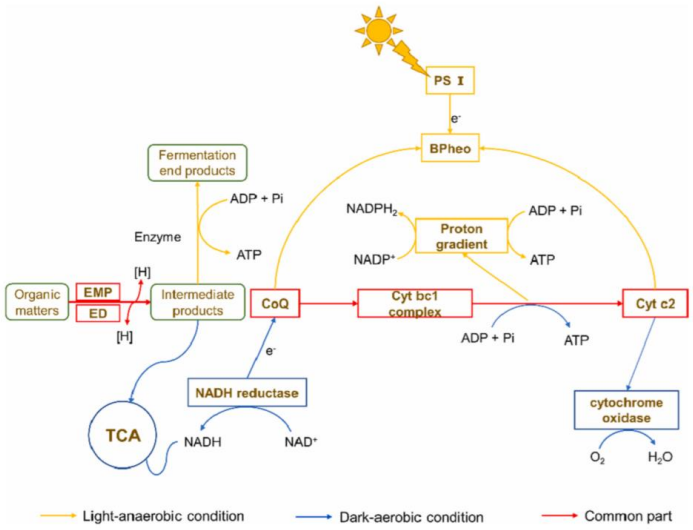

Figure 2 Metabolic pathways of PNSB under different conditions (Lu et al. 2011)[19]. Yellow lines stand light-anaerobic pathway; blue lines for dark-aerobic conditions; red lines for common paths.

2.3 What are raceway reactors?

Open raceway reactors were the first culture systems used for microalgae production and currently are the most common at industrial scale. They started being developed from the 50-60's last century and, since then, they represent the large majority of the global microalgae production on a commercial scale[40]. Their major positive aspects consist in their basic-skilled operation requirements and the low construction cost and energy consumption: from 2 to 8 W/m3 at 20 cm depth[41]. Drawbacks such as low bio-mass concentrations, poor gas-liquid mass transfer, and lack of temperature control have to be considered in the final decisional process. Nonetheless, despite the numerous system's inefficiencies and the availability of other better performing technologies (e.g. tubular reactors), they still remains broadly applied.

Their basic design includes at least two parallel open channels through which the wastewater circulates by means of a paddlewheel. Raceways reactor are often constructed of concrete or compacted earthenware often covered with plastic liner to mitigate hydraulic losses and guarantee laminar fluid dynamic[42]. Figure 3 reports the projections (areal and side view) of a standard raceway reactor, showing the relative dimensions of the paddlewheel and the sump. For microalgae production, to favour an optimal gas exchange ratio of O_2 and CO_2, a sump is often designed, but there are other possible configurations. On industrial scale, dimensions vary from 1.000 to 5.000 m^2 with an investment cost in a range from 0.13 to 0.37 M€/ha at 100 ha scale[40].

According to the most cited literature reviews regarding the fluid-dynamic of the raceway reactor, the most influencing parameters for the biomass production are the water channel velocity, the water depth and the water mixing[41,43,44]. Shortly, mixing is important to keep biomass in suspension and affects the photosynthesis efficiency and photoinhibition. Water depth strongly influences the areal productivity of biomass and determines many physical and chemical parameters as the temperature and light gradient. Finally, water velocity is the major factor which determines the Reynolds number: a crucial parameter for head losses and the real hydraulic retention time in the reactor.

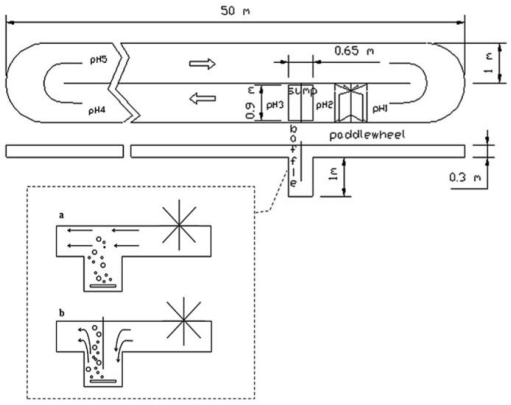

Figure 3 Schematic areal and vertical view of a standard raceway reactor for microalgae modelling according to Mendoza et al,. 2013 [45].

Figure 4 Picture of a 5 m^2 standard raceway reactor for microalgae taken from the paper of Chiaramonti et al. (2012)[44].

2.4 PNSB influencing parameters

A comprehensive literature review of PNSB literature was conducted through Scopus in order to find the main parameters which determine their growth in wastewater reactors. From the literature review it emerged that PNSB are being rediscovered in the last decades as more and more interest was given to the production of bio-hydrogen. Since their discovery, PNSB are correctly thought to be influenced by light. However, in years of studies and research, a wider range of parameters were found to influence their growth. According to one of the last scientific review, Figure 5 gathers the most studied biotic and abiotic factor studied for PNSB[46].

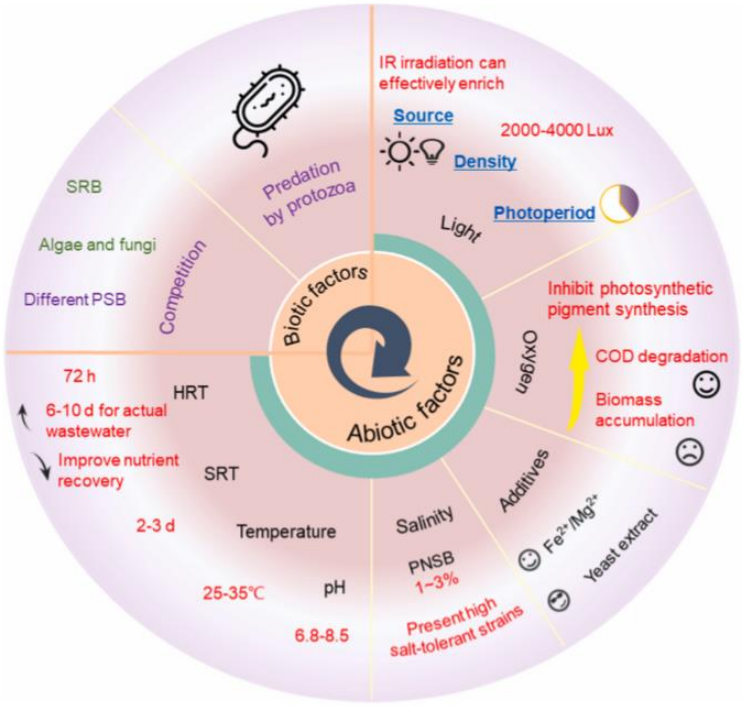

Figure 5 Summary of the most important and studied factors influencing the growth of PNSB according to the literature review of Chen et al., 2020[46].

2.4.1 Light: the major factor to select PNSB

In the literature, the effects of lights have been deeply investigated to optimize the growth of PNSB. As bacteriochlophylls and carotenoids are the primary pigments that allow the photosynthesis in PNSB, the visible light spectrum (340-740 nm), especially blue and red light was found the optimal range[47]. However, a common selective tool to select PSNB over other phototrophic bacteria is infrared light (IR), 0.7-1 nm, as the chlorophyll present in most of microalgae and cyanobacteria does not absorb this wavelength (Figure 6). For that reason, a practical solution for the selection and enrichment of PNSB biomass is the application of IR filter[32]. In most of studies, the widest used wavelength is 850 nm, as it is in both of the absorption spectrum of bacteriochlophyll a and b.

Similarly to microalgae or other cyanobacteria, light intensity should be in a range to activate photosynthesis but not repress it. Chen et al. (2020) assessed this range between 2000-5000 Lux (16-40 W/m^2) for wastewater treatment applications, but this scientific field is broad, complex and yet not fully understood[46]. More importantly, the light intensity and wavelength is not the only factor, but the light propagation in the reactor and the reactor geometry are crucial aspect to consider for a proper comparison.

Seasonal and environmental light variability adapted the evolution strategies of PNSB bacteria as some species can significantly grow or be hindered by alternated and low-light conditions. Day and night variations significantly affect the metabolic pathway of bacteria: extensions of the light phase compared to the dark phase generally increased the bacteriochlorophyll content and biomass yield ($mgCOD_{con}/mgCOD_{bio}$)[18]. However, both continuous and flashing light are known to cause inhibition. In a laboratory set-up the best light-dark cycle for growth and organic removal was evaluated to be of 2h/1h [10]. On the contrary, a more recent research found that with a 24h/24h cycle a greater biomass concentration was measured, but with the lowest protein content[48].

In the end, light has been a largely investigated factor for the growth of PNSB and, yet, its effect has not been universally quantified. Nonetheless, it remains the fully fledged essential variable to select the growth of PNSB in any photobioreactor.

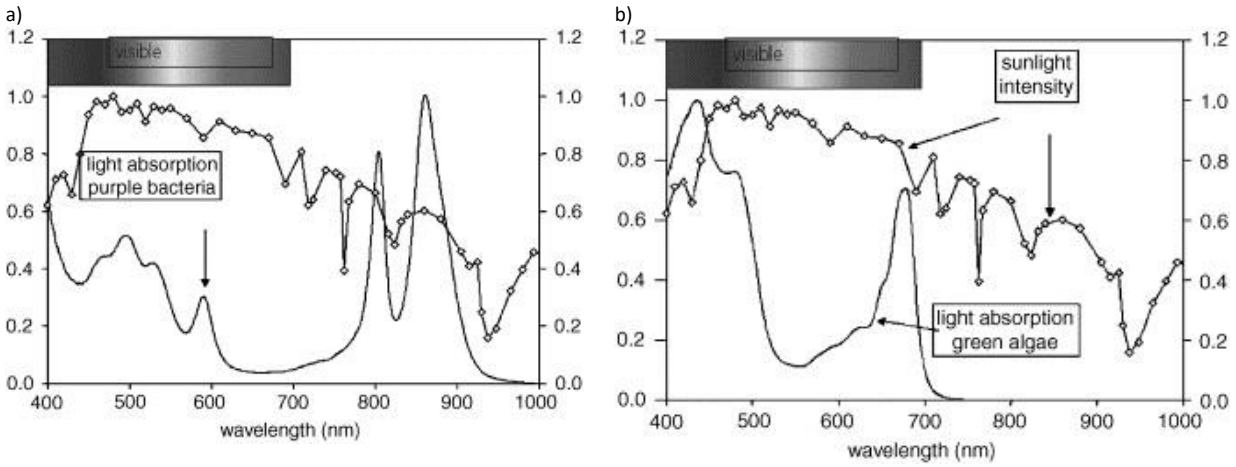

Figure 6 Sunlight and light absorption by purple bacteria (a) and green algae (b) [49]. For PNSB, absorbance peaks are usually in a range between 800-860 nm, for green algae, peaks stand within 600-700 nm.

2.4.2 Oxygen: a divisive variable so far

The oxygen influence on PNSB growth is one of the more discussed topic found in the literature. At first, PNSB were discovered as anoxygenic photosynthetic bacteria, so oxygen was thought to limit their growth. All the literature agrees on the fact that oxygen damages the reaction centre for the

anoxygenic photosynthesis, hindering the production of carotenoids and bacteriochlorophyll visibly fading their original purple colour [50,51]. Nonetheless, it was observed several time PNSB species that could tolerate and growth under light or dark aerobic conditions [20,52]. At this regard, the scientific literature is not unambiguous and many different conclusions have been reached. Firstly, there is a general distinction between aerobic and semi-aerobic conditions which is not universal, complicating the interpretations of experimental results. In addition, single-strain experiments and mixed culture experiments are sometimes compared even though they investigate distinct conditions.

More recent studies on single strain of purple bacteria reported a considerable increase in the final biomass concentration and COD removal despite a lower biomass to substrate yield [20,53]. According to these researches, on the contrary of what was previously thought, some PNSB species can grow even faster in pure chemotrophic pathway. In Figure 7 it is given an example of some results by Lu et al. (2018) showing the difference COD removal under different metabolic pathways[20]. Differently, Alloul et al. (2020) observed that PNSB could grow faster under pure photo-anaerobic conditions than in aerobic conditions[18]. However, most of these experiments were conducted with pure culture without taking into account the biotic competition. When compared to other aerobic chemotrophic family, PNSB showed a lower growth rate and affinity with oxygen, implying that they might not prevail standard chemotrophic bacteria under these circumstances (3 *vs* 6 d^{-1} and 0.5 *vs* 0.2 mgO_2/L)[21,52]. In the literature, it was found only one case-study in which light-aerobic conditions were found to be beneficial for the selectivity of photosynthetic bacteria[54].

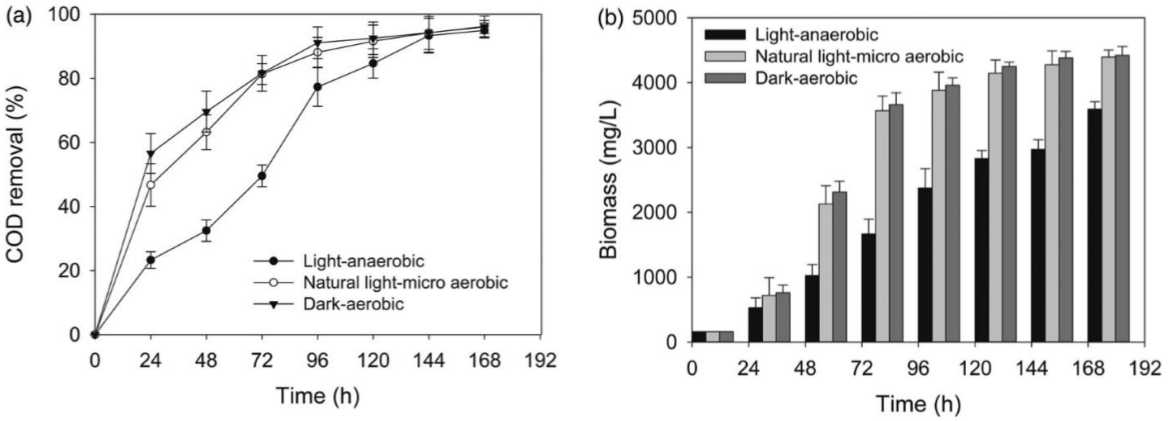

Figure 7: COD removal (a) and biomass concentration in mgTSS/L (b) for different light-oxygen conditions measured in the paper of Lu et al. (2018)[20]

In conclusion, light-micro-aerobic conditions are considered the most acceptable conditions to allow a certain abundance of PNSB bacteria competing with other chemoheterotrophic bacteria. However, oxygen concentration should be always a limiting factor to avoid out-competition of standard chemoorganoheterotrophs, thus the recommended dissolved oxygen levels (DO) are usually below

0.50 mgO_2/L. Sometimes, instead of the standard DO meters, it was suggested to control the oxygen controlling the oxygen reduction potential (ORP) between -200/-300 mV, as suggested in the paper of Kaewsuk et al (2010)[29].

2.4.3 Carbon source: acidified wastewater and more

The majority of studies investigated the preference of a specific VFA for the growth of their metabolism. However, it appeared that, for PNSB species, a mixture of VFAs favours the growth compared to a specific type (Figure 8)[55]. Among VFAs, acetate, but also propionate and butyrate are typically preferred, but it is generally accepted the fact that PNSB favour low fatty acid chain[56]. In this regard, hydrolysis and pre-acidification, as proposed in the Saraswati project, it is commonly suggested as a pre-treatment steps to promote PNSB[5]. Having said that, some PNSB species were found able to degrade directly macromolecules photoheterophically, even though at a considerable lower pace[17,57]. Substrate preference through the chemoheterotrohic pathway has not been deeply studied, but it appeared to be less affected by the specific type of complex substrate or VFA. Actually, PNSB seemed to grow faster with sucrose and glucose than with VFAs when performing a chemoheterotrophic metabolism[52].

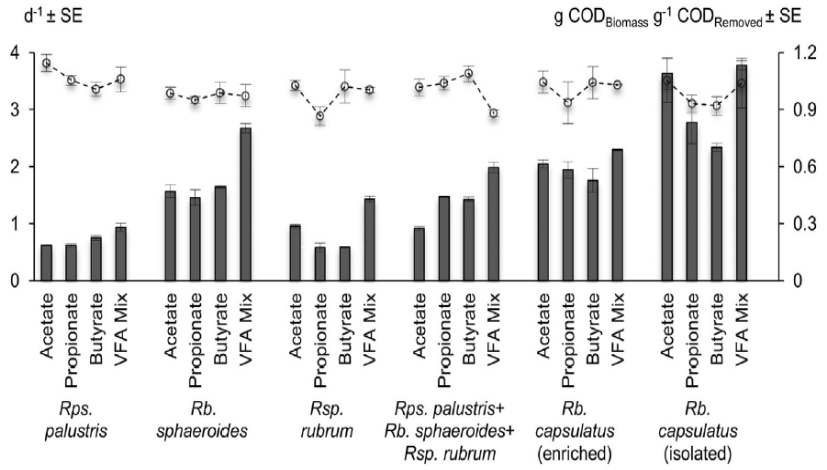

Figure 8 PNSB growth rate (left) and biomass yield (right) with different substrate medium: acetate , propionate, butyrate, VFA mix (Alloul et al. 2019)[55].

2.4.4 Other parameters: details can make the difference

Metabolisms are a series of complicated processes in which many factors contribute in a direct or indirect way. In the previous sections, the most examined variables concerning the growth of PNSB

under semi-aerobic conditions were reported, although, there are several of other parameters that should be at least mentioned for a complete understanding of PNSB.

2.4.4.1 Nitrogen

PNSB mainly use nitrogen during anabolism as a fundamental nutrient for biomass growth, even though some denitrifying strains were also discovered [58]. Nitrogen abundance also regulates the bio-hydrogen production by PNSB as ammonia seriously hinders hydrogenase enzyme activity; moreover it was found that high level of ammonia lead to a higher protein content in the dry cells [59]. Therefore, in most studies, this topic is faced regulating and comparing the C/N ratio. In many industrial wastewater, the C/N ratio is generally high and then bio-hydrogen production is of particular interest. Under other circumstances, as in municipal or agricultural streams, C/N ratio is relatively low and then protein content can reach higher level up to 80-90% [46]. In conclusion, nitrogen presence could be as well a factor regulating the metabolic pathway of PNSB, but it has been mainly studied combined with the H_2 recovery, which is not the main focus of this thesis.

2.4.4.2 Temperature and pH

Most of strains of purple non-sulphur bacteria are classified as mesophilic bacteria, and in nature their proliferation happens in temperate water, between 25-35 °C. They were discovered also to survive at low temperature, but not beneath 10 °C [60]. From the literature review, it emerged that most of the long-term experiments were conducted in controlled temperature environments, while has not been yet investigated rapid and long-term change of temperature on these bacteria in open photobioreactor. However, one research, which investigated the effects of temperature for *Rhodospirillum rubrum* under illuminated semi-aerobic conditions, concluded that PNSB growth rate obeys to the Arrhenius law for temperatures below 40 °C[61].

In general pH dependency of PNSB is not particular strict and these bacteria can adapt in a pH range between 6.8 and 8.5. In several batch experiments with an initial pH around 7.5-8.0 it was obtained the best performance [46]. It is important to consider that organic removal, especially VFAs for PNSB, would lead to a final increase in the pH in the exponential growth phase. Thus, as for microalgae reactors, pH can be an important control tool to monitor for semi-continuous reactors .

2.5 Raceway reactor influencing parameters

2.5.1 Physical and Hydraulic parameters

Raceway reactors are characterised by a high surface to volume ratio to optimize the light contact with the microorganisms. In the literature, water depth is often designed in a range between 15-30 cm. Channel width is around 1/5-1/10 of the channel length and the width of the bend is often equal to the channel width or slightly higher[44]. Paddlewheels configuration, shape and dimensions are considered important as they do not only provide mixing with the influent, but they should free enough energy for water's eddy to enhance vertical mixing avoiding prolonged photoinhibition[64].

Water flow is the most important parameter to control the hydraulic losses in the reactor; in the literature a value between 0.15-0.30 cm/s is often suggested. At this regard, Manning or Colebrook formula are typically considered in the literature [41]. Head loss coefficient is a typical parameter to be estimated to calculate the power requirement of the reactor. Mainly it has to consider the friction losses along the channel, in the bends and through the paddlewheel[44]. Finally, the design and the operational condition of the sump are of major importance as it enhance the gas exchange with the atmosphere. However, for the cultivation of PNSB, it might be prevented in order to control and minimize the oxygen transfer rate (OTR).

2.5.2 Light distribution

In open raceway reactors the light reaching the surface is dependent on the position of the reactor itself and the position of the sun. Then, latitude, longitude, hours and seasonal change are the major parameters influencing the radiation intensity on the surface of the raceway reactor[40]. As for PNSB, infrared wavebands are particularly important, diffusive light should be majorly considered. In 2002, Katsuda et al. (2002) proposed the first attenuation model for *Rhodobacter caspsulatus* according to Lambert-Beer equation[65]. This equation is often used for its applicability, but in the literature can be found other more accurate models as, for instance, the bidirectional scattering model and the full radiative transfer equation[66]. Based on the author's knowledge author, these model have not been applied for PNSB bacteria, so they will not be considered.

2.5.3 Mass Transfer

For raceway reactors gas transfers are particularly relevant in the paddlewheel and in the sump where most of the CO_2 and O_2 exchange occurs. Nevertheless, along the channel, the elevated surface to volume ratio can enhance the exchange of gasses between the water and air. According to Mendoza et al. (2013), with a fixed gas flow rate of rate of 6 m^3h^{-1} , the mass transfer rate coefficient of CO_2

were measured as 165, 64,0.87, 0.98 h^{-1} for the paddlewheel, the sump, the straight and the bend channel[40]. As it appears, next to the paddlewheel is where occurs the fastest exchange ratio, but it has to be considered that the length of the channel is around 50 times higher. Moreover, biological activity on these ratio has to be considered. At the moment, there aren't specific studies on the exchange ratio regarding PNSB applications, but the same considerations could be valid. The two main gases to taken into account are oxygen, carbon dioxide, and additionally ammonia. Finally, others factors could be included in the mass transfer, as the vertical and longitudinal diffusion after the paddlewheel mixing or the diffusion of soluble and particulate matter varying with the flow characteristics.

2.6 Modelling PNSB in raceway reactor

At present, the mechanistic model elaborated by Puyol et al. (2017) is the most complete and available model in the scientific literature for a mixed-culture of purple phototrophic bacteria (PPB) for wastewater treatment[17]. The code is available and can be run with Matlab (MATLAB R2015a, The MathWorks Inc., Natick, MA) and it is compatible with the International Water Association (IWA) Activated Sludge Model (ASM) for further implementations in the biotechnological application[67,68]. These factors were the main reasons why this model was taken as reference and starting point for this project. It was evaluated on a long-term dynamic photo-anaerobic membrane bioreactor (PAnM) with satisfactory results. Under strictly anaerobic conditions and a constant infrared light source, the photoheterotrophic metabolism was assumed to dominate, once accurately inoculated. Purple phototrophic bacteria (PPB) were the only form of biomass considered in the reactor; their multifunctional metabolism was summarized in four reactions. Six processes were simulated with PPB as only form of biomass. The PPB bacteria were summarized with four reactions: two photoheterotrophic, one fermentative chemoorganoheterotrophic and one autotrophic. Furthermore, hydrolysis and decay were included. In conclusion, the model was composed by six processes and 10 variables. The Petersen matrix used by Puyol et al. (2017) is shown here below.

Component (C) →	i	1	2	3	4	5	6	7	8	9	10
j	Process↓	S_S	S_{ac}	S_{IC}	S_{h2}	S_{IN}	S_{IP}	S_I	X_{PB}	X_S	X_I
1	Hydrolysis/ fermentation	$f_{ss,xs}$	$f_{Sac,xs}$	$f_{iC,xs}$	$f_{h2,xs}$	$f_{IN,xs}$	$f_{IP,xs}$	$f_{si,xs}$	0	−1	$f_{xi,xS}$
2	Acetate uptake	0	−1	$f_{IC,ph,ac}$	0	$-f_{N,B}Y_{PB,ph}$	$-f_{P,B}Y_{PB,ph}$	0	$Y_{PB,ph}$	0	0
3	Photoheterotrophic uptake	−1	0	$-f_{IC,ph}S_s$	0	$-f_{N,B}Y_{PB,ph}$	$-f_{P,B}Y_{PB,ph}$	0	$Y_{PB,ph}$	0	0
4	Chemoheterotrophic uptake	−1	$(1-Y_{PB,ch})$ $f_{ac,ch}$	0	$(1-Y_{PB,ch})$ $f_{h2,ch}$	$-f_{N,B}Y_{PB,ch}$	$-f_{P,B}Y_{PB,ch}$	0	$Y_{PB,ch}$	0	0
5	Autotrophic uptake	0	0	$-f_{IC,a}$	$-f_{h2,a}$	$-f_{N,B}Y_{PB,a}$	$-f_{P,B}Y_{PB,a}$	0	$Y_{PB,a}$	0	0
6	Decay of XPB	0	0	$-\sum_{i=8-9} Ci \times f_{C,i}$	0	$-\sum_{i=8-9} Ci \times f_{N,i}$	$-\sum_{i=8-9} Ci \times f_{P,i}$	0	−1	1	0
		Soluble substrate (mgCOD L^{-1})	Acetate (mgCOD L^{-1})	Inorganic carbon (molC_HCO3 L^{-1})	H^2 (mgCOD L^{-1})	Inorganic nitrogen (mgN_NH_4 L^{-1})	Inorganic phosphorous (mgP_PO_4 L^{-1})	Soluble inert (mgCOD L^{-1})	Phototrophic biomass (mgCOD L^{-1})	Biodegradable particulate (mgCOD L^{-1})	Particulate inert (mgCOD L^{-1})

Rate equations:

j1: $\rho_{HYD} = k_{HYD}X_S$

j2: $\rho_{ACT} = k_{M,ac}X_{PB}\left(\frac{S_{ac}}{K_{S,ac}+S_{ac}}\right)I_{FA}I_{IN}I_{IP}I_E I_{C\_S}$

j3: $\rho_{PHT} = k_{M,ph}X_{PB}\left(\frac{S_s}{K_{S,s}+S_s}\right)I_{FA}I_{IN}I_{IP}I_E I_{C\_ac}$

j4: $\rho_{AUT} = k_{M,IC}X_{PB}\left(\frac{S_{IC}}{K_{S,IC}+S_{IC}}\right)I_{FA}I_{IN}I_{IP}I_E$

j5: $\rho_{CHE} = k_{M,ch}X_{PB}\left(\frac{S_B}{K_{S,B}+S_B}\right)I_{FA}I_{IN}I_{IP}$

j6: $\rho_{DEC} = k_{DEC}X_{PB}$

Limiting factors:

Competitive inhibition: $I_{C\_S} = \frac{S_{ac}}{S_{ac}+S_S}$ $I_{C\_ac} = \frac{S_S}{S_S+S_{ac}}$

N: $I_{IN} = \left(\frac{S_{IN}}{K_{S,IN}+S_{IN}}\right)$ P: $I_{IP} = \left(\frac{S_{IP}}{K_{S,IP}+S_{IP}}\right)$ Free Ammonia: $I_{FA} = \left(\frac{K_{I,FA}}{K_{I,FA}+S_{NH3}}\right)$ Light: $I_E = \left(\frac{S_E}{K_{S,E}+S_E}\right)$

Figure 9 Petersen's Matrix taken developed in the photo-anaerobic mechanistic model from Puyol et. al. (2017)

2.7 From the literature review to the model development

Together with collecting general background, the literature review particularly aimed to identify those variables which could characterize the growth of PNSB in a raceway reactors and that could be easily implemented in a model. In conclusion, the following parameters were selected as:

- light intensity and variability;
- oxygen presence and the oxygen transfer rate, determining the so-called semi aerobic conditions;
- biotic competition with standard chemoorganotrophic bacteria;

The mechanistic model from Puyol et al. (2017)[17] was considered sufficiently extensive and robust and was taken as reference for this project. Nevertheless, most of above mentioned variables needed to be included to simulate raceway reactors conditions. Therefore, important adjustments and modifications were studied and developed in order to adapt it to the raceway reactor. These aspects will be exhaustively explained in the next section where the model and its equations are be presented and discussed.

3 Material and Methods

*This section gathers all information needed to answer the second and the third research questions. The first three subsections explain in detail the model structure, variables and implemented equations (3.1**Fout! Verwijzingsbron niet gevonden.** – 3.3). Then, the attention is shifted at the tuning process that was needed to parametrise the model with the experimental results (3.4 – 3.5). The last subsection reports the necessary information to understand the structure of the sensitivity analysis answering at the third research question.*

3.1 General model configuration

In a raceway reactor system, there are significant physical and environmental conditions that are distant from the model developed by Puyol et al (2017). Therefore, some changes are required to simulate an open raceway reactor which are shown at Table 1. For instance, due to the contact with atmosphere and the paddlewheel rotation the gases transfer rates should be included. Mainly, oxygen and carbon dioxide kinetic should be considered. The oxygen transfer rate (OTR) would promote respiring chemoheterotrophic growth, inducing biotic competition between standard chemoheterotrophic bacteria (X_{HET}) and PNSB (X_{PB}). As mentioned in the literature review, to favour PNSB, wastewater has to be previously acidified through fermentation. Therefore, it is reasonable to assume that the influent wastewater would contain fermenting bacteria (X_{FR}) which might still impact the biological activity of the raceway reactor. As well, the natural light intensity variations will determine a possible switch between the phototrophic and chemotrophic metabolism among PNSB, which was controlled with a cybernetic model, an internal regulatory process to deal with mixotrophi metabolism and multiple substrate[69]. Moreover, the different water levels would impact the average light intensity, so a light attenuation model should be included. At last, a continuous stirred tank reactor (CSTR) mass balance was changed to a sequencing batch reactor (SBR) system, because the laboratory experiments operated under semi-continuous conditions.

Table 1 Main differences between the model from Puyol et al. (2017) and the present model[17]

	Puyol et al. (2017)	**Present model**
Biomass	X_{PB}	X_{PB}, X_{HET}, X_{FR}
Conditions	Anaerobic (closed)	Semi-aerobic (gas-transfer with atm)
Substrate	- S_S (glucose) - S_{AC} (acetate)	- S_S (glucose) - S_{VFA} (volatile fatty acids) - S_{AC} (acetate)
Growth	Monod	Monod and cybernetic
Metabolisms	- X_{PB} ◦ Photoheterotrophic ◦ Chemotrophic (anaerobic&fermentative) ◦ photoautotrophic	- X_{PB} ◦ Photoheterotrophic ◦ Chemotrophic (aerobic&anoxic) ◦ Chemotrophic (anaerobic)

		- X_{HET} ○ Chemotrophic (aerobic&anoxic) ○ Chemotrophic (anaerobic) - X_{FR} ○ Fermentative
Light	Constant Light: I_0	Lamber-Beer I_{av}
Reactor conditions	CSTR	SBR
pH	dynamic	constant

In order to facilitate the comprehension of the biological and physical processes in the raceway reactor a simplified representation of the conceptual model is shown with Figure 10. Three populations of bacteria were simulated in the model: purple phototrophic bacteria (X_{PB}) respiring chemoheterotrophic bacteria (X_{HET}) and fermentative bacteria (X_{FR}). The reasons of this subdivision was assessed as a balance between the vastness of microbial species and the simplification requested for a simulation of the model. Similarly, the wastewater organic composition can be expressed as one or a multitude of substrates. In this model, four variables were chosen: the complex soluble compounds (S_S), acetate (S_A), soluble volatile fatty acids (S_{VFA}) and the suspended organic particulate (X_S). Together with the organic substrate, microbes consume many other chemical components, typically grouped with the terms of macro-nutrients (nitrogen, phosphorous and sulphur) and micro-nutrients (potassium, magnesium, iron, etc.). In this model, as in the model from Puyol et al (2017), soluble inorganic nitrogen (S_{IN}) and soluble inorganic phosphorus (S_{IP}) were taken into considerations as they are important parameters for wastewater treatment and environmental discharge regulations. During bacterial organic oxidation, inorganic carbon (S_{HCO3}) in form of CO_2 or HCO_3^- is typically produced, inducing an important change in the water alkalinity. On the other hand, oxygen (S_{O2}) or other electron acceptors as sulphate, hydrogen or iron are consumed. In this model, only soluble oxygen would be considered, whereas the other electron acceptors like nitrate or sulphate would not be modelled. Soluble and particulate inert compound (S_I, X_I) can be as well included in the model, to consider hydrolysis and decay processes which close the cycle . The figure shows the alteration of the light and dark phase (sun/moon) which influences the metabolic switch between phototrophic and chemotrophic metabolism and the different gas transfer rate during the night (dotted line) as the paddlewheel is usually switched off at night. In the next sections the major model components and variables included in the model are explained more details, giving the essential information on biological and chemical reactions.

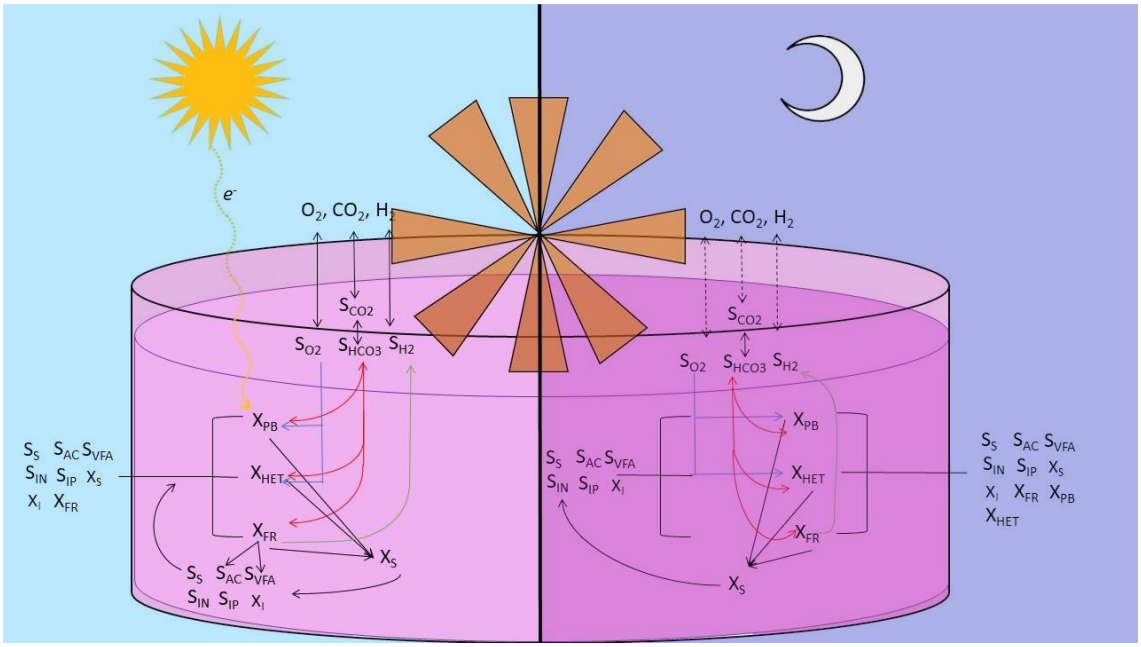

Figure 10 Conceptual model showing the biological and physical interactions in the raceway reactor during the day (left) and during the night (right). Influent, mainly composed with soluble substrate (complex substrate – S_S, acetate – S_{AC}, volatile fatty acid – S_{VFA}) is uptook by microorganisms (PNSB – X_{PB}, standard chemoheterotrophic bacteria – X_{HET}, fermentative bacteria – X_{FR}) according to the specific metabolic pathway. During the day, X_{PB} use electrons from light (e^-) to perform anoxygenic photosynthesis to achieve photoheterotrophic growth. Oxygen, is exchanged during the chemoheterotrophic metabolism by X_{PB} and X_{HET}. Bicarbonate (S_{HCO3}) is exchanged and equilibrium with soluble carbon dioxide in the water (S_{CO2}) is calculated and balanced with the gas transfer. During the night, whether the paddlewheel is turned off, the gas transfer is strongly hindered, affecting the aerobic chemoheterotrophic and photoheterotrophic growth. Decay of microorganisms is also considered forming organic particulate (X_S) which would be hydrolysed into the major compounds, closing the cycle.

3.2 Model variables

The chemical composition of the influent has an important role in the biological activity that would take place in the reactors. The multitude of organics substrates in water can be summarized with one elemental formula to adjust case by case. In the Anaerobic Digestion Model (ADM), the substrate is divided in many specific compounds (acetate, propionate, valerate, amino acids etc…), whereas in the Activated Sludge Models (ASMs) wastewater is most frequently simulated only with two substrates (readily biodegradable substrate and acetate) [68,70]. In the raceway reactor, influent wastewater would be most likely pre-treated by an anaerobic digestor, thus it is reasonable to assume a large fermentation of the substrate. Nevertheless, depending on the performance of the anaerobic digestor, a certain concentration of the original complex substrate would remain in the wastewater. Therefore, a distinction between the already acidified wastewater and the complex substrate is essential. For these reasons, in the model, three soluble substrates were assumed: complex substrate (S_S) and two acidified compounds, acetate (S_A) and soluble volatile fatty acids (S_{VFA}). In this study, S_{VFA} was defined as a mixture composed by 80% propionate, 10% valerate, 10% butyrate[71].

Consequentiality the elemental formula can be approximated to $C_{3.33}H_{6.67}O_2$. The elemental formula assumed for S_S for many modelling purposes is glucose ($C_6H_{12}O_6$), but more sophisticated and realistic compositions can be implemented ($C_{10}H_{19}O_3N$)[17,72]. The ratio between S_A and S_{VFA} could radically change according to the duration of the previous fermentation process, thus it is not fixed, but determined on the specific circumstances. In conclusion the soluble available substrate can be summarized like follows:

- *S_S [mgCOD/L]: Complex soluble substrate.* In standard ASM model, this organic component represents the soluble fraction of COD which is readably at use of bacteria.
- *S_A [mgCOD/L]: Acetate.* Acetate represents the end products of fermentation. It can be rapidly and directly assimilated by purple heterotrophic bacteria and oxygenic heterotrophic bacteria, but it is usually considered a dead-end product for fermenting bacteria (not methanogenic).
- *S_{VFA} [mgCOD/L]: Volatile fatty acids chains.* This fraction, it is not usually found in the standard ASM model as it is considered in the S_s fraction whereas in the ADM model, it is divided for each volatile fatty acid component (e.g. butyrate, valerate, etc).

Apart from the soluble components, the organic fraction can be also present in particulate form. In ASMs and ADM models, organic particulate is usually defined into two or three components [68,70]. Organic fraction that cannot be directly assimilated by bacteria, because it has to be firstly hydrolysed. Similarly to the Puyol's model, in this project the particulate matter was divided into two components[17]:

- *X_I [mgCOD/L]: Inert particulate organic material.* This fraction is not degraded in the system. However, it can be oxidized by chemical reactions, so it is expressed in mgCOD/L. Typically, within the processes of hydrolysis and bacterial decay, X_I is produced.
- *X_S [mgCOD/L]: Slowly biodegradable substrates.* With this parameter, the literature refers to all high molecular weight, colloidal and particulate organic substrates which must be hydrolysed before they can be assimilated. Because of the previous fermentation treatment, it is expected that *X_S* would represent only a small fraction of the incoming COD. As chemical reaction, X_S hydrolysis mainly forming S_S, S_A and S_{VFA}.

Nutrients as nitrogen and phosphorus are important elements that can greatly affect bacterial growth under limiting conditions. Regarding nitrogen removal, according to most of wastewater treatment model, there are four variables simulating the nitrogen cycle (N_2, NH_4^+, NO_3^- and NO_2^-). Nonetheless, after a fermentation step, because of the low ORP (-300 -100 mV), $NO_3^-$and NO_2^- can be assumed a limited fraction compared to NH_4^+ [73]. Moreover, in the raceway reactor, the reduced OTR and the

negative ORP is assumed insufficient to allow any form of nitrification. Similar conclusions can be assumed for the phosphorus components which is primarily considered as ortho-phosphate. One last aspect is the nitrogen and phosphorus bound with particulate and soluble components which was not included, as it was considered already hydrolysed. Then, in conclusion, in this model, nutrients are simulated as explained below:

- S_{IN} *[mgN/L]: Inorganic soluble nitrogen.* This variable simulates NH_4^+ assimilation by bacteria during their growth.
- S_{IP} *[mgP/L]: Inorganic soluble phosphorus.* This variable simulates PO_4^{3-} assimilation by bacteria.

Catabolism produces a considerable amount of CO_2. In closed anaerobic bioreactor the partial pressure of CO_2 is an important aspect determining equilibrium in water. However, in a raceway reactor (pH 7.0-8.5), the CO_2 fraction is irrelevant and minimal compared to the HCO_3^- concentrations. Thus in the model, it will be assumed that the CO_2 produced by biological activity is instantaneously transformed to HCO_3^- while a certain fraction is transferred to the atmosphere (S_{CO2}, S_{HCO3}). As well, the soluble oxygen concentration (S_{O2}) is a variable determined by the catabolic processes and governed by gas exchange with the atmosphere. In conclusion, three more variables are added into the system:

- S_{CO2} *[mg CO_2/L]: Soluble Carbon dioxide.* In this model this variable is not dependent on biological activity, but only from chemical-physical processes as pH and gas transfer, in function of S_{HCO3}.
- S_{HCO3} *[mmolHCO_3^-/L]: Bicarbonate.* This variable simulates bicarbonate variations because of biological activity.
- S_{O2} *[mg O_2/L]: Soluble oxygen* . The model can simulate the oxygen uptake from the biological activity and oxygen transfer because of paddlewheel rotation.

The last variables that are described in the model are those representing the biomass. As mentioned before, three main groups of bacteria in the raceway reactor were considered. This subdivision was based on the microbial analysis of some experiments performed under illuminated semi-aerobic conditions. *Acinetobacter*, *Dysgonomas* and *Arcobacter* were found the most abundant species competing with PNSB bacteria in raceway reactor[18]. In another experiment, *Bacteroidales* and *Pseudomonadales* were measured as the most abundant anaerobic and aerobic chemotrophic bacteria[21]. These microorganisms can mainly perform a respiring chemotrophic metabolism, oxidising the organic substrate with a inorganic electron acceptor as oxygen, but they can grow as well under

anaerobic conditions. In ASMs models they are usually referred as Ordinary Heterotrophic Organisms (OHOs), but in this model they were classified as respiring heterotrophic bacteria (X_{HET})[74].

- X_{PB} *[mgCOD/L]: Purple non-sulphur bacteria.* If properly inoculated and controlled into the raceway reactor, these organisms can grow and compete with heterotrophic bacteria. The elemental formula used in this model was $C_1H_{1.8}O_{0.38}N_{0.18}P_{0.014}$ as standard value found in the literature[63].
- X_{HET} *[mgCOD/L]: Respiring heterotrophic bacteria.* These bacteria are assumed to be the main competitor against X_{PB}. They are the main responsible for hydrolysis of particulate substrates X_S and can use all degradable organic substrates under aerobic/anoxic conditions. In presence of oxygen they can use it as an optimal acceptor. Under anoxic/anaerobic condition, they can use different type of electron acceptors (e.g. NO_3^- and SO_4^-), which, however, are not considered in this model. Their elemental formula is usually $C_1H_{1.8}O_{0.5}N_{0.2}P_{0.014}$ [75].
- X_{FR} *[mgCOD/L]: Fermenting heterotrophic bacteria.* These organisms are fermenting bacteria that can degraded components except from S_A. They can grow under anoxic/anaerobic conditions, while they are hindered by oxygen presence. They are distinguished by aerobic fermentation as they would be mainly present in the prior anaerobic digestor. As X_{HET} their elemental formula is assumed to be $C_1H_{1.8}O_{0.5}N_{0.2}P_{0.014}$[75].

3.3 Model processes

In this section all processes of the raceway reactor are discussed and the specific equations are given. At first, the focus was turned to the physical-chemical processes: the gas transfer equation, the light attenuation model and the mass balance are given. Then the attention shifted to the biological processes, firstly describing the stoichiometry and lastly the kinetic.

3.3.1 Physical processes

3.3.1.1 Gas transfer rate with the atmosphere

In a raceway reactor, because of the interaction between water surface and atmosphere, the solubility of each component is function of the Henry's constant an the relative atmospheric pressure. For oxygen and carbon dioxide the partial pressure in atmosphere were assumed respectively 21% and 0.004%. Henry's constant values were taken at standard temperature of 298 K and considered to be constant at 0.012 and 0.034 $\frac{mol}{L \cdot atm}$ for O_2 and CO_2. In conclusion, the saturation concentration (C_s) for

oxygen and carbon dioxide in water were equal to 8.3mg O_2/L and 0.04 mg CO_2/L at the standard temperature.

In case of microalgae modelling in a raceway reactor, the gas balance is typically written as

$$\frac{dO_2}{dt} = kl_a(C_s - C) + P - R \qquad \textit{Eq. 1}$$

Where $kl_a$is the reaeration coefficient (h^{-1}), P is the amount of oxygen produced by photosynthesis and R is the consumption oxygen rate by oxygenic respiration[76].

The term P is assumed to be zero because of the absence of microalgae in the model and R is mainly dependant on biological activity. The reaeration coefficient becomes an important value to define. This constant can be determined with a tracer gas experiment [77]; otherwise a range of values can be taken from literature (page 15). According to Mendoza et al. (2013) the reaeration coefficient for a raceway reactor is around 1 h^{-1} [45].

3.3.1.2 Light attenuation model

The propagation of light in water is an important parameter which defines the photosynthetic activity of the raceway reactor. Different approaches are available to simulate the light behaviour, from the Lambert-Beer approach to more complex flux model[66].

The Lambert beer law is widely used in literature because of its simplicity and applicability. It is a one dimensional equation that describes the absorption of light in a fluid as follows:

$$I = I_0 * 10^{-\varepsilon \cdot C \cdot L} \qquad \textit{Eq. 2}$$

Where I is the light at a certain depth, I_0 is the intensity radiation, ε is mass attenuation coefficient [$m^2 \cdot g^{-1}$], C is the TSS concentration [$g \cdot m^{-3}$], and L is the depth of the raceway reactor [m]. To be more accurate ε should be analysed for each wavelength, but in his research Hoon Kim measured a constant values for the interested wavelength of anoxygenic photosynthesis, with a value around 0.12 $m^2 \cdot g^{-1}$ for wavelengths between 299-900 nm[78]. In this model, ε was considered equal to 0.07 $m^2 \cdot g^{-1}$ as in the research of Solimeno[76]

Since the depth of a raceway reactor is moderately shallow and the culture is well considered well mixed, it is a common assumption to consider the average light intensity as expressed in the formula below:

$$I_{avg} = \frac{1}{L}\int_0^L I\, dL \qquad \textit{Eq. 3}$$

Solimeno et al. (2016)[79] directly expressed the equation for a raceway reactor in function of the depth (L) with I_0 expressed in µmol·m^{-2}·s^{-1} which can be converted to W/m^2 multiplying for a value between 4.57 and 5.00.

$$I_{avg} = \frac{I_0(1 - e^{-\varepsilon \cdot C \cdot L})}{\varepsilon \cdot C \cdot L} \qquad \textit{Eq. 4}$$

3.3.2 Reactor geometry and mass balance

Industrial raceway reactors are usually modelled in three zones: channel, paddle-wheel, and sump[40]. The channel can be simulated as an ideal or real plug-flow reactor; the paddle-wheel area and the sump as a continuous stirred tank (CSTR), but, in the sump, it is usually considered a gradient for the gas transfer of oxygen and carbon dioxide. On the contrary, laboratory-scale or pilot-scale raceway reactor, due to their reduced dimensions, are more commonly considered as one single CSTR. In this research, the model was firstly compared with laboratory experiments performed with a 100L raceway reactor under batch and sequencing batch reactor (SBR). Therefore, the mass balances in the model are measured accordingly. SBR systems work on a fill and draw cycles principle which should be fine-tuned considering the natural light variations for outdoor photobioreactor. A standard SBR cycle is composed in five steps: fill, react, settle, decant, and idle[80]. In case of raceway reactors, one potential schematization is reported at Figure 11.

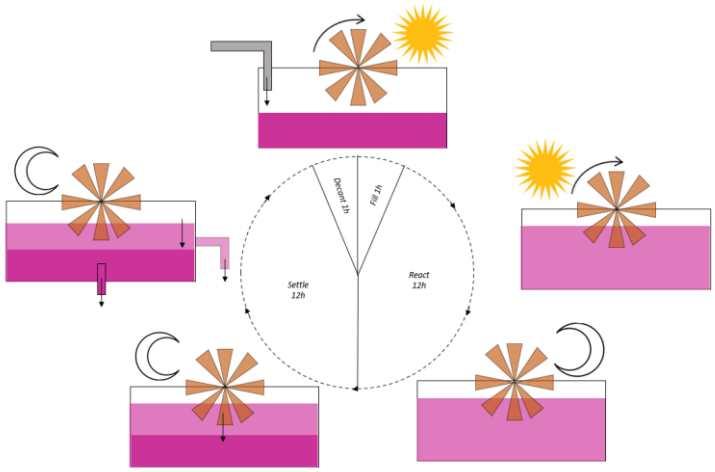

Figure 11 Schematization of the cycle of raceway reactor under sequencing batch reactor conditions. During the day the reactor is filled with the influent reaching and the paddlewheel is turned on promoting gas transfer. At night the paddlewheel is stopped, slowing the reactions processes and promoting settling of biomass. At last, supernatant and sludge is taking out.

The following formulas contain the mass balance equations for the soluble and particulate components for one SBR system. The reactor volume is not constant so its variability should be considered as a differential equations (Eq. 5). Hydraulic and sludge retention time (HRT, SRT) are the main parameters which determine the mass balance for the soluble and particulate fraction. In general, SRT is managed with a recirculation flow, which in this case was not simulated. However, after the settling, a large part of biomass would have sedimented on the bottom of the reactor. Therefore, it would not be extracted in the effluent, if not previously mixed by the paddlewheel. In conclusion, the control of the paddlewheel activation can regulate different HRT and SRT. In the mass balance, this aspect can be regulated with the factor f_{SRT} (Eq. 6). The other two equations report the mass balance for the soluble (S) and particulate (X) fraction (Eq. 7-8) with r_s and r_x that represent the global process rate (consumption/production) which are explained in the next subsections.

$$\frac{dV}{dt} = Q_{in}(t) - Q_{out}(t) \qquad \text{Eq. 5}$$

$$f_{SRT} = \frac{HRT}{SRT} \qquad \text{Eq. 6}$$

$$\frac{dS}{dt} = \frac{(Q_{in}(t) * S_{in} - Q_{out}(t) * S + \frac{dV}{dt} * S)}{V_o} + r_s \qquad \text{Eq. 7}$$

$$\frac{dX}{dt} = \frac{(Q_{in}(t) * X_{in} - Q_{out}(t) * X + \frac{dV}{dt} * f_{SRT} * X)}{V_o} + r_X \qquad \textit{Eq. 8}$$

3.3.3 General stoichiometry

3.3.3.1 The metabolism of purple non-sulphur bacteria - X_{PB}

As known, PNSB can perform multiple metabolisms. In this study, their behaviour was simulated for each substrate and metabolic pathway. In the following paragraphs all the processes of their metabolism is reported starting from their photoheterotrophic metabolism, then showing their respiring and fermentative chemoheterotrophic metabolism.

Photoheterotrophic pathway

The phototrophic pathway diverges based on the electron donor used in the anoxygenic photosynthesis, lithotrophic or organotrophic, and on the carbon source, autotrophic and heterotrophic. In this model, it was considered only the photoorganoheterotrophic metabolism, ignoring the photolithoautotrophic pathway which is significantly slower[17].

In black box models, the phototrophic metabolism is commonly simulated only by the anabolic reactions, as the catabolism is promoted by the photosynthetic activity which is an inner conversion inside the microbial cell. Moreover, PNSB, when they grow photoorganoheterotrophically, perform a cyclic photophosphorylation, thus the electrons' transfer is difficult to examine. Under these circumstances, according to the experimental results, the biomass to substrate yield ($Y_{X/S}$) of PNSB usually varies between 0.8-1.2 $mgCOD_x/mgCOD_s$. Thus, for the three substrates (S_{AC}, S_{VFA}, S_S) the phototrophic metabolism results as in Eq. 9.1-3:

$$-0.5712C_2H_3O_2^- - 0.18NH_4^+ - 0.014PO_4^{-3} - 0.29H^+ + C_1H_{1.8}O_{0.38}N_{0.18}P_{0.014} + 0.31H_2O + 0.142HCO_3^- \qquad \textit{Eq. 9.1}$$

$$-0.285C_{3.33}H_{5.67}O_2^- - 0.18NH_4^+ - 0.014PO_4^{-3} - 0.196H^+ - 0.048HCO_3^- + 1C_1H_{1.8}O_{0.38}N_{0.18}P_{0.014} + 0.392H_2O \qquad \textit{Eq. 9.2}$$

$$-0.190C_6H_{11}O_6^- - 0.18NH_4^+ - 0.014PO_4^{-3} + 0.09H^+ + 1C_1H_{1.8}O_{0.38}N_{0.18}P_{0.014} + 0.391H_2O + 0.142HCO_3^- \qquad \textit{Eq. 9.3}$$

The previous equations are specifically reported for a $Y_{X/S}$ equal to 1 $mgCOD_x/mgCOD_s$; in case of a lower yield, a portion of substrate would end as CO_2/HCO_3^-, whereas the inorganic carbon could be used as external carbon source when yield increases above one [81].

Aerobic respiration pathway

The chemotrophic metabolism of PNSB bacteria under oxygenic condition has recently been object of debate and discussion. As stated in the previous sections, oxygen tolerance and consumption can very between species and conditions (Page 11). However, the vast majority of experiments in mixed culture stated that in micro-aerobic condition PNSB would activate an oxygenic respiration pathway and compete in a certain way with standard chemoheterotrophic bacteria (X_{HET}).

In this study, it was considered that a biomass to substrate yield could vary between to 0.20-0.50 $mgCOD_x/mgCOD_s$. Thus, the stochiometric reactions for the three substrate (S_{AC}, S_{VFA}, S_S) can be written as in the equations below (Eq. 10.1-3) in which the yield is set equal to 0.20 $mgCOD_x/mgCOD_s$.

$$2.856C_2H_3O_2^- + 0.18NH_4^+ - 0.014PO_4^{-3} - 4.57O_2 + C_1H_{1.8}O_{0.38}N_{0.18}P_{0.014} + 0.392H_2O + 4.712HCO_3^- + 1.995H^+ \quad \textit{Eq. 10.1}$$

$$-1.432C_{3.33}H_{5.67}O_2^- + 0.18NH_4^+ - 0.014PO_4^{-3} - 4.57O_2 + 2.098H^+ + 3.754HCO_3^- + 1C_1H_{1.8}O_{0.38}N_{0.18}P_{0.014} + 0.392H_2O \quad \textit{Eq. 10.2}$$

$$-0.952C_6H_{11}O_6^- + 0.18NH_4^+ - 0.014PO_4^{-3} - 4.57O_2 + 3.9H^+ + 1C_1H_{1.8}O_{0.38}N_{0.18}P_{0.014} + 0.392H_2O + 4.65HCO_3^- \quad \textit{Eq. 10.3}$$

Anaerobic respiration and dark fermentative pathway

In the literature, the anaerobic respiration and the dark fermentative pathway of PNSB has been minorly investigated [82,83]. Puyol et al.(2017) combined together these two metabolisms and in this report it was used the same structure. It was assumed that PNSB were able to ferment only complex substrate (S_S) involving acetate and H_2 as end products and they were able to convert S_{VFA} volatile fatty acids anoxically with different electron donors as NO_3^-, Fe^{2+} and As^{3+} [82,83]. It have to be mentioned that usually these metabolisms are characterised by a very slow growth rate compared to the phototrophic and chemotrophic metabolism and rarely it was observed any type of growth. For instance, in Puyol et al. (2017) model, this specific growth rate lower than the decay rate[17]. In conclusion, PNSB anoxic and anaerobic metabolism is represented according to the following equations (Eq. 11) calculated with a yield of 0.1 $mgCOD_x/mgCOD_S$ and without the electron acceptors.

$$-5.713C_2H_3O_2^- + 0.18NH_4^+ - 0.014PO_4^{-3} - 20.176H_2O + C_1H_{1.8}O_{0.38}N_{0.18}P_{0.014} + 10.426HCO_3^- + 45.985H^+ \quad \textit{Eq. 11.1}$$

$$-2.863C_{3.33}H_{5.67}O_2^- + 0.18NH_4^+ - 0.014PO_4^{-3} - 20.2H_2O + 8.534HCO_3^- + 1C_1H_{1.8}O_{0.38}N_{0.18}P_{0.014} + 46.85H^+ \quad \textit{Eq. 11.2}$$

$$-1.904C_6H_{11}O_6^- + 0.18NH_4^+ - 0.014PO_4^{-3} - 20.16H_2O + 1C_1H_{1.8}O_{0.38}N_{0.18}P_{0.014} + +10.42HCO_3^- + 49.764H^+ \quad \textit{Eq. 11.3}$$

Hydrogen production or photo fermentative metabolism

In most recent year, the scientific community especially researched in what is called photo-fermentative metabolism to enhance the hydrogen production[16]. During photoheterophic growth, thanks to the nitrogenase enzyme ATP molecules are used for the production of ammonia and nitrogen[84]. However, it is known that this enzyme is extremely sensitive to oxygen and requires strictly anaerobic conditions, thus these reactions should not happen in the raceway reactor. Additionally, PNSB can also use substrate, producing hydrogen and carbon dioxide according to the equation (Eq. 12) identified by Koku et al. (2002)[85]. These reactions were observed to happen under excess of of light and substrate and with specific organic compounds as malate. Besides it was still observed that in presence of oxygen they are strongly limited. In conclusion, photo-fermentative metabolism was not included in the model, but it might be easily implemented with the equation (Eq. 12)

$$-C_xH_yO_z - (2x-z)H_2O + (y/2+2x-2)H_2 + xCO_2 \qquad \textit{Eq. 12}$$

3.3.3.2 The metabolism of respiring chemoheterotrophic bacteria - X_{HET}

Under semi-aerobic conditions, a multitude of oxygenic and anoxic heterotrophic bacteria will grow in a raceway reactor. Oxygen, nitrate and sulphate would be the most likely electron acceptors in the catabolism. Because of the low oxygen transfer rate, the low ORP of the system, and of a previous anaerobic digestor, reasonably nitrate level can be ignored. Nitrate is rarely present in raw wastewater, and it is generally formed after a first aerobic system. Nonetheless, nitrate can be found in some industrial and agricultural wastewater such as livestock and poultry farming[58]. On the contrary, sulphate is a largely present component in blackwater which can sustain to sulphate reducing biological activity. In this research, this aspect was not taken into consideration even though PNSB are even hindered by sulphide which is generated by sulphate reducing bacteria[86]. In this model, ASMs models and BioWin software were studied and the general stoichiometry (anabolism and catabolism) was incorporated in the model[70]. The anabolic and catabolic reactions were calculated adjusting the mass and the charge balance. According to the standard value of the ASM models, $Y_{X/S}$ can vary between 0.3-0.7 $mgCOD_x/mgCOD_s$; however, under low oxygen concentration (below 0.5 mgO_2/L) it reaches its minimal values.

$$-1.313C_2H_3O_2^- - 0.2NH_4^+ - 0.014PO_4^{-3} - 1.575O_2 + 0.472H^+ + 1.641HCO_3 + 1C_1H_{1.8}O_{0.5}N_{0.2}P_{0.014} + 0.42H_2O \qquad \textit{Eq. 13.1}$$

$$-0.658C_{3.33}H_{5.67}O_2^- - 0.2NH_4^+ - 0.014PO_4^{-3} - 1.575O_2 + 0.563H^+ + 1.202HCO_3 + 1C_1H_{1.8}O_{0.5}N_{0.2}P_{0.014} + 0.42H_2O \qquad \textit{Eq. 13.2}$$

$$-0.438C_6H_{11}O_6^- - 0.2NH_4^+ - 0.014PO_4^{-3} - 1.575O_2 + 1.348H^+ + 1.639HCO_3^- + 1C_1H_{1.8}O_{0.5}N_{0.2}P_{0.014} + 0.42H_2O \quad \textit{Eq. 13.3}$$

The final metabolism for respiring bacteria is expressed for the three substrate (S_{AC}, S_{VFA}, S_S) in the equation below that were calculated with a yield equal to 0.4 $mgCOD_x/mgCOD_s$. (Eq. 13.1.1-3). To consider the anoxic and anaerobic metabolism, the same equations were considered, changing the yield between 0.2-0.3 $mgCOD_x/mgCOD_s$. It is important to recall that the electrons acceptor was not considered in this case.

3.3.3.3 Fermenting chemoheterotrophic bacteria - X_{FR}

As already mentioned, the influent would be characterised by a certain presence of fermenting bacteria. Consequently, despite the lower standard SRT of the raceway reactor, fermenting bacteria might still have a relevant impact on the biological conversions. For instance, it is reasonable to think that they would mainly characterize the biological activity during the dark phase. In this research the catabolic reactions were assumed to produce H_2 (electron acceptor) as reported in the following equations for S_S and S_{VFA} (Eq. 14.1-2). These catabolic reactions were taken from the anaerobic digestion models, ADM1 and ADM2[68].

$$-C_6H_{12}O_6 - 4H_2O + 2C_2H_3O_2^- + 2HCO_3^- + 4H_2 + 4H^+ \quad \textit{Eq. 14.1}$$

$$-C_{3.33}H_{5.67}O_2^- - 3.1H_2O + 1.2C_2H_3O_2^- + 0.9HCO_3^- + 1.1H^+ + 3.1H_2 \quad \textit{Eq. 14.2}$$

Fermenters are mostly characterized by a low yield (0.05 – 0.20 $mgCOD_x/mgCOD_s$) due to the little free energy available from their catabolism. In the following equations, the overall metabolism for fermenting bacteria metabolism is calculated with a yield equal to 0.1 $mgCOD_x/mgCOD_s$.

$$2.63C_{3.33}H_{5.67}O_2^- - 0.2NH_4^+ - 0.014PO_4^{-3} - 6.90H_2O + 2.65H^+ + 2.02HCO_3 + 1C_1H_{1.8}O_{0.5}N_{0.2}P_{0.014} + 7.34H_2 \quad \textit{Eq. 15.1}$$

$$-1.750C_6H_{12}O_6 - 0.2NH_4^+ - 0.014PO_4^{-3} - 5.86H_2O + 6.51H^+ + 3.20HCO_3^- + 1C_1H_{1.8}O_{0.5}N_{0.2}P_{0.014} + 3.14C_2H_3O_2^- + 3.14H_2 \quad \textit{Eq. 15.2}$$

3.3.3.4 Hydrolysis and Decay

Hydrolysis is a chemical and biological processes in which complex undissolved organic substrates is transformed into soluble and partly degradable substrates. Depending on the chemical composition of the organic particulate, the soluble substrates (S_s) can vary its chemical composition. In general, proteins and carbohydrates mainly decompose to sugars and amino acids, while lipids degrade to fatty acids and alcohols[87]. Moreover, the environmental conditions (e.g. aerobic/anoxic/anaerobic)

determine the outcomes of the soluble substrates. In this model, the process of hydrolysis is modelled according to Puyol et al. (2017)[17].

As well the decay process is an important aspect to consider in the biological activity. It can be simulated in different ways, but, in standard ASM models with Monod growth, it is simulated as a deactivation of biomass (μ-k_{dec}). In this model, the decay rate was assumed equal and constant for all the group of bacteria (X_{PB}, X_{HET}, X_{FR}). During this process, nitrogen and phosphorus are released based on the biomass composition, while carbon is released into organic particulate (X_S).

In conclusion, the decay and hydrolysis coefficient were taken equal to 0.09 d^{-1} and 0.071 d^{-1} and followed a first order kinetic[17]. It should be noted that these factors are particularly situation specific, but these values are comparable with the kinetics under anaerobic conditions, around 0.1 d^{-1} [68].

3.3.4 Kinetic and growth model

In the literature, a multitude of mathematical models have been developed for purple non-sulphur bacteria[16]. A first and simplified method to study bacterial growth is Monod equation, which has the main advantage to be easily incorporated or combined with the ASMs and ADM models.

One of the most peculiar aspects of purple non-sulphur bacteria is their multi-versatile metabolism. Thus, one of the main critical aspects to model is the regulation of their metabolic pathway. When mixotrophic bacteria are modelled, one shared common rule is to avoid summing all different growth rates and define a certain function which is able to consider a preferred metabolic pathway [88]. Similarly, this concept can be also applied when multiples substrates are simulated[89]. From these studies, it emerged that the maximum overall growth of a biological group ($\mu_{mixed,max}$) is limited asymptotically (e.g. $\mu_{max,1}$ or $\mu_{max,2}$).

$$\mu_{mixed} \neq \sum \mu_j \qquad \text{but } \mu_{mixed,max} = \textit{either } \mu_{max,1} \text{ or } \mu_{max,2}$$

One possibility to tackle this problem is the application of the cybernetic model. The cybernetic model is an internal regulatory behaviour of microorganism to optimize their growth under a multiple substrates or mixotrophic conditions[69]. For instance, it was used to simulate the oxygenic and anoxygenic fermentation processes in which yeast can degrade different substrates with different electron acceptors or the autotrophic and heterotrophic growth of *Spirulina sp.*[89]. The picture below reports the experimental results of these studies.

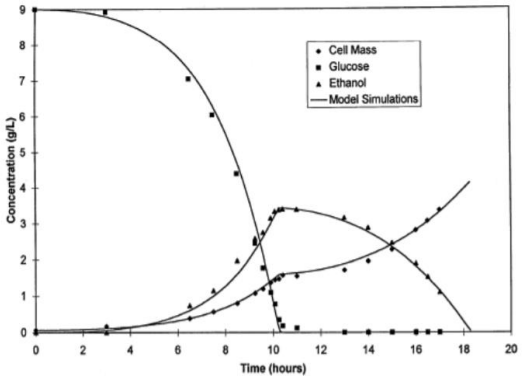

Figure 12 Simulations of the cybernetic model and experimental data for Saccharomyces cerevisiae in the study from Kompala et Dhinakar (2011)[89])

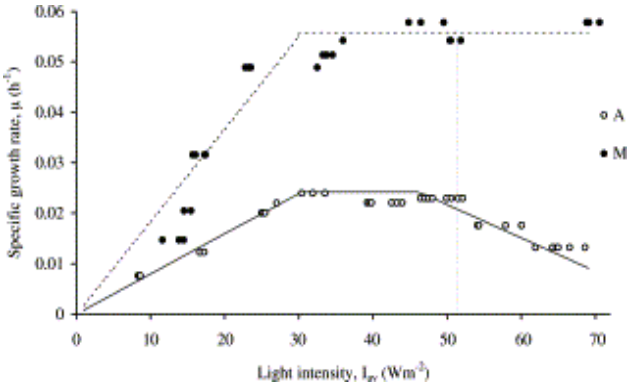

Figure 13 Influence of average light intensity on specific growth rate for Spirulina sp. with autotrophic metabolism (--) and mixotrophic metabolism (- -) in the paper of Chojnacka et al. (2004)[88]

Briefly, the Monod growth rate equation is modified from the original formula with a parameter E_R which refers to the relative amount of the key enzyme (Eq. 16):

$$\mu_j = \frac{\mu_{max,i} \times E_R \times S_S}{K_S + S_S} \qquad \textit{Eq. 16}$$

This last parameter can be written as $E_R = e/e_{max}$ in which e is the intracellular key enzyme content and the maximum level of intracellular enzyme (e_{max}) can be calculated as:

$$e_{max} = \frac{\alpha}{\mu_{max,i} + \beta} \qquad \textit{Eq. 17}$$

in which α and β are enzyme synthesis and degradation rate constants.

The key enzyme regulating the growth of PNSB was not found in the literature. However, experimental data can already give an indication of the preferential substrate for specific metabolic pathway[21,55]. For this reason E_R was substituted with a arbitrarily factor to regulate the preference for certain substrate ($f(S_i)$), specific for each parametrisation (Appendix C). Therefore the growth rate in the model is expressed as :

$$\mu_j = \frac{\mu_{max,i} \times f(S_s) \times S_S}{K_S + S_S} \qquad \textit{Eq. 18}$$

The inclusion of a regulatory function to simulate the switch between different metabolic pathways is achieved with the addition of the cybernetic variables μ_i and v_i determined as

$$\mu_i = \frac{\mu_i}{\sum_j u_j} \; and \; v_i = \frac{\mu_i}{max_j u_j} \qquad \textit{Eq. 19}$$

Together with $f(S_i)$, these variables become important parameters to determine the growth rate of a specific biological group.

In conclusion, when operating with multiple substrates and metabolic pathways the mass balance for a chemostat reactor according to Kompala et Dhinakar (2011)[89] becomes:

$$\frac{dX_i}{dt} = (\sum_i \mu_i v_i - D)X_i \qquad \textit{Eq. 20}$$

3.3.4.1 Growth inhibitory factor

The Monod growth model is not only regulated by substrate availability but as well from other compounds essential for the biological growth as nutrients and oxygen. In this model, apart from nutrients and oxygen, light was also included. In standard ASM models, growth inhibition factor (I_i) are typically expressed as a fraction $I_i/(K_{S,i} + I_i)$ where the I_i is the limiting compounds variable and $K_{S,i}$ is the relative half velocity constant. In this study, based on the specific metabolic pathway a maximum of three limiting parameters were considered. Due to the low K_S values for nutrients (0.2 mgN/L and 0.08 mgP/L) limitation of nutrients availability was not considered[17]. Temperature (Arrhenius equation) and pH were not taken into account as these variables were assumed fixed, despite the fact that they could be important (e.g. pH in fermentation)[68]. Then, mainly oxygen and light availability, together with substrate, were chosen. From the literature review emerged that anoxygenic photosynthesis is inactivated with increasing level of oxygen concentration[38,90]. As well, this was chosen for the anoxic and fermenting pathway to select the preference of the aerobic pathway. Table 2 summaries the main growth inhibitory factor used in the model. It is important to mention that the relative half velocity constant might change for the specific metabolic pathway and the biological group.

Table 2 Major growth inhibitory factor for the four metabolic pathway: substrate, light, and oxygen.

Metabolic pathway	Substrate	Light	Oxygen
Phototrophic pathway	$\frac{S_i}{K_{S,i} + S_i}$	$\frac{I_{IE}}{K_{S,IE} + I_{IE}}$	$\frac{K_{S,O2}}{K_{S,O2} + S_{O2}}$
Aerobic pathway	$\frac{S_i}{K_{S,i} + S_i}$	[-]	$\frac{S_{O2}}{K_{S,O2} + S_{O2}}$
Anaerobic pathway	$\frac{S_i}{K_{S,i} + S_i}$	[-]	$\frac{K_{S,O2}}{K_{S,O2} + S_{O2}}$

Fermenting pathway	$\frac{S_i}{K_{S,i} + S_i}$	[-]

3.4 Model layout and the tuning process with experimental data

The general model structure can be summarized in four categories (physical processes, stoichiometry, kinetic and reactor geometry) which schematically classify the four processes explained in detail in the previous paragraphs (paragraphs 3.3.1-3.3.44). A simplified schematization of the model layout is shown in Figure 14**Fout! Verwijzingsbron niet gevonden.**. These equations are characterized by constant input parameters that have to be adjusted in order to proper simulate the reactor performance of a raceway reactor.

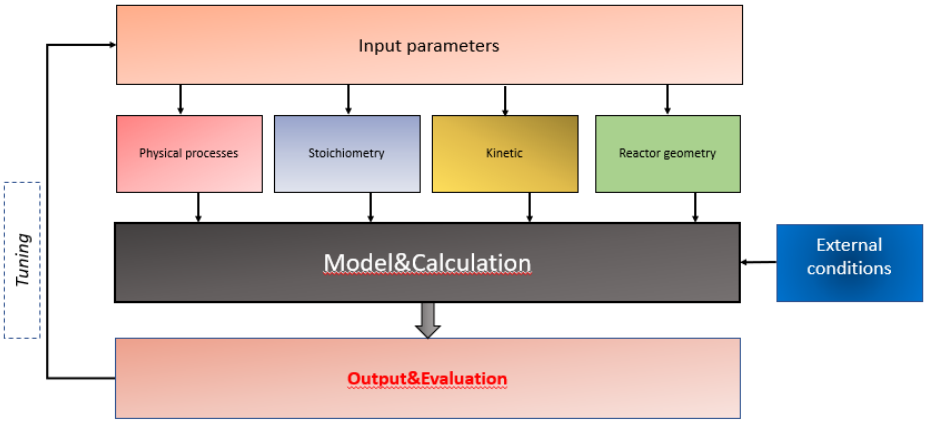

Figure 14 General model configuration for the tuning process. Input parameters are divided into four categories (Physical processes, stoichiometry, kinetic and reactor geometry). The external conditions were fixed and the model was run. The output are evaluated with experimental results. Then, changing the input in the specific boundaries the model is tuned more accurately to the experimental data in order to reduce the errors of the simulations.

In this project the model has been tuned with seven laboratory experiments performed by Alloul et al. (2020)[18]: firstly, it was compared with four batch experiments, then with three steady-state sequencing batch reactors (SBR). The specific aspects of these experiments are faced in the coming sections (paragraph 3.5). However it is important to distinguish beforehand which input parameters were considered already fixed and those that had to be tuned. An extensive list of the most important input parameters is reported at Table 3. Some of these parameters, as the reaeration coefficient or the reactor geometry, were not changeable as they were specific of the experiments. In other cases, as for the decay and hydrolysis rate, these factors were fixed to simplify the parametrisation procedure. For the remaining components, a range of acceptable values was determined from the scientific literature. However, the available experimental data were not sufficiently consistent to achieve a mathematical calibration of these parameters. Then trial and error was used to tune the model to the experimental results. The attention was primarily given to the parameters determining

the growth of PNSB bacteria, while for the other two biological groups, BioWin manual was used as main reference[74].

Table 3 Most relevant input parameters used in the proposed model

Input Parameters

Physical processes		**Model tuning**	**Value**	**Reference**
kl_a	Reaeration coefficient [h^{-1}]	fixed	1	Alloul et al. (2020)[18]
C_s	Gas saturation concertation (mg/L)	fixed	8.3	Henry Constant
I_0	Radiation intensity on the surface [W/m^2]	fixed	54	Alloul et al. (2020)[18]
ε	Attenuation constant [m^2/g]	fixed	0.07	Solimeno et al. 2017
T	Temperature [K]	fixed	301	Alloul et al. (2020)[18]
pH	pH []	fixed	7.0-7.5	Alloul et al. (2020)[18]
L	Water depth [m]	fixed	0.1-0.2	Alloul et al. (2020)[18]
Stoichiometry		**Model tuning**	**Values**	**Reference**
$Y_{XPB,PH}$	Biomass yield phototrophic growth (X_{PB}) [$mgCOD_x/mgCOD_s$]	tuned	0.8-1.2	Nakajima et al. (1997)[37]
$Y_{XPB,CH}$	Biomass yield chemotrophic growth (X_{PB}) [$mgCOD_x/mgCOD_s$]	tuned	0.2-0.5	Capson-Tojo et al. (2021)[21]
$Y_{XHET,AN}$	Biomass yield Anaerobic growth (X_{PB}) [$mgCOD_x/mgCOD_s$]	tuned	0.05-0.2	BioWin[74]
$Y_{XHET,CH}$	Biomass yield Chemotrophic growth (X_{HET}) [$mgCOD_x/mgCOD_s$]	tuned	0.3-0.7	BioWin[74]
$Y_{XHET,AN}$	Biomass yield Anaerobic growth (X_{HET}) [$mgCOD_x/mgCOD_s$]	tuned	0.1-0.3	BioWin[74]
Y_{XFR}	Biomass yield Fermenting growth (X_{FR}) [$mgCOD_x/mgCOD_s$]	tuned	0.05-0.2	BioWin[74]
Kinetic		**Model tuning**	**Values**	**Reference**
$f(S_i)$	Subtrate preference factor	tuned	0-1	Arbitrarly
$\mu_{max,ph,XPB}$	Maximum growth rate phototrophic growth (X_{PB}) [h^{-1}]	tuned	0.04-0.18	Nakajima et al. (1997)[37]
$\mu_{max,ch,XPB}$	Maximum growth rate chemotrophic growth (X_{PB})	tuned	0.05-0.15	Alloul et al. (2020)[18]
$\mu_{max,an,XPB}$	Maximum growth rate Anaerobic growth (X_{PB}) [h^{-1}]	tuned	~0	Mohsin et al. (2017)[82]
$\mu_{max,ch,XHET}$	Maximum growth rate for chemotrophic growth (X_{HET}) [h^{-1}]	tuned	0.125 – 0.25	BioWin[74]
$\mu_{max,ch,XAN}$	Maximum growth rate for Anaerobic growth (X_{HET}) [h^{-1}]	tuned	0.003-0.01	BioWin[74]
$\mu_{max,ch,XFR}$	Maximum growth rate Fermenting growth (X_{FR}) [h^{-1}]	tuned	0.003-0.017	BioWin[74]
$K_{S,IE}$	Half velocity constant for Light inhibition W/m^2	tuned	10-20	Katsuda et al. (2002) [65] Cerruti et al. (2020)[91]
$K_{S,O2,PH}$	Half velocity constant for O_2 inhibition phototrophic [mgO_2/L]	tuned	0.5-2	Arbitrarly
$K_{S,O2,CH,PB}$	Half velocity constant O_2 inhibition chemotrophic (X_{PB}) [mgO_2/L]	tuned	0.4-1.0	Capson-Tojo et al. (2021)[21]
$K_{S,O2,CH,HET}$	Half velocity constant O_2 inhibition chemotrophic (X_{HET}) [mgO_2/L]	tuned	0.05-0.5	BioWin[74]
k_{dec}	Decay constant rate [h^{-1}]	fixed	0.0029	Puyol et al.(2017)[17]
k_{hyd}	Hydrolis constant rate [h^{-1}]	fixed	0.00375	Puyol et al.(2017)[17]
Reactor Geometry		**Model tuning**	**Values**	**Reference**
V	Volume [m^3]	fixed	0.1	Alloul et al. (2020)[18]
A	Area [m^2]	fixed	0.5	Alloul et al. (2020)[18]
HRT	Hydraulic retention time [d]	fixed	2	Alloul et al. (2020)[18]
SRT	Sludge retention time [d]	fixed	2	Alloul et al. (2020)[18]
dV/dt	SBR cycle	fixed	1/1/22h	Alloul et al. (2020)[18]

3.5 Experimental data for the parametrization of the model

3.5.1 Four batch experiments

Four batch experiments were performed by Alloul et al. (2020)[18] to better understand the growth of PNSB in raceway reactor and the impact of three main operational control tools as paddlewheel rotation, light cycle and surface area. A VFAs solution was used as substrate composed by acetate, propionate and butyrate in a ratio of 1/1/1 gCOD/L. All experiments started with a VSS concentration of 0.02 gVSS/L and optical density at 660 nm (OD_{660}) was measured to extrapolate exponential growth. A halogen lamp was used as light source and its intensity was measured equal to 54 W/m^2 at the water surface. The initial and final TCOD and SCOD were measured in order to analyse the COD removal, final biomass and yield of the reactions. The table below summarizes the theoretical conditions of the four experiments.

Table 4 Summary of the operational condition for the batch experiments (Alloul et al.2020). Optical densitity (OD_{660}), initial substrate concentration (COD_{in}), oxygen transfer rate (OTR); volume (V)

Scenario	*Inoculum [gVSS/L]*	*OD_{660} [Abs]*	*CODin [mgCOD/L]*	*OTR [mgO_2 /L/h]*	*Paddlewheel [on/off]*	*Light [on/off]*	*V [L]*
BATCH 1	0.02	0.073	3000	8.5	24h / 0h	12h / 12h	100
BATCH 2					24h / 0h	24h / 0h	100
BATCH 3					12h / 12h	12h / 12h	100
BATCH 4					24h / 0h	12h / 12h	50

In the experiments, the optical density variation was used to estimate the growth rate (μ [h^{-1}]) according to the formula:

$$\mu = \frac{LN(OD_{660,t+1}) - LN(OD_{660,t})}{\Delta t} \qquad \textit{Eq. 21}$$

The biomass concentration (mgCOD/L) can be extrapolated according to the formula below (Eq. 22). The ratio 1.15 gCOD/gTSS was measured from the experimental results which differs from standard 1.42 gCOD/VSS ratio. The ratio between absorbance (A_{660}) and TSS was found in the paper of Alloul et al. (2020) and Cerruti et al. 2020 [18,63].

$$X_b = \frac{OD_{660} \times 1.15 \frac{gCOD}{gTSS}}{2.50 \frac{A_{660}}{gTSS/L}} \times 1000 \qquad \textit{Eq. 22}$$

To estimate the quality of the simulation, four fixed parameters and four dynamic variables were taken into consideration. More precisely, the average growth rate (μ_{mean}), the final biomass ($X_{b,end}$), the biomass to substrate yield ($Y_{x/s}$) and the relative abundance of PNSB (%PNSB) were calculated. In this case, the relative error (e_{rel}) was calculated as the absolute difference between the model and the simulations divided by the experimental value.

Correspondingly, the four dynamic variables are the biomass concentration (X_b), the oxygen concentration (O_2), the substrate concentration (SCOD) and the growth rate (μ). In this case, relative standard error (RSE) and the root-mean-squared-error(RMSE) were calculated to compare the experimental results with the simulations. The three formulas for the error comparison are reported here below :

$$e_{rel} = \frac{|y_i - Y_i|}{Y_{i,avg}} \qquad \textit{Eq. 23.1}$$

$$RSE = \sqrt{\frac{\sum(y_i - Y_i)^2}{\sum(y_i - Y_{i,avg})^2}} \qquad \textit{Eq. 23.2}$$

$$RMSE = \sqrt{\frac{\sum(y_i - Y_i)^2}{n}} \qquad \textit{Eq. 23.3}$$

Eq. 23 Error estimation for model and experimental comparison. Relative error (e_{rel}), relative standard error (RSE) and root-mean-squared-error (RMSE). The model results are expressed as y_i, experimental results as Y_i, the average of the experimental results ($Y_{i,avg}$).

In the model the extrapolation of these parameters was assessed through these calculations, reported here below.

$$X_{BIO} = X_{PB} + X_{HET} + X_S + X_I \qquad \textit{Eq. 24.1}$$

$$\mu_t = \frac{LN(X_{BIO}(t)) - LN(X_{BIO}(t + \Delta t))}{\Delta t} \qquad \textit{Eq. 24.2}$$

$$COD_{rem,t} = TCOD_{in} - S_{AC,t} - S_{VFA,t} - S_{I,t} \qquad \textit{Eq. 24.3}$$

$$Y_{\frac{x}{s}} = \frac{X_{BIO,end} - X_{BIO,in}}{TCOD_{in} - SCOD_{end}} \qquad \textit{Eq. 24.4}$$

$$\%PNSB = \frac{X_{PB}}{X_{HET} + X_{PB}} \qquad \text{Eq. 24.5}$$

Eq. 24 Parameter estimation for batch experiment from the model simulations

3.5.2 Three sequencing batch reactor experiments

Under similar conditions, three steady state sequencing batch reactor (SBR) experiments were performed by Alloul et. al (2020)[18]. The substrate concentrations and compositions remained equal to the batch experiments (3 $gCOD_{in}$ /L 1/1/1 acetate/propionate/butyrate). In this case, the reactor operated with a hydraulic and sludge retention time (HRT and SRT) of 2 days. A summary of the operational conditions is reported at Table 5.

Table 5 Summary of operational conditions for the SBRs experiments (Alloul et al. 2020). Hydraulic retention time (HRT); sludge retention time (SRT); influent substrate concentration (COD_{inf}); oxygen transfer rate (OTR); volume (V)

Scenario	HRT [d]	SRT [d]	CODinf [mgCOD/L]	O_2 [mg O_2 /L/h]	Paddlewheel [on/off]	Light [on/off]	V [L]
SBR 1	2	2	3000	8.5	24h / 0h	12h / 12h	100
SBR 2					12h / 0h	12h / 12h	100
SBR 3					24h / 0h	12h / 12h	50

The reactor run for several weeks; after five sludge retention time it was considered under stable conditions and samples after the light and dark phase were extracted. Standard chemical analysis were performed to assess the reactor performance as biomass concentration (mgCOD/L), TSS productivity (gTSS/d) and relative PNSB abundancy[18]. Dynamic variables were not measured, so it was possible to calibrate the model only with steady-state results.

The simulations were started with similar initial conditions to the final conditions of the batch experimental results and they were run for 45 days. It was observed that, after 10-15 days the beginning of the simulation, the reactor reached a biological stability. In order to compare experimental and simulated values four parameters were chosen: the removed COD (COD_{rem}), the effluent biomass (X_{BIO}), the measured yield ($Y_{x/s}$) and the PNSB abundance (%PNSB). These parameters were calculated from the simulation as in Eq. 24. As for batch experiments, to assess the quality of the calibration the relative error (e_{rel}) was calculated for the fixed parameters, as in Eq. 23.

3.6 Structure of the sensitivity analysis

The third research question aimed to evaluate the effects of the most impacting variables on the production and abundance of PNSB in the raceway reactors. To answer this question a one-at-a-time (OAT) sensitivity analysis was defined, assessing the impact of instantaneous and long term perturbations. Moreover, with these simulations, it was possible to study more representative scenarios than laboratory experiments, for instance approaching some aspects relatively to the Saraswati project conditions.

In general, the operational conditions of the second SBR simulation (SBR2 - Table 5) were taken as reference study, since they are the most likely for practical applications. Therefore, the input parameters that were determined after the tuning with the SBR simulations were considered (Table 12) and occasionally changed. Two approaches were undertaken: the first assessed the impact of instantaneous turbulences, the latter studied the steady state of different operational conditions.

The study of instantaneous turbulences helps to understand the response of the system at perturbations. Three variables were studied simulating three diverse type-events: a peak of suspended solids in the influent, a drop of the available substrate and the impact on the light intensity variations. In these scenarios, the model was run for 45 days and once it had reached a steady state conditions (10-15 days), the system was disturbed for ten straight days. By doing so, it was possible to study the effects and the recovery of the system.

On the other hand, long term turbulences conditions would help to individuate new steady-state conditions to optimize the reactor performance like the TSS productivity, the COD removal or the PNSB abundance. For these long-term simulations, it was proposed to analyse the impact of the influent particulate, of longer sludge retention time, including new biological groups as fermenting bacteria (X_{FR}) and microalgae (X_{MA}). As the model was changed new variables had to be included, so the model needed to be adjusted accordingly.

A summary of the sensitivity analysis is reported in Table 6 which classifies the events as long or short terms and it shows the effects of equations implemented in the model.

Table 6 Summary of the sensitivity analysis scenarios. The

Short-term perturbations			
Name	*Range*	*Effect*	*Notes*
Peak of TSS (X_S)	X_S = 0-1000 mgCOD/L	Absorbance & scattering of light	1.15 mgCOD/mgTSS
Natural light	I_0 = 0-300 Wm^{-2}	Light variability an cycle	$K_{S,IE}$ = 25 W/m^2
Drop of COD_{in}	COD_{in} = 500-3000 mgCOD/L	Higher oxygen availability	[-]
Long-term perturbations			
Name	*Range*	*Effect*	*Note*
TSS disturbance (X_s)	X_S = 0-400 $mgCOD_{XS}/L$	Absorbance & scattering of light	1.15 mgCOD/mgTSS
SRT extension	SRT =2-10 [d]	TSS concentration	[-]
Fermenters impact	SRT =2-10 [d]	Biotic competition	X_{FR} ; S_s (glucose)
Microalgae impact	SRT =2-10 [d]	Higher oxygen availability	X_{MA}

Particulate compounds: total suspended solids scenario

In these simulations the original influent concentration (3 gCOD/L – 1 /1/1 acetate/ propionate/ butyrate) was altered adding a particulate fraction (mgCOD/L). In the proposed model, the particulate fraction is divided in four categories: X_{PB}, X_{HET}, X_s, X_I. With the assumption that the majority of the incoming particulate wastewater was biodegradable, only X_s was increased in a range from 0 to 1000 mgCOD/L and from 0 to 400 mgCOD/L for the short and long term sensitivity analysis respectively (Table 6). Then, the influent particulate fraction was then converted to mgTSS/L according to the same ratio found in the experimental values (1.15 mgCOD/mgTSS) [18]. Giving the Lambert-Beer equation utilized in the model, an increase of particulate concertation, would impact the average light intensity of the model and then the phototrophic growth. Figure 15 shows an explicative example of the negative repercussion of TSS concentration on the average light intensity (I_{av}) and the Monod inhibitory factor of light (I_{IR}).

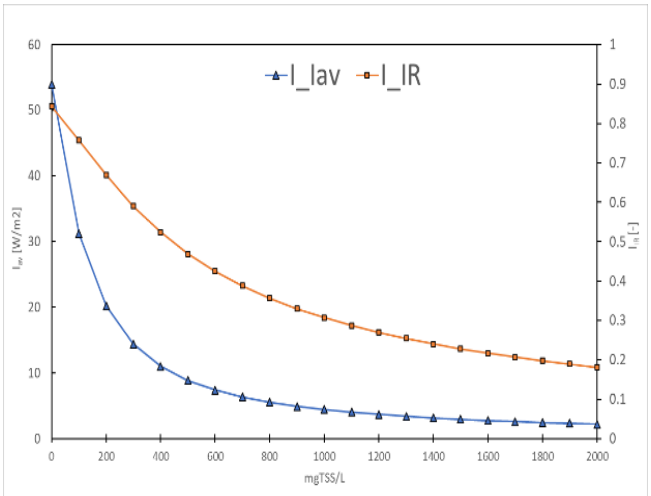

Figure 15 On the left, the Impact of total suspended solids (mgTSS/L) on the average light intensity I_{AV} [W/m2]. On the right, the direct correlated light inhibited constant I_{IR} used in the Monod growth with a half velocity constant of 10 W/m2 (Table 3)

3.6.1 Light intensity and cycle perturbations: natural light scenario

These scenarios aim to assess the impacts of the light intensity variations on the performance and the PNSB abundance of the raceway reactor. In these simulations artificial light was replaced by natural light. At this regard, it has to be mentioned that the sun's irradiation profile is markedly different from the one of the halogen lamp used in Alloul et al. (2020)[18,49]. In fact, only a small portion of the sunlight spectrum enter in the optimal range for the growth of PNSB bacteria (750-1000 nm). Thus, the Monod terms of phototrophic growth ($K_{S,IE}$) should be adjusted accordingly to these conditions. In the literature, most of outdoor studies focused on tubular closed photobioreactor for the optimization of hydrogen production[92,93]. According to Carlozzi et al. (2006) when solar radiation is expressed in $MJm^{-2}d^{-1}$ the half velocity constant for irradiation ($K_{S,IE}$) is around 7 $MJm^{-2}d^{-1}$ [94]. Assuming a conversion factor of 1 W m^{-2}= 0.0864 MJ $m^{-2}d^{-1}$ K_{IR} becomes 81 W m^{-2}. Similarly, Puyol et al. (2017) used a $K_{S,IE}$ around that value (88 W m^{-2})[17]. However, in this studies scattering and absorbance of light by particulate components was not taken into account. On the other hand, Berberoglu estimated a much lower $K_{S,IE}$ (25 W m^{-2}) and included a inhibition irradiation constant ($K_{I,IE}$ = 120 W m^{-2}) to consider the excess of light[93]. More importantly, Berberoglu (2010), the water depth was divided into layers and average light intensity was estimated for each one. In a recent master thesis at TUDelft, Hoon Kim (2018) found out a similar $K_{S,IE}$ (20 W m^{-2}) applying Lambert-Beer equation [78]. Thus, for these simulations K_{IR} was increased from 10 to 25 W m^{-2} but $K_{IR,I}$ was not considered as the model does not dived the raceway reactor in layers.

To assess the effect of natural light under similar circumstances to the Saraswati project, diffuse radiation data were collected from photovoltaic Geographical Information System (PVGIS) for the Indian region. Average hourly radiation measurements for typical meteorological year (TMY) were calculated for each month. In these simulations, it was studied the reactor performance during the month of September. To understand the effects of light variation, one reference scenario was simulated with a constant average hourly light source (*scenario μ*). Instantaneous decrease of light, simulating hypothetical atmospheric perturbations, were calculated as the difference between the average hourly light source and one or two time the standard deviation measured from September data (*scenarios μ-1STD, μ-2STD*). The perturbation was started on the 10th day of the simulation and lasted for ten straight days. Finally, it was simulated the reactor performance with dynamic TMY data for the month of September (*scenario Sept.*). Figure 16 reports the hourly light intensity for the three proposed scenarios.

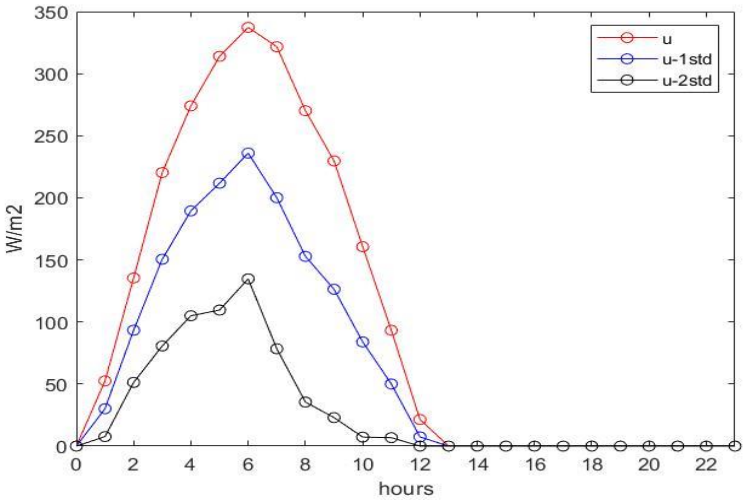

Figure 16 Daily light intensity at the water surface expressed in W/m^2 for three natural light scenarios perturbation (μ; μ-1STD; μ-2STD). Scenario μ used the average of the hourly light intensity data for the month of September. During the perturbations μ-1STD and μ-2STD the average September light intensity was reduced by 1 or 2 time the hourly standard deviation calculated during the month of September.

3.6.2 Biotic competition: fermenting bacteria and microalgae scenario

In these scenarios biotic competition was extended with two other type of biological group : fermenting bacteria (X_{FR}) and microalgae (X_{MA}). In the original model fermenting bacteria were already included (Page 31), but they were not considered in the comparison with experimental results (Page 38). The main reason to study fermenting bacteria was to approach a more realistic scenarios as wastewater has to be pre-treated by an anaerobic digestor to favour acidification of the influent.

Therefore, the influent concentration would be characterized with a certain concentration of fermenting bacteria (X_{FR}) and a not converted complex substrate (S_S).

Microalgae were not directly included in the model. However their potential impact was studied stoichiometrically on the steady state conditions. In both cases, fermenting bacteria and microalgae are characterized by a lower growth rate, thus it was decided to study the impact of longer retention time in a range between 2-10 days.

4 Results

This section gathers the results answering the second and the third research questions (page 3). In the first two subsections (4.1 - 4.2) the results of the model simulations, compared with the experimental data performed by Alloul et al. (2020)[18], are reported quantifying the quality of the model simulations. The last subsection (4.3) shows the results of the sensitivity analysis partitioning into short and long terms impacts for a total of six different scenarios as previously explained at *Table 6.*

4.1 Simulations of the batch scenarios

The interpretation of the experimental results are of primary importance in order to correctly parametrize the model. An overview of the batch experiments performed by Alloul et al. (2020)[18] is reported in Appendix F. The four model scenarios run with the same input parameters found after the tuning process (Appendix C). To start the simulations, the initial conditions were set according to the specific batch measurements.

Figure 17 (a-d) contains the results of the experiments and of the simulations for the batch scenarios from 1 to 4. The straight lines stand for the simulated values while dots, linked by dashed line, stand for the experimental results. Biomass (black line), oxygen (blue line) and soluble substrate (green line) were displayed when the experimental data were available. The best similarity to the experimental curves was observed in scenarios 2 and 3 (Figure 17 b-c). On the other hand, scenarios 1 and 4 had some important deviations: scenario 1 simulates a greater growth rate but a similar yield (Figure 17 a); vice versa for scenario 4 which shows a similar growth rate and yield, but a markedly different final biomass (Figure 17 d). For all 4 simulations, oxygen depletion is correctly simulated in the first hours but the reoxygenation, towards the end of the experiment, is generally modelled more rapidly.

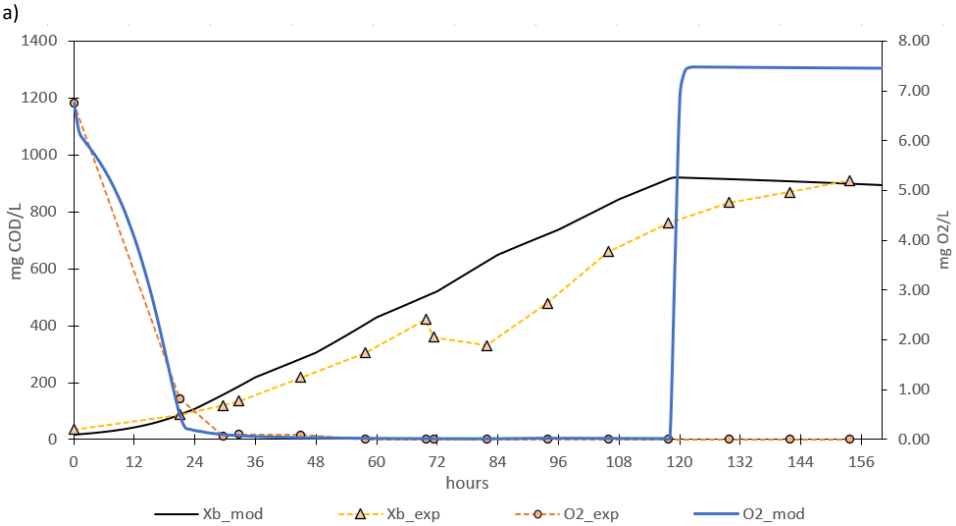

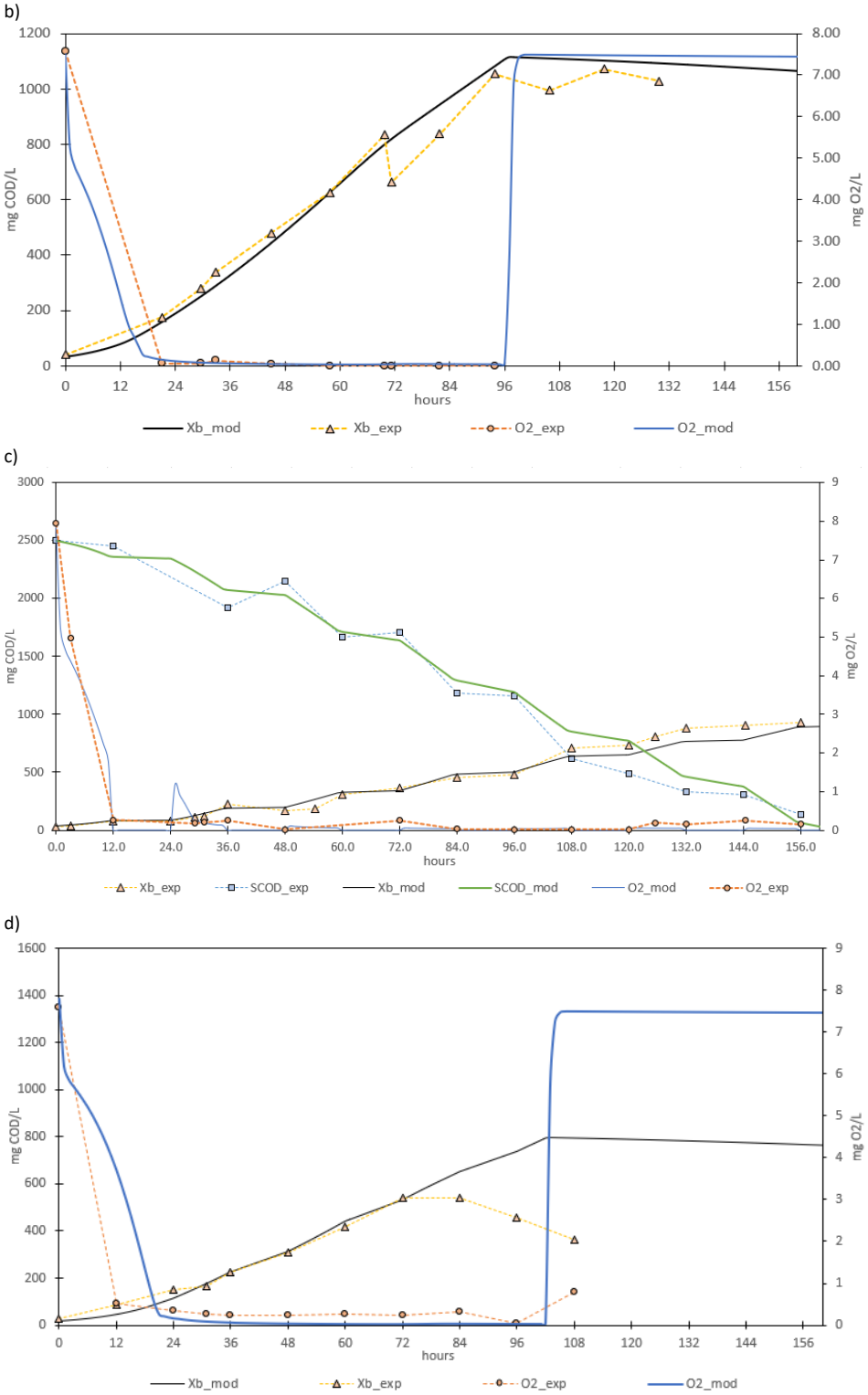

Figure 17 Comparison of the experimental results and simulations. Figures from a to d are respectively for scenarios from 1 to 4. $X_{b,mod}$: simulated biomass (mgCOD/L); $X_{b,exp}$: measured biomass (mgCOD/L); $O2_{mod}$: simulated oxygen (mgO_2/L); $O2_{,exp}$: measured oxygen (mgO_2/L /L); $SCOD_{mod}$: simulated soluble substrate (mgCOD/L); $SCOD_{,exp}$: measured soluble substrate (mgCOD/L).

Figure 18 (a-d) shows the comparison between the model simulations (bar chart) and experimental results (squared dots) and the specific relative error (diamond dots). Final biomass and average growth rate have a high similarity and errors measure mostly below 10% (Figure 18 a-b). Scenario 4 simulates the greatest error, estimating a higher biomass concentration (50% more). Figure 18 (c-d) reports the yield and the PNSB abundance. In this case, the simulations are satisfying only for the first two scenarios. It might be argued that for scenarios 3 and 4 the yield measurement were relevantly inaccurate (50% and 70%). However, this aspect was already considered as a possible outcome of the simulation as the COD measurements were not consistent (Appendix F). In fact, scenario 3 measures the highest yield of the experiments (0.7 mgCOD/mgCOD) while PNSB abundance is only 20% of the microbial community, discording with the fact that PNSB abundance should be the major and only factor increasing the yield.

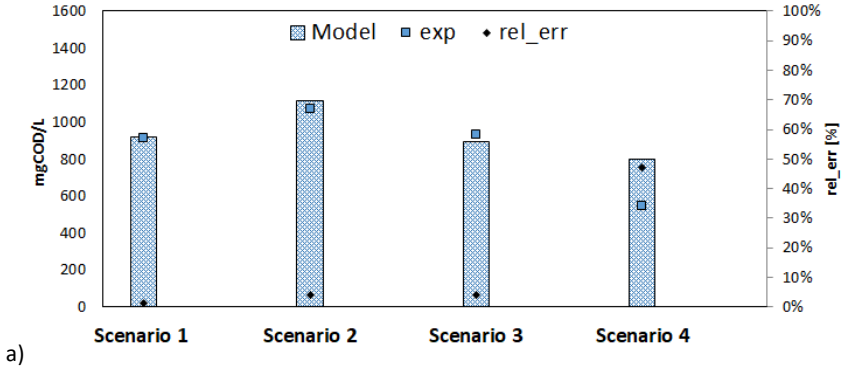

a)

b)

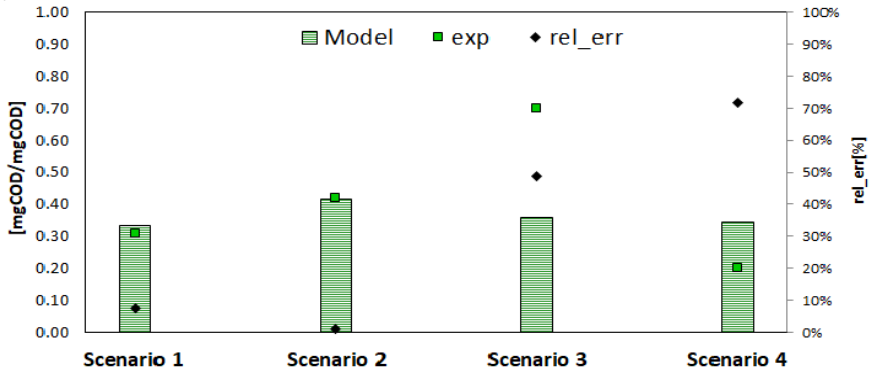

c)

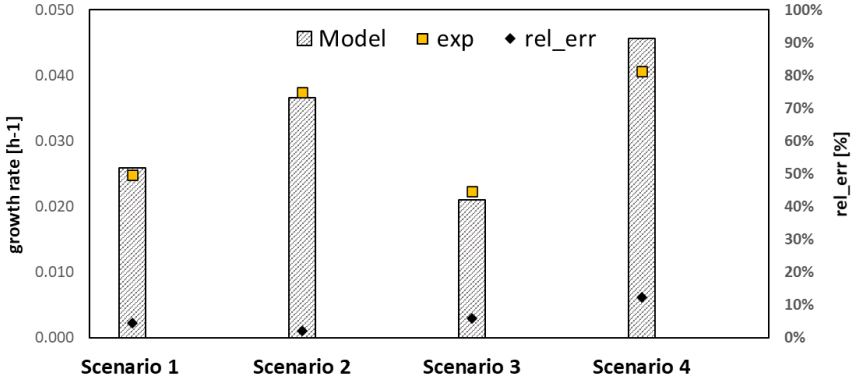

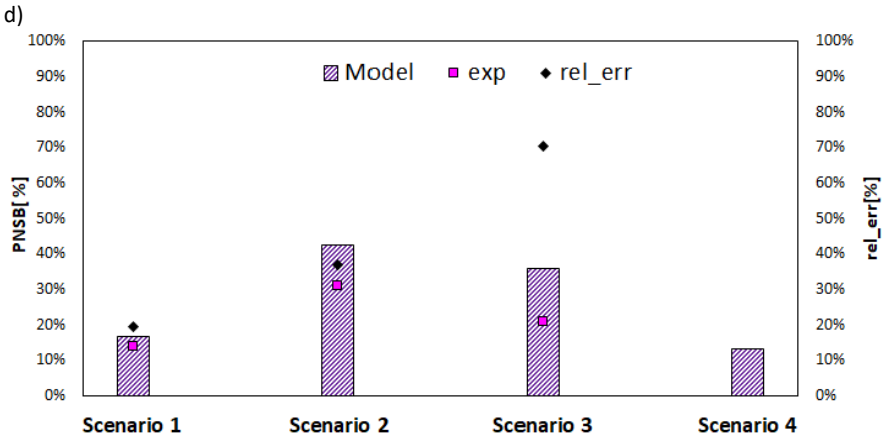

Figure 18 Comparison of experimental (squared dots) and model simulations (bar charts) results (right axis) and the specific relative error with diamond dots (left axis). Figures, from a to d, respectively show final biomass [mgCOD/L], growth rate [h^{-1}], yield [mgCOD/mgCOD] and PNSB abundance [%].

As well, dynamics variables were important to evaluate the quality of the batch simulations. Table 7 contains the relative standard error (RSE) and the root mean squared error (RMSE). From the experimental results, biomass and growth rate measurements were the most available and reliable information, whereas soluble substrate consumption was available only for scenario 3 and oxygen was measured only in the first hours of the experiments. As it appears in Figure 19, scenario 3 measures the best fitting with RSE below 0.05 for biomass (X_B), substrate (S_{COD}) and oxygen (O_2) and 0.26 for the growth rate (μ). Then, scenarios 2, 4 and, at last, 1 succeed in terms of quality as reported in Table 7 and in Figure 19. The RMSE for the growth rate (μ) represented around 15% of the average growth rate (μ_{mean} – Table 15) for scenarios 2,3,4 and 35% for scenario 1.

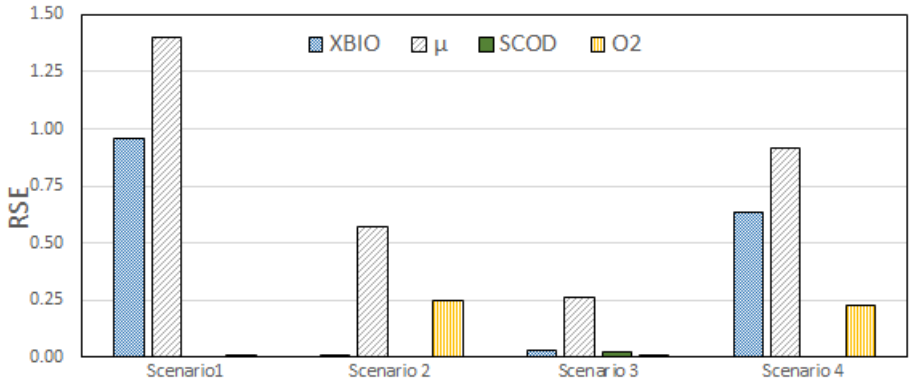

	Scenario1	Scenario 2	Scenario 3	Scenario 4
XBIO	0.96	0.01	0.03	0.63
μ	1.40	0.57	0.26	0.92
SCOD			0.02	
O2	0.00	0.25	0.01	0.23

Figure 19 Relative standard error (RSE) for the four dynamic variables from the batch experiments: biomass concentration (X_B), growth rate (μ), substrate concentration (SCOD) and oxygen concentration (O_2).

Table 7 Relative standard error (RSE) and root-mean-squared-error (RMSE) for biomass concentration (X_{BIO}), oxygen concentration (O_2), substrate concentration (SCOD) and growth rate (μ).

Scenario	RSE				RMSE			
	X_{BIO}	O_2	SCOD	μ	X_{BIO} [mgCOD/L]	O_2 [mgO_2/L]	SCOD [mgCOD/L]	μ [h^{-1}]
BCH 1	0.96	3.87	[-]	1.40	132	3.34	[-]	0.0106
BCH 2	0.01	0.25	[-]	0.57	23	0.22	[-]	0.0051
BCH 3	0.03	0.01	0.02	0.26	56	0.19	135.65	0.0038
BCH 4	0.05	0.23	[-]	0.92	44	0.98	[-]	0.0057

In conclusion, the model was fitted in order to have the closest similarity with scenario 3 as it was the only scenario with SCOD hourly data. In addition, its operational conditions are the most likely to be applied in a real case scenarios . This condition was achieved for all fixed parameters and dynamic variables apart from the biomass to substrate yield parameter ($Y_{x/s}$). However, despite the errors which could be significant, as for scenario 1, the simulations followed the corresponding trends for all fixed parameters that were observed during the experiments. Then, it can be concluded that the model is able to adequately simulate the four different scenarios and the relative impact of three different operational control tools (paddlewheel rotation, light cycle, and surface to volume ratio) partly answering at the second research question.

4.2 Simulations of the sequencing batch reactor scenarios

In order to simulate the sequencing batch reactor experiments the model was run for a 45 consecutive days to reach steady state conditions. For each simulation, the initial conditions were set close to the final results obtained from the batch experiments. As from theory, it was observed that after five time the SRT, around the 10th day of the simulation, the system reached a steady state condition. A figurative example of the model simulation is reported at Figure 20. It shows the hourly soluble substrate concentration (green line), total and PNSB biomass concentration (X_{BIO} – black line, X_{PB} - purple line), for the second SBR scenario between the 20th and 30th day of the simulation (Table 5). The figure includes some text boxes that helps to understand the SBR operation. The peak of soluble substrate corresponds at the influent addition at the beginning of the light phase; the minimum substrate value indicates the end of the dark phase and the effluent extraction; the alteration of the light and dark cycle is appreciable thanks to the different biomass growth, which is minimal in the dark phase (absence of oxygen and light).

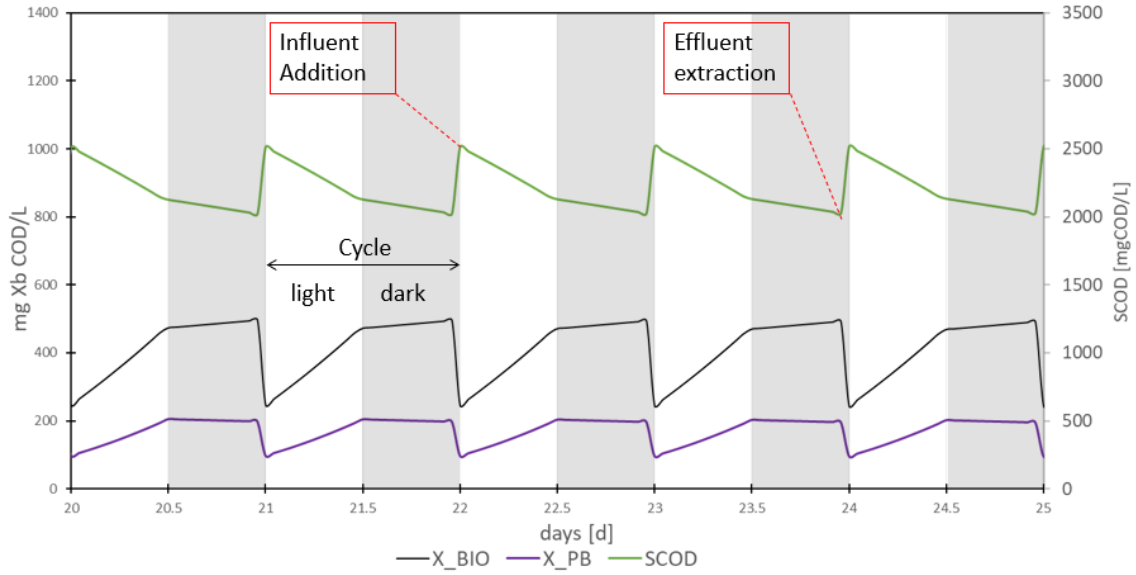

Figure 20 Explicative example of a SBR cycle in the raceway reactor. On the left axis, total biomass (X_{bio}) and purple bacteria biomass (X_{PB}) in mgCOD/L; on the right axis the total soluble COD concentration (SCOD). The figure shows the influent addition at the beginning of the light phase, a reaction phase and the extraction of the effluent at the end of the dark phase.

An extensive overview of the experimental results is discussed in detail in the paper from Alloul et al.(2020)[18]. In this report the attention was exclusively turned to the quality of the simulations. The tuning process identified the a set of input parameters for the three scenario, even though it diverges from the one found in the batch experiments (Appendix C). As for the batch experiments, the relative error (e_{rel}) was the main indicator determining quality of the simulations. Figure 21 (a-d) displays the

comparison of the mean average experimental results (squared dots) and the simulations results (bar charts) and the relative error (circular dots) for samples after the light and dark phase. Figure 21a shows that the COD removal is coherently simulated for all samples and scenarios as the relative error is below 10% (~100 mgCOD/L). Biomass concentration appears adequately simulated even thought for scenarios 1 and 2 the relative error increases up to 20%, around 150 mgCOD/L (Figure 21b). Similar considerations are valid for the biomass to substrate yield, reported in Figure 21c. Also in this case, scenarios 1,2 are less appropriately fitted with the experimental results than scenario 3. Vice versa the abundance of PNSB appeared to be better simulated in scenarios 1 and 2 than in scenario 3. Reasonably, scenarios 1 and 2 are closer to each other than scenario 3. Thus, looking at the different operational conditions (Table 5), it can be deduced that different water level has a more drastic and uncertain impact than the paddlewheel rotation. The paddlewheel rotation would promote linearly the growth of heterotrophic bacteria, while the variation in light intensity is exponentially correlated with the phototrophic growth due to Lamber-Beer equation (Eq. 1, Eq. 2).

Table 8 contains the experimental results and model simulations with the absolute and relative error for the SBR simulations. When the error is negative, the model overestimates the experimental results. The experimental results are shown here in triplicate or duplicate for each type of sample with the relative standard error of the measurements. On average, for each parameter, the specific relative error varies in a range of ±20%.

In conclusion, the model was fitted in order to have a close similarity to all scenarios. Despite the considerable errors for some parameters as the total biomass for scenarios 1 and 2 or the PNSB abundance in scenario 3, the simulations followed the corresponding trends for all fixed parameters that were observed during the experiments. Finally, the proposed model was able to sufficiently simulate the three different SBR scenarios and impact of the control tools as the paddlewheel rotation and surface area or water level, partly answering at the second research question proposed in this project.

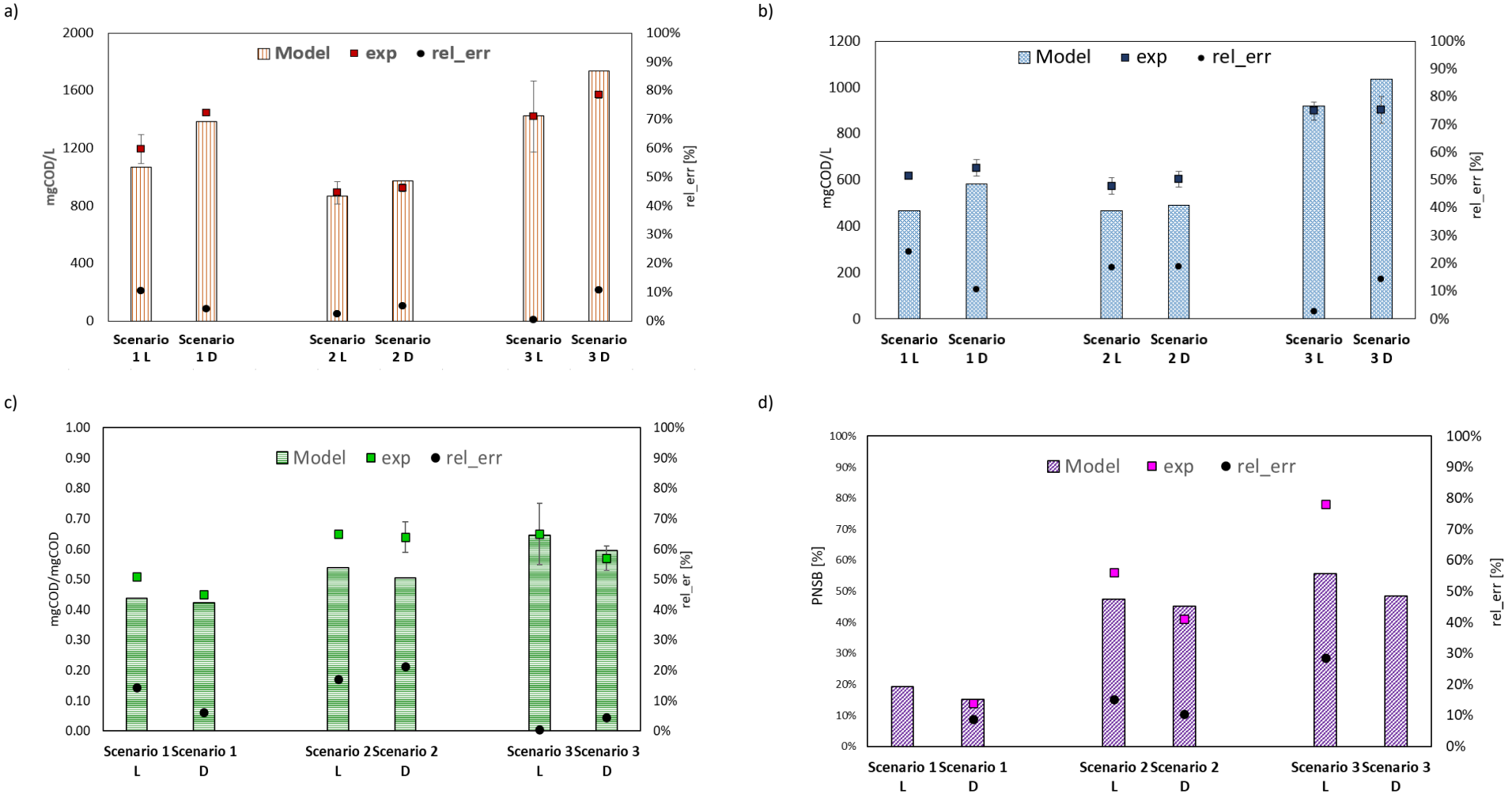

Figure 21 Comparison average experimental results and model simulation for the four fixed parameters : (a) COD removal [mgCOD/L]; (b) biomass [mgCOD/L]; (c) yield [mgCOD/mgCOD]; (d) relative PNSB abundance [%]. For each graph, on the left axis it is reported the relative error [%].

Scenario		COD rem					Xbio					Yx/s					%PNSB				
		Exp.	*SE*	*Model*	*Abs.err*	*rel_err*	*Exp.*	*SE*	*Model*	*Abs.err*	*rel_err*	*Exp.*	*SE*	*Model*	*Abs.err*	*rel_err*	*Exp.*	*SE*	*Model*	*Abs.err*	*rel_err*
SBR 1	After day cycle	1181	18	1070	111	9%	612	7	467	145	24%	0.52	0.002	0.437	0.08	16%		[-]	0.19		
		1207			137	11%	622			155	25%	0.52			0.08	15%					
	After night cycle	1397	102	1382	15	1%	660	31	584	76	12%	0.47	0.015	0.422	0.05	11%	0.14	[-]	0.15	-0.01	-9%
		1605			223	14%	692			108	16%	0.43			0.01	2%					
		1329			-53	-4%	604			20	3%	0.45			0.03	7%					
SBR 2	After day cycle	835	79	869	-34	-4%	538	51	468	70	13%	0.64	0.000	0.538	0.11	16%	0.56	[-]	0.48	0.08	15%
		947			78	8%	610			142	23%	0.64			0.11	16%					
	After night cycle	969	29	973	-4	0%	556	30	490	66	12%	0.57	0.050	0.504	0.07	12%	0.41	[-]	0.45	-0.04	-10%
		887			-86	-10%	622			132	21%	0.70			0.20	28%					
		919			-54	-6%	634			144	23%	0.69			0.19	27%					
SBR 3	After day cycle	1167	245	1425	-258	-22%	846	33	921	-75	-9%	0.72	0.093	0.646	0.08	11%	0.78	[-]	0.56	0.22	29%
		1279			-146	-11%	938			17	2%	0.73			0.09	12%					
		1815			390	21%	910			-11	-1%	0.50			-0.14	-29%					
	After night cycle	1609	24	1737	-128	-8%	840	52	1034	-194	-23%	0.52	0.040	0.595	-0.07	-14%	0.00	[-]	0.48		
		1549			-188	-12%	984			-50	-5%	0.64			0.04	6%					
		1553			-184	-12%	888			-146	-16%	0.57			-0.02	-4%					

Table 8 Summary of the comparison between the simulations and the experimental results for the four parameters (COD_{rem}, X_{bio}, $Y_{x/s}$ and %PNSB). Four each parameter it is reported the experimental (exp) and its relative standard error (SE) results. The column model give the outcome of the simulation. The last two columns are respectively the absolute error and the relative error (abs_{err}, rel_{err}).

4.3 Short and long-term perturbations: the results of the sensitivity analysis

In the next subsections the results of the sensitivity analysis are exposed and discussed. The aim of this study was the investigation of those factors that were not evaluated during the experimental results, but, they appeared to be really significant for stability and performance of the system. Firstly, the results of the instantaneous perturbated scenarios are reported studying the stability and recovery of the system, then, long-term perturbated scenarios are discussed defining new steady-state and the boundary limits of the reactor performance (Table 6).

4.3.1 Instantaneous perturbated scenario: negative effects of TSS peaks in the influent

In these simulations, the influent particulate fraction ($X_{s,in}$) was varied in a range from 100 to 1000 mgCOD/L. In this case the perturbation has a length of 10 days, from the 15th to the 25th of the simulation.

Figure 22 shows the reactor performance calculated as a twenty day average since the beginning of the TSS perturbation, thus considering the recovery of the system. As it emerges, the PNSB effluent concentration constantly declines from 220 mgCOD/L to 50 mgCOD/L and so their abundance which shrinks from 47% to 10%. As well, the COD removal rate steadily decreases from 450 mgCOD/L/d to 365 mgCOD/L/d. On the contrary, TSS productivity remains stable around 260 mgCOD/L/d until $X_{S,in}$ is lower than 300 mgCOD/L and then starts increasing up to 300 mgCOD/L/d. However, it should be recalled that these last two parameters are directly correlated with the perturbation as X_S is expressed in mgCOD/L (Eq. 24).

Figure 23 shows the impact of the influent TSS perturbation on the effluent concentration of purple bacteria (X_{PB}). After 10 days of perturbation the PNSB concentration touched a minimum value, after which they start repopulating the raceway reactor. For TSS peaks between 500-1000 mgCOD/L, PNSB were not completely washed out, but they reached low minimum concentration (below 20 mgCOD/L) and long recovery time (more than 20 days). In these scenarios PNSB abundance plumbed below 10% at the minimum. Thus, it can be said that such perturbations would be critical for the stability of PNSB in the system. With particulate concentration up to 300 mgCOD/L (260 mgTSS/L), PNSB were initially strongly affected but, they also showed a rapid recovery to original steady state variable (10-15 days).

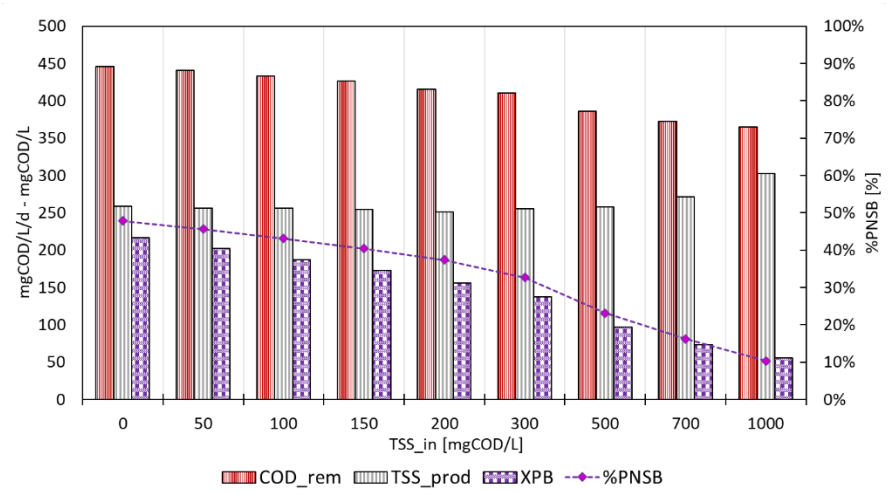

Figure 22 Reactor performance calculated as a twenty day average since the beginning of the perturbation (peak of TSS): on the left axis COD removal ratel (COD_{rem}), TSS productivity (TSS_{prod}) expressed in mgCOD/L/d and purple bacteria concertation (X_{PB} – mgCOD/L); on the left axis PNSB abundance (%PNSB) the right axis.

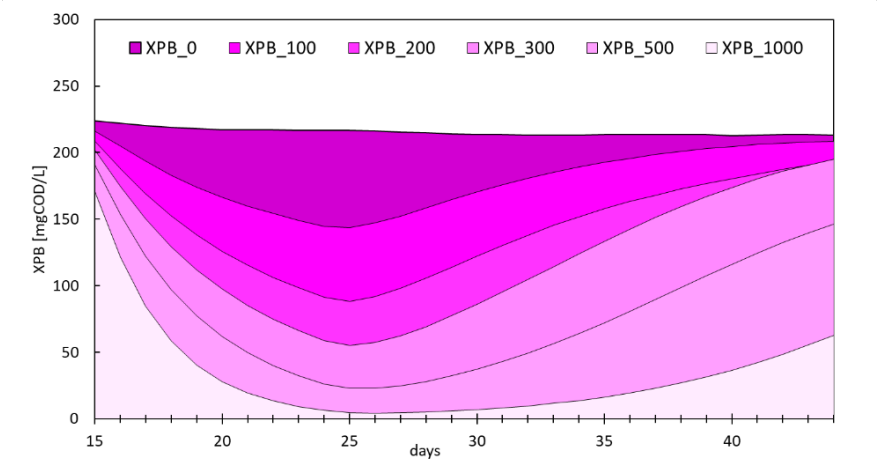

Figure 23 Daily effluent PNSB concentration since the beginning of the TSS perturbation with TSS peaks between 0 to 1000 mgCOD/L ($X_{PB,0}$ – $X_{PB,1000}$). A darker colours implies a higher concentration of X_{PB} due to a lower peak of TSS.

These simulations pointed out a strong dependency between the influent TSS in the system and the PNSB abundancy of the raceway reactor. In the literature, it wasn't found any experiment studying in detail this correlation. Nonetheless, the research of Martinez et al. (2018), investigating the effects of suspended particles and turbid media for the growth of microalgae, individuates turbidity as one of the main factor affecting the growth of phototrophic bacteria[96].

4.3.2 Instantaneous perturbated scenario: effects of natural light cycle and variability

In these simulations, artificial light was replaced by natural sunlight using meteorological data from the Indian region (Kolkata). Four simulations were run with different natural light variations. In the first scenario (scenario μ), no perturbation was considered; in the second and third scenarios, the light

intensity was reduced for ten straight days of nearly 40% and 75% respectively (scenarios *µ-1std*, *µ-2std*); the last scenario was run with real September data (scenario *Sept.)*.

Figure 24 shows the reactor performance for the four simulations. These values were calculated as average results of the next 20 days since the perturbation. Scenario µ allows a TSS productivity of 330 mgCOD/L/d with a relatively abundance of 60% and 670 mgCOD/L/d of COD removal. The variations of the natural light intensity seem particularly significant for the extreme scenario (*µ-2STD)* where the TSS production, COD removal and PNSB abundance drop to 184 mgCOD/L/d, 441 mgCOD/L/d and 25%. Interestingly, the scenarios *µ-1STD* and *Sept.* measure similar performance: approximately 260 mgCOD/L/d for TSS productivity, 500 mgCOD/L/d for COD removal and nearly 50% of PNSB abundance.

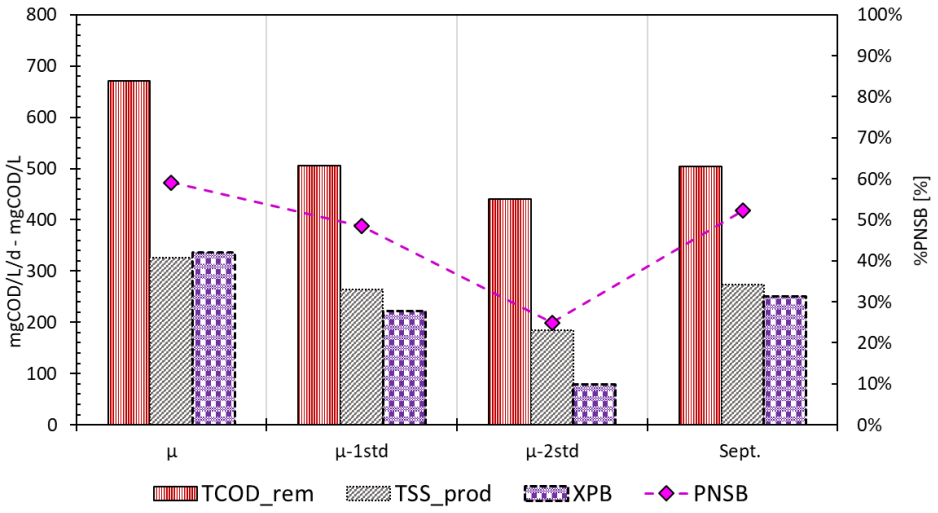

Figure 24 Raceway reactor performance calculated as a twenty day average since the beginning of the perturbation (light intensity variation): COD removal ($TCOD_{rem}$), TSS productivity (TSS_{prod}) expressed in mgCOD/L/d and purple bacteria concertation (X_{PB}) in mgCOd/L on the left axis; PNSB abundance (%PNSB) are reported on the right axis.

Figure 25 shows hourly PNSB concentration in the raceway reactor for the four simulations from the first day of perturbation to the following 20 days. In the first scenario, PNSB concentration was constant around 350 mgCOD/L. The minimum concentration of PNSB is reached with scenario *µ-2STD* falling below 20 mgCOD/L, whereas, in simulation *µ-1STD,* PNSB do not decline below to 150 mgCOD/L. In the scenario with the real September data the PNSB concentration fluctuates between 150 mgCOD/L and 330 mgCOD/L.

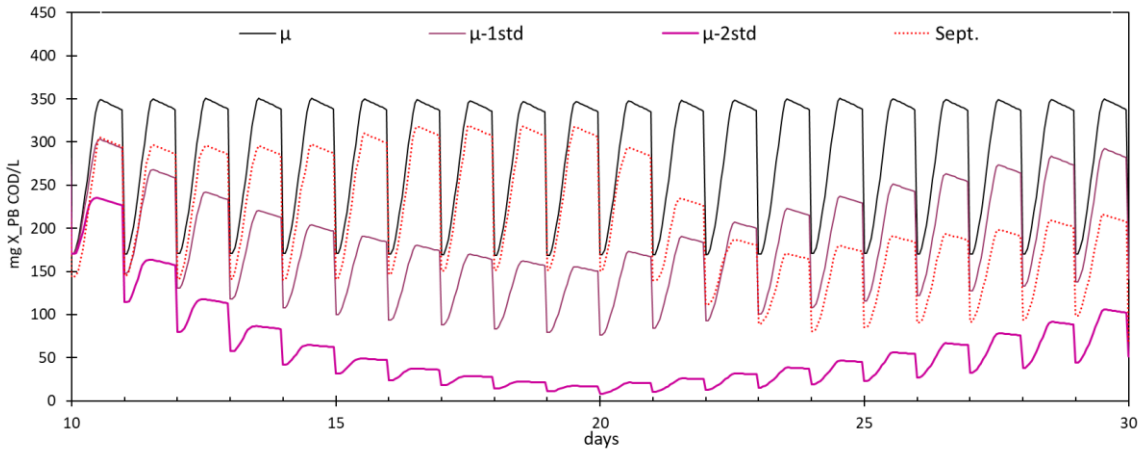

Figure 25 Hourly PNSB concentration [mgCOD/L] for the four simulated scenarios studying the short term perturbation of natural light variation and cycle. Monthly average light data from the month of September (μ); light intensity variability (μ-1STD, μ-2STD); real September radiation (Sept.).

As expected, variations of light intensity have an important impact on the stability of phototrophic bacteria. However, it was found that the light cycle has as well an important effect. For instance, the daily average light during the scenarios μ-1STD and μ-2STD measures 46 and 120 Wm^{-2} while, it was 54 Wm^{-2} in the laboratory experiments (Table 5). Even considering that for these simulations two different light half velocity constant ($K_{S,IE}$ equal to 10 and 25 W/m^{-2}), it can be said that a hourly variability of natural light has a relevant effect when compared to constant artificial light. Finally, these simulations helped to understand the raceway reactor operability with natural light and light cycle. According to the given radiation intensity, PNSB bacteria can be cultivated and extracted during the month of September in India and, as direct conclusion, weekly and seasonal variations should be carefully studied for the stable production of PNSB.

4.3.3 Instantaneous perturbated scenario: decline of PNSB with drop of soluble substrate

The assumption of a constant influent wastewater is unlikely to happen in real wastewater applications. In these scenarios it was simulated the effects of a significant drop in the incoming substrate (COD_{in}) such as it would be limiting. Despite the fact the model was not conceived for such event, the theoretical limitation of the substrate would lead to an increase of the oxygen concentration. This should benefit the chemotrophic pathway, favouring standard chemotrophic bacteria over the group of purple bacteria. To run these simulations the influent wastewater was reduced from 3 gCOD/L to 0.5-1.25 gCOD/L maintaining the same proportion of acetate, propionate

and butyrate (1/1/1 gCOD) for 10 days starting from the 10th day of simulation.

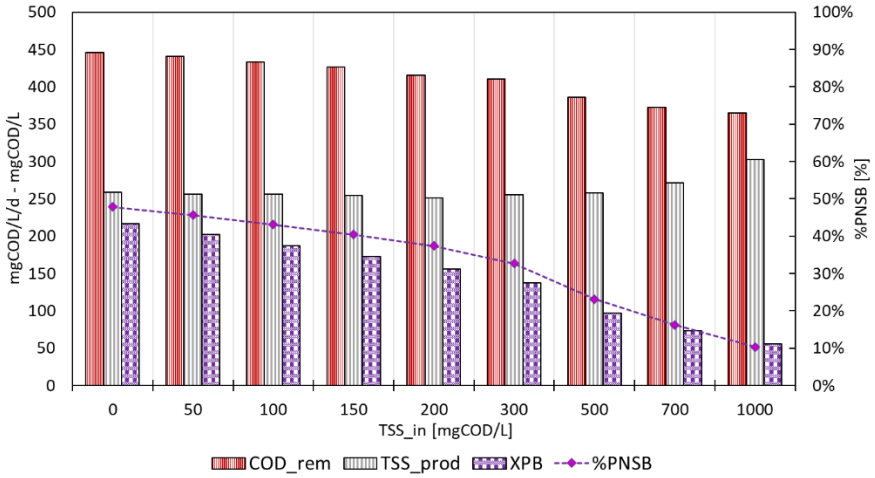

Figure 22 Figure 26 shows the reactor performance calculated as a twenty day average since the beginning of the TSS perturbation, thus including the recovery of the system. The effects are especially visible when COD_{in} is lower than 0.5 gCOD/L at which PNSB abundance plunges at 20%. When the influent concentration remains higher than 1000 mgCOD/L, despite being negatively affected in terms of TSS productivity, COD removal and PNSB abundance, the system performance is relatively close to the reference scenario with 3 gCOD/L.

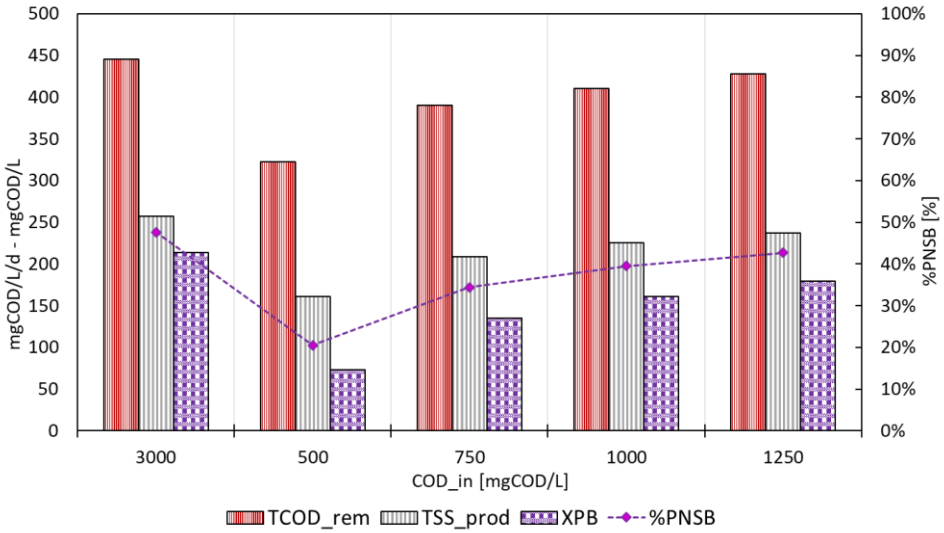

Figure 26 Raceway reactor performance calculated as a twenty day average since the beginning of the perturbation (drop of soluble substrate scenario). COD removal (TCODrem), TSS productivity (TSSprod) and purple bacteria concertation (XPB) on the left axis; PNSB abundance (%PNSB) the right axis.

Observing in detail Figure 27, which reports the hourly PNSB and oxygen concentration in the raceway reactor, it is appreciable the effect of a lower incoming substrate. PNSB biomass starts decreases since the beginning of the perturbation (10th day) while oxygen concentration slightly increases reaching

peaks up to 0.06 mgO_2/L. The decline of PNSB implies a slower growth rate which was found related to three factors: the limiting substrate, the heterotrophic competition (X_{HET}) and the phototrophic switch. In the end, the coupled effects of the first two factors is thought to be the main reason of PNSB decrease.

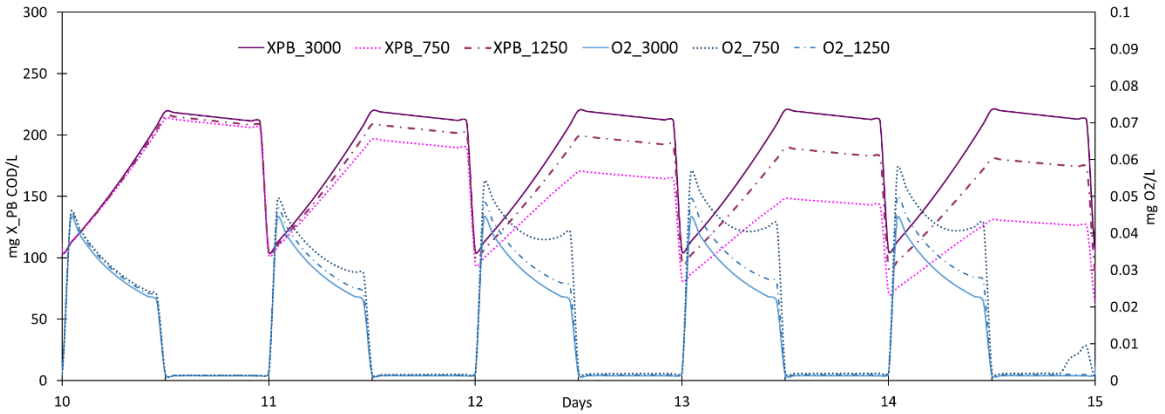

Figure 27 Hourly PNSB (left axis) and oxygen (right axis) concentration since the beginning of the instantaneous perturbations (drop of soluble substrate scenario). The legend refers to the influent substrate during the perturbation varying from 750 – 1250 mgCOD/L ($X_{PB,750-3000}$ – $O_{2,\ 750-3000}$)..

In conclusion, a drop of the COD concertation is most likely coupled with an increase of the oxygen concentration (Figure 27). From the simulations, it can be said that these events promote the chemoheterotrophic growth against the phototrophic growth. In the literature, the more recent papers evidenced the negative impact of oxygen concentration on PNSB abundance in mixed culture, arriving at the conclusion that PNSB would be rapidly outcompeted by standard heterotrophic bacteria[21]. Nonetheless, Figure 27 only measures very little changes in the oxygen concentration (+0.02 mg O_2/L) and the impact of oxygen concentration was never measured is such small variation. In fact, standard dissolved oxygen meter can detect no more than ±0.10 mg O_2/L, and the previous mentioned research studied semi-aerobic conditions with O_2 not below 0.25 mg O_2/L.

4.3.4 Long-term perturbated scenario: the negative prolonged impact of TSS

In these simulations, the influent biodegradable particulate concertation (X_S) was varied from 0 to 400 mg COD/L corresponding to 0 to 348 mgTSS/L (1.15 mgCOD/mgTSS). These scenarios want to assess the limitary boundaries of influent TSS on the PNSB concentration with an HRT and SRT of 2 days. The simulations were run for 45 days and the system was evaluated at equilibrium after 30 days and the reactor performance was evaluated as average between the 30th to the 45th day.

Figure 28 shows the reactor performance for the simulations with different influent TSS concentration. As it emerges, PNSB can not sustain influent TSS concentration greater than 300 mgCOD/L (246mgTSS/L) as their abundance drops well below 10%. Similarly, in the TSS peak scenario (page 55), COD removal constantly decreases from 450 mgCOD/L/d to 350 mgCOD/L/d. The TSS productivity remains stable around 250 mgCOD/L/d and then starts increasing above 300 mgCOD/L/d. Looking in detail at the particulate composition of the effluent, it is visible how, according to the model, X_S replaces PNSB while it doesn't affect X_{HET} which remains stable (Figure 29). As consequence, X_{BIO} increases with influent TSS concetration greater than 200 mgCOD/L.

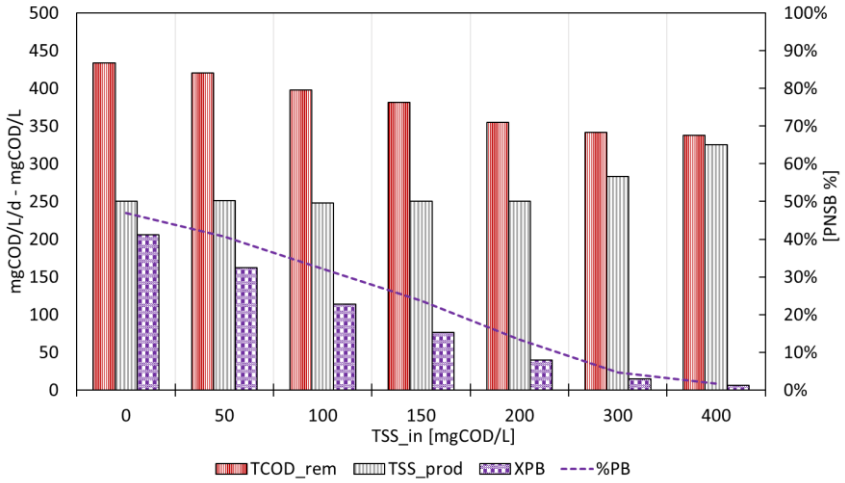

Figure 28 Raceway reactor performance compounds simulating the long-term impact of influent suspended solids (mgTSS/L): COD removal ($TCOD_{rem}$), TSS productivity (TSS_{prod}) and PNSB concertation (X_{PB}) on the left axis; PNSB abundance (%PNSB) the right axis.

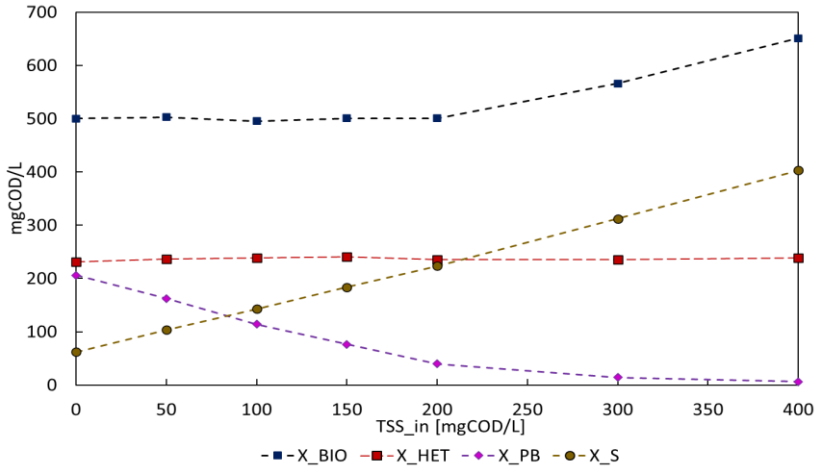

Figure 29 Effluent concentration of main particulate compounds simulating the long-term impact of influent suspended solids (mgTSS/L): total biomass (X_{BIO}), heterotrophic bacteria (X_{HET}), PNSB (X_{PB}), organic substrate (X_S) expressed in mgCOD/L.

In conclusion, according to the simulations, TSS in the influent strongly impact the stability of PNSB bacteria and the limitiray boundaries to have a minimum abundance of 20% of PNSB is around 200 mgCOD/L of X_S (180 mgTSS/L). These conclusions agree with the results from the previous simulations, underling the negative impact of TSS on the relative abundace of PNSB. However, in this case, relatively slow processes as decay and hydrolysis (0.09 and 0.07 d^{-1}) play a more significant role on the equilibrium of the system and should be investigated more in detail.

4.3.5 Long-term perturbated scenario: the benefits of SRT extension

One possible countermeasure to minimize the effect of TSS in the influent is the extension of the SRT: PNSB would be minorly washed out while standard chemotrophic bacteria would not further develop as oxygen remains the growth limiting factor. However, a longer SRT would also increase the TSS concentration and favour anoxic growth of bacteria (X_{HET}), in turn, limiting phototrophic growth. These simulations were run with a incoming TSS influent concentration equal to 300 mgCOD/L (261 mgTSS/L) and extending the SRT from 2 to 10 days.

Figure 30 shows the results of the reactor performance calculated as average between the 30th to 45th day. The COD removal linearly increases (R^2=0.96) from 375 mgCOD/L/d to 1000 mgCOD/L/d and so the TSS productivity from 283 mgCOD/L/d to 560 mgCOD/L/d (R^2 = 0.95). With the intial SRT of two days the PNSB abundance was less than 10%; it reaches a maximum, around 30%, between 4 and 5 days and then starts decreasing, settling around 20%. Figure 31 shows the compositon of the main particulate fraction reporting the concenration of PNSB (X_{PB}), heterotrophic biomass (X_{HET}), and slowly biodegradable substrate X_S. The growth of PNSB indicates a logistic curve stabilizing around 480

mgCOD/L with SRT higher than 5 days. On the other hand, the concentration of X_{HET} and X_S steadily increase measuring the best regression with a power lines, which are especially appreciable with SRT higher than 7 days. However, the growth of X_{HET} is expected to slow down when the substrates would be start to become limiting.

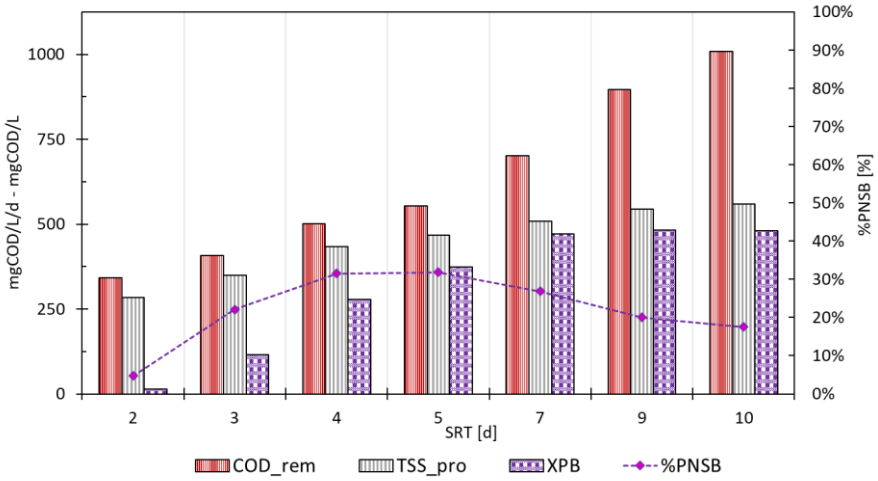

Figure 30 Raceway reactor performance for the scenario varying SRT: COD removal ($TCOD_{rem}$), TSS productivity (TSS_{prod}) and purple bacteria concertation (X_{PB}) on the left axis; PNSB abundance (%PNSB) the right axis.

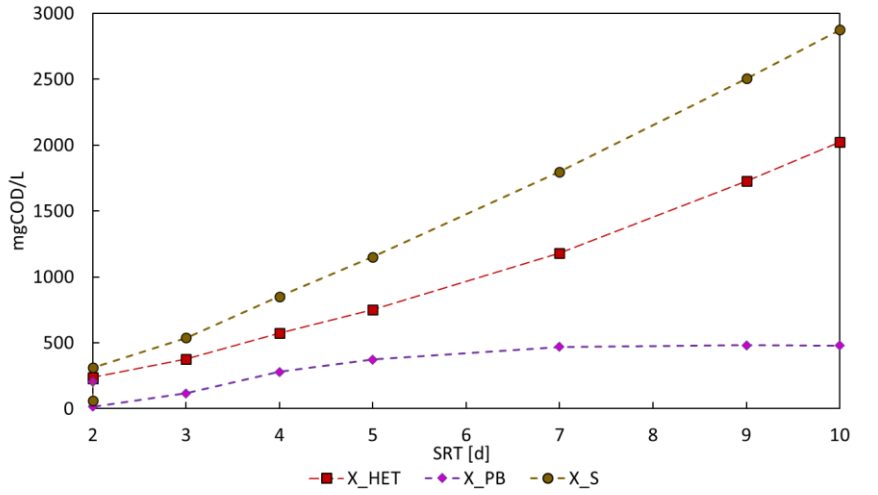

Figure 31 Effluent concentration of main particulate compounds for the scenario with varying SRT: chemoheterotrophic bacteria (X_{HET}), PNSB (X_{PB}), organic substrate (X_S) expressed in mgCOD/L.

It can be concluded that a certain extension of the SRT is beneficial for the proliferation of PNSB bacteria. Under these conditions, the optimal concentration and abundance of PNSB was obtained with a SRT of 5 days. However, an excessive SRT can favour the anoxic/anaerobic growth of X_{HET} and an accumulation of X_S in the system which would limit the phototrophic growth. Logistic growth model

has been severely applied for the growth of phototrophic microorganism in order to incorporate the light attenuation directly in the growth equation[16,97]. In these simulations, it was observed an overall increase of the TSS productivity in contrast with what was found by Alloul et al. (2020)[18]. These distinct results can be partially justified underling the different experimental conditions, mainly reactor geometry, and the fact that, in reality, the hydrolysis rate is dependent by the SRT [98].

4.3.6 Long-term perturbated scenario: increasing pressures from fermenters and microalgae with longer SRT

Fermenting bacteria

In these scenarios, the composition of the influent concentration (3 gCOD/L) was changed from the original 1/1/1 gCOD of acetate, propionate and butyrate to 1.5/1.0/0.5 acetate (S_{ac}), propionate (S_{VFA}) and glucose (S_s). Apart from including the two new variables S_S and X_{FR} as explained in the previous section (page 31), the input parameters needed to change accordingly in order to set a preferred substrate. The input parameters to indicate the substrate preference ($f(S_i)$) were modified accordingly to have similar reactor performance with the experimental results and the simulations exposed previously discussed (page 51). As mentioned in the literature review, PNSB bacteria prefer fermented compounds, so S_A and S_{VFA}, over complex substrate (S_S), especially when they perform the phototrophic metabolism (page 13).

To determine the effects of fermenting bacteria, the sludge retention time was increased from 2 to 8 days as it was found to be the optimal range for SRT from the previous simulations. As it is shown in Figure 32, the relative abundance of PNSB is maximized between 3 and 4 days SRT with values around 60% of the total microbial community constantly declining with longer SRT. Total PNSB concentration (X_{PB}) and COD removal rate (COD_{rem}) constantly rises, reaching a threshold, with SRT longer than 6 days, around 1000 mgCOD/L and 900 mgCOD/L/d respectively. In regard of the TSS productivity, this parameter remains stable around 450 mgCOD/L/d with SRT higher than 3 days.

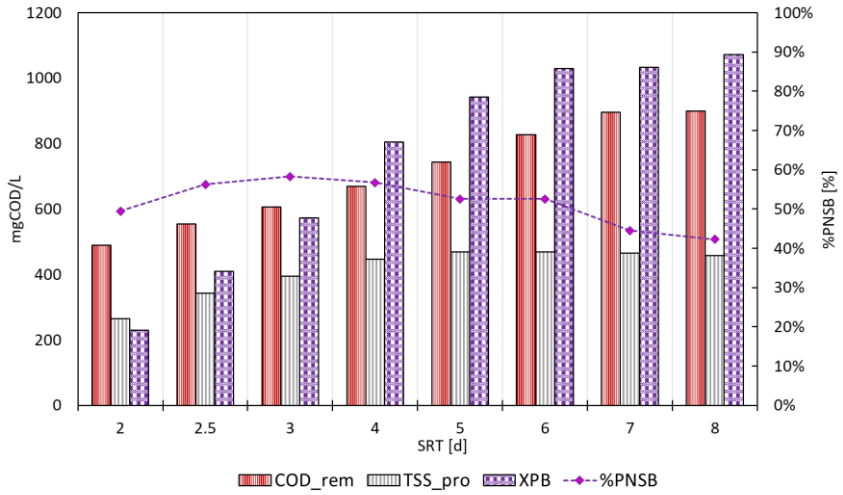

Figure 32 Raceway reactor performance with different SRT for the fermenting bacteria scenario: COD removal ($TCOD_{rem}$), TSS productivity (TSS_{prod}) and purple bacteria concertation (X_{PB}) on the left axis; PNSB abundance (%PNSB) on the right axis.

Figure 33 shows the absolute concentration of the major particulate compounds (X_{HET}, X_{PB}, X_S, X_{FR}). According to these simulations fermenting bacteria start to be consistently present with a SRT longer than 5 days, yet remaining a minor fraction compared to the other two biological groups. Within 2-5 days of SRT the relative increase of purple bacteria is higher than chemotrophic bacteria and so the total concentration. After this point, X_{HET} increases relatively faster than X_{PB} and they finally overtake when SRT are longer than 8 days. Similarly to the previous scenarios, the increase of the X_S fraction is more than linear and closer to a power regression line. This fact is mainly related to the fact that hydrolysis rate was assumed constant. These simulations suggest that within an SRT of 2-5 days oxygen is a greater limiting factor than light and so the growth of PNSB is favoured over the standard chemotrophic bacteria. At a certain point, the total biomass concentration and the growth of anaerobic and fermenting bacteria would limit the phototrophic pathway such as the relative abundance of PNSB would start declining. Additionally, it implies that the anoxic group of bacteria becomes consistent with a SRT longer than 4 days

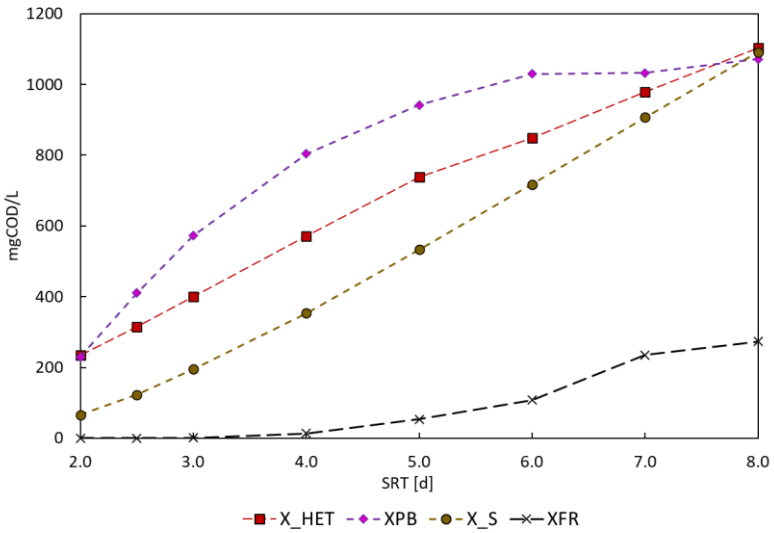

Figure 33 Effluent concentration of main particulate compounds for the fermenting bacteria scenario: chemoheterotrophic bacteria (X_{HET}), PNSB (X_{PB}), organic substrate (X_S) and fermenting bacteria (X_{FR}) expressed in mgCOD/L.

Microalgae

Microalgae were not directly included in the model. However, their potential impact was studied stoichiometrically on the steady state conditions. The main concern of microalgae proliferation is the production of oxygen in their anabolism. According to Solimeno (2017), for every mgCOD of microalgae produced, 0.97 mgO_2 of oxygen is released[76]. The impact of microalgae was simulated with a higher oxygen transfer rate (OTR) of the system, which is directly correlated with the volumetric mass transfer rate K_{la} (Eq. 1) . Originally, it was assumed to be close to 8.5 mgO_2/L/h matching a K_{la} of 1 h^{-1} (Table 5). In these simulations OTR was varied between 1.0-1.75 h^{-1} assuming that microalgae would produce between 0 to 6.4 mgO_2/L/h. According to the software BIO_ALGAE the net growth rate for microalgae (μ_{MA}) in raceway reactor could vary between 0.003-0.007 h^{-1} [95]. Thus the microalgae concentration to sustain such an oxygen production can be estimated as OTR_{MA}/μ_{MA}. With the given net growth rate, the minimum sludge retention time to sustain steadily microalgae should be equal to $1/\mu_{MA}$ (6-14 days). With these assumptions the most realistic scenarios to simulate the microalgae effect is a SRT of 6 days and a K_{la} of 1.25 h^{-1}. The results of the simulation presented a PNSB abundance which corresponds to a decline of 8% compared to the original scenario (40% *vs* 48%) However, because of the higher retention time (6 days) the effluent concentration of purple non-sulphur bacteria reached 711 mgCOD/L which is three times more than the original scenario (Table 8) . In conclusion, it can be said that impact of microalgae does not seem one of the major threats for the stability of PNSB bacteria. In contrast with PNSB bacteria, microalgae are negatively affected by heavily

polluted wastewater, because the proliferation of standard heterotrophic bacteria would limit their phototrophic growth. This is also one of the main reason why microalgae are used as a common tertiary treatment to recover macronutrient as nitrogen and phosphorus.

In conclusion, the additions of fermenting bacteria and microalgae coupled with the extension of sludge retention time was found to favour PNSB growth and abundance whether the SRT was below 5-6 days. When the SRT was extended over 6 days the anoxic and fermenting microorganisms and microalgae started to be relevant, limiting the growth of PNSB. However, these simulations were performed with a constant hydrolysis and it was observed a steady increase of the X_S fraction. At last, in order to properly simulate the anoxic chemotrophic pathway, the presence of electron acceptors to perform catabolic reactions, as sulphate or iron and other minerals should be evaluated.

5 Discussion

5.1 Critical aspects of the simulations

5.1.1 Batch simulations: lag-phase, stationary phase and initial conditions

The batch simulations were of primary importance for this research, due to the lack of dynamic SBR data that is currently available in literature. Nonetheless, batch conditions can importantly differ from steady state reactor. One of the main aspect that the proposed model does not consider is the lag-phase. In this initial phase, the inoculated microorganisms adapt themselves to the reactor conditions and do not immediately grow exponentially. According to the scientific literature, there are different mechanistic and deterministic models which simulate the lag-phase more accurately than the simple Monod equation [99]. In the laboratory experiments, the inoculum was cultivated in a photobioreactor under strictly anaerobic conditions, in which the phototrophic growth was the main metabolic pathway. In fact PNSB, mainly *Rhodobacter capsulatus*, represented around 75% of the initial microbial community. Moreover, the initial conditions of the raceway reactor, were characterized by an oxygen concentration almost at saturation conditions (O_2 > 7.0 mg/L). As mentioned in the literature, anoxygenic photosynthesis is carried by enzymes whose efficiency depend on oxygen tension[100]. Therefore, it is possible to assume that in the first hours the PNSB community were more hindered by these new conditions than standard chemotrophic bacteria.

As well, toward the end of the simulations, the model gets apart from the experimental results (Figure 17). In theory, this phase represents the end of the exponential growth and the beginning of the stationary phase. Usually, Monod equations do not represent appropriately this phase whereas Herbert-Pirt equations, with the introduction of the maintenance coefficient (q_s), simulates it with more accuracy. Mainly, this factor is able to modify the apparent biomass to substrate yield of the system, which is especially noticeable when substrate starts to be limiting[101]. At TU Delft university, a new model has been recently implemented studying the effect of the light/dark cycle on PNSB under anaerobic conditions using Herbert-Pirt equations[91]. Nonetheless the Monod growth equation remains the most widely used for wastewater treatment applications as indicated in the ASM and ADM models [68,70].

One last point regarding the batch experiments concerns the constant initial conditions on the microbial community of the inoculum. For all simulations, it was chosen to start with an inoculum composed by 75% and 25% of X_{PB} and X_{HET} respectively. This proportion was taken from the results of Alloul et al. (2020), assuming it was constant for all different scenarios[18]. However, in similar study

consistent fluctuations were observed in the initial microbial community of the inoculum [21]. Finally, because one of the main focus of this research was the relative abundance of PNSB, the information on the microbial community at the beginning of the batch experiments should be considered crucial for a more correct parametrization of the model.

In conclusion, this model was originally conceived to investigate the raceway reactor performance under SBR operational conditions. However, the availability of dynamic experimental data was considered essential as it would have actually helped the parametrisation process and given more consistency to the results answering the second research question. The suggested implementation for specifically for the batch experiments, the lag-phase, the stationary phase should be introduced and have more experimental data on the dynamic variations of the relative abundance of PNSB.

5.1.2 SBR simulations: dark-phase, hydrolysis and predation and biofilm growth.

As shown in the results section, the model was able to sufficiently simulate the trends for four fixed parameters selected to represent the reactor performance and the biotic competition under SBR conditions ($TCOD_{rem}$,X_{BIO}, $Y_{X/S}$, %PNSB). However, the relative error was overall higher when compared with the batch simulations. More specifically, biomass and yield resulted considerably underestimated for scenarios 1 and 2 and, in general, it was not observed a significant decrease in the PNSB relative abundance of between the light and dark phase (Table 8). In this regard, additional measurements, especially during the dark phase, would help the tuning process, but the implementation or amelioration of the model equations could possibly reduce the inaccuracy of the simulations. For instance, it should be recalled that hydrolysis and decay were not experimentally tested by Alloul et al. (2020) and that these equations were directly implemented as in the paper of Puyol et al. (2017) [17,18]. Nonetheless, these processes, are known to be particularly case specific and the variety of the wastewater composition and the reactor operational conditions play an important role[102]. On the other hand, it could be claimed that minor processes, like endogenous respiration and predations, could be relevant during the dark phase in which the growth rate is almost stopped. In the literature, it wasn't found any study focusing on these aspects, but, looking at the microalgae modelling, these processes are known to be relevant, especially during the dark phase[79,103].

Other important point regarding the SBR experiments is the calculation of the real sludge retention time. During the experiments performed at the De Koningshoeven brewery (Tilburg), biofilm formation was observed on the walls and paddlewheels was observed (Appendix EAppendix). Despite it was periodically removed, its formation implies and affects the sludge retention time of the system.

A quantitative estimation of this process was challenging and not in the scope of the experiments, even though it denotes some relevant difference from the actual operational conditions and the modelling simplification. The raceway reactor, used for the laboratory experiment, had an extended vertical surface area (1.2 m^2). Even considering a low biofilm productivity (10 $gVSS/m^2/d$) [104], the biomass production, due to biofilm growth, is estimated to represent around 10-30% of the total TSS productivity. Without adding new equations, this aspect could be easily implemented in the model slightly extending the sludge retention time, possibly overcome the underrated values of total biomass and yield (Table 8). In fact, from the results of the sensitivity analysis, it was observed that an extension of SRT would mainly promote total biomass and abundance of PNSB in the system (page 62).

In conclusion, it can be said that the SRT simulations were able to replicate the experimental results performed by Alloul et al. (2020). Nevertheless, the model should reconsider some equations, in particular hydrolysis and the decay processes. Moreover the implementation of new processes as endogenous respiration and predation might explain more accurately the dark phase which was difficult to reproduce. At last, another possible way to solve the underestimation of the total biomass concentration and yield might be a relatively extension of the SRT from theoretical values which can be justified by the experimental observation of biofilm formation during the experiments.

5.2 Future model improvements

5.2.1 Incorrect aspects of the simulations

The model was intended as a first attempt to simulate the growth of PNSB in a mixed culture and semi-aerobic conditions. Even though the model was able to sufficiently simulate the seven experimental scenarios, some aspects of the simulations remain of difficult interpretation. For instance, in batch experiments, when substrate becomes limiting, the reoxygenation curve distanced importantly, increasing much faster than the experimental results (Figure 17). The reason of this behaviour lies in the fact that in the model there is not any other compound than soluble substrate consuming oxygen. Actually, physical and biological processes in wastewater are much more complex and would not allow such a rapid reoxygenation. Therefore, the addition of other oxygen consuming processes as endogenous respiration or nitrification could strengthen the accuracy of the oxygen balance. These biological activity are usually considered in the ASM models and should be implemented in the future[70]. Besides, oxidations reactions mainly of iron, sulphide and magnesium might be important in anaerobic environments. At this regard, it is important to recall that one of the major aspects differentiating the ADM models from the ASM models is indeed the inclusion of chemical reactions of most abundant minerals[105,106]. As already mentioned in the previous paragraphs,

hydrolysis was considered with a first-order kinetic as in most ADM models kinetic because of the experiments of Puyol et al. (2017), but in standard ASM models it is usually expressed in function of the standard chemotrophic bacteria[107]. Even though of minor importance, the assumption of an equal decay rate for all the three biological groups is incorrect for an accurate simulation[70,74,76].

One last important remark concerns exclusively the two scenarios in which paddlewheel was stopped during the dark phase (Table 4,Table 5). The model structure always assumes perfectly mixed conditions which are problematic to accept in the dark phase because of biomass sedimentation. The implementation of this aspect is challenging, as it includes several new variables and equations. Nevertheless, during the dark phase, the biological reactions are slower than during the light phase, therefore a simplification was considered still acceptable for the purpose of this project.

5.2.2 Future implementation of the model

As already discussed, the model was simplified since the complexity of wastewater modelling, the availability of experimental data and the objective of the project. In this section, it will be briefly discussed the most relevant implementations that could ameliorate the accuracy and universality of the model.

Starting from the biological and chemical processes, temperature and pH should be included in the model. It is a well-known fact that the biological activity is importantly correlated with these two variables, not only influencing the overall performance of the reactor, but also determining the microbiological selection[60,108]. Similarly, anoxic and anaerobic growth of heterotrophic bacteria should better implemented, introducing the availability of electron acceptors, with particular emphasis on nitrate and sulphate. Possibly, specific biological groups like denitrifiers, sulphate reducing bacteria (SRB) and sulphur oxidizing bacteria (SOB) might be requested for certain type of wastewater [74,105].As well, biological competition of the phototrophic pathway can be further investigated. PNSB and microalgae are not the only phototrophic bacteria and *cyanobacteria* or *green-sulphur bacteria* could compete under certain conditions (e.g. sulphate enriched wastewater)[27]. At this regard, during the experiments performed the brewery, it was observed a visible change in raceway reactor colour, turning greenish, after a spill of a brewing session (Appendix E). Measurements at the spectrometers reported a considerable shift of the wavelength peaks from 805-860 nm to 735-780 nm, which is characteristic of green-sulphur bacteria[109]. One last remarks concerns the PNSB metabolism can be ulteriorly extended including the photoautotrophic or chemolithoautotrophic pathway which can play a role with limited or not degradable substrate[110,111].

At the same time, new physical processes can be improved and implemented. The reactor can be divided into multiple-layer to avoid the dependency on the average light intensity as in the research of Berberoglu et al. (2010)[93]. Besides, Lambert-Beer equation is the most simple light attenuation model that can be applied and bidirectional scattering model or full radiative transfer model have been already applied to microalgae modelling[66]. Finally, the reactor was simulated as one single CSTR, whereas it could be interesting the subdivision into a series of CSTR in which the reaeration coefficient would change based on the distance from the paddlewheel [40,112]. This aspect would be particularly important for the up-scaling phase of the raceway reactor. Other available approach could opt for computational fluid dynamic (CFD) models, including a larger series of parameters and reactions as mixing and hydraulic losses [113].

5.3 Sensitivity analysis

The sensitivity analysis pointed out some important results that should be considered for the next and practical and simulating development of the raceway reactor. According to the model instantaneous and long-term perturbations can markedly destabilize the PNSB abundance in the reactor. These findings suggest that TSS removal both in form of organic, inorganic and biological fraction (X_S, X_{FR}, X_I) should be monitored and minimized as much as possible (page 55, 60). Therefore, the incoming influent should be pre-treated with a sedimentation or even microfiltration unit. However, these results were conducted based on the assumption that the absorption spectrum of all different particulate fraction was equal, whereas the phototrophic activity of PNSB is mainly influenced by a specific wavelength range (780-900 nm). Therefore, experimental studies should analyse more in detail the effect of turbidity on the growth of PNSB to better individuate the boundaries of total and influent TSS concentration in order allow a sufficient phototrophic activity. These studies have not been conducted yet for PNSB, but it might be assumed a very similar theory behind the effect of turbidity as the one studied for microalgae in the research of Martinez et al. (2018)[96].

Another important aspect observed after the tuning of the model and the sensitivity analysis is the little contribution of the chemotrophic pathway for PNSB. The lower half velocity constant for oxygen in heterotrophic bacteria ($K_{S,O2,HET}$ = 0.1 mgO_2/L) would limit the chemotrophic switch of PNSB as they are characterized by a $K_{S,O2,PB}$ of 0.5 mgO_2/L. Moreover, an according to the sensitivity analysis and increase of the oxygen availability or a greater OTR would mainly advantage the proliferation of heterotrophic bacteria at the expenses of PNSB (page 58, 64). These results are in line with the most recent research at this regard[21]. Therefore, the oxygen transfer rate should be examined carefully and correlated with the paddlewheel mixing and the relative reaeration coefficient (kl_a) for the specific

conditions. Moreover, in real wastewater, dissolved oxygen meter should be replaced with an oxygen reduction potential meter. In synthetic waster, due to the relative minor presence of inorganic electrons acceptors as nitrate and sulphate, oxygen appears the main compound to monitor. On the other hand, the complexity of real wastewaters includes a series of electrons acceptors which can thrive anoxic growth, competing with PNSB[27].

Light intensity variations were studied relatively to the Saraswati project, using radiation measurements in the Kolkata region only for the month of September. Under these conditions the PNSB concentration was even higher than in the experimental values, but the light availability, cycle and variability should be considered during for the stability of the reactor (page 56). This aspect would have important implications during the winter and the monsoon period where the light-dark cycle and the light intensity can important diverge from the September scenario. As explicative example a yearly simulation was run with the hourly daily variations and it was observed that PNSB abundance dropped during November until February below 30% and there was a significant reduction in the month of June and July (monsoon period) (Appendix D - Figure 34).

Lastly, the regulation of the sludge retention time was found to be one of the most efficient operational control tools to promote and stabilize the abundance of PNSB. The simulations individuated the best retention time between 3 to 5 days. With these conditions and an appropriate oxygen transfer rate the extension of SRT exclusively favour PNSB compared to other group (X_{HET}, X_{FR}, X_{MA}). These values are in line with most of the literature review but it has to recalled that the model does not properly assess the impact of anoxic growth [46]. Moreover, with longer SRT it was observed a relative increase of the biomass productivity which should be beneficial for the extraction of valuable resources as single cell proteins. These observations were in contrast with the experimental results of Alloul et al. (2020), but they can be justified because of a constant hydrolysis rate and the different experimental conditions. In fact, these experiments were conducted in smaller reactors, using the same light intensity, then affecting the light availability[18].

6 Conclusion

The primary aim of this thesis was to develop a mechanistic model able to simulate the nutrient removal and recovery, and the growth dynamics of the purple non-sulphur bacteria (PNSB) in a raceway reactor. The thesis objective was divided in three research questions which reached the following conclusions.

- The influence of light, oxygen availability, biotic competition, and the carbon source were found and selected as the most important parameters to include in the mechanistic model in order to simulate raceway reactors conditions and study the nutrient removal and PNSB dynamic.

- The model of Puyol et. al (2017)[17] was used as the starting point for the development of the model, but several adjustments were requested. Mainly, the cybernetic growth model was used to control the versatile metabolisms of PNSB and the multitude of substrates.

- The model was able to simulate seven laboratory experiments (4 batch, 3 SBR) under different operational conditions (light, oxygen availability, surface -area) performed by Alloul et al. (2020)[18]. The COD removal rate was ranged between 450-780 $mgCOD_x/mgCOD_s$, the yield between 0.40-0.65 $mgCOD_X/mgCOD_S$ and the PNSB abundance between 10-65%. On average the relative error was below ± 20%.

- The sensitivity analysis individuated influent TSS concentration (TSS>250 mgTSS/L) and COD concentration (COD <1000mgCOD/L), and hourly light intensity variations as relevant parameters negatively affecting PNSB abundance in the system (from 48% to 10%).

- An extension of the SRT from 2 to 5 days was found to favour the abundance of PNSB from 48% to 60% and the TSS productivity from 230 to 400 mgTSS/L/d.

Several improvements and implementations were suggested in the discussion section. The anoxic and anaerobic chemoheterotrophic growth, especially during the so called dark phase, should be improved taking into account the availability of the electron acceptors as sulphate, nitrate, and iron. As well, hydrolysis and decay should be investigated more in detail for raceway rector conditions. Temperature and pH dependency should be implemented as they are known to be relevant for fermentative

growth. The effects of turbidity and total suspended solids was observed to be one of the major compounds disturbing the stability of PNSB. At this regard, specific experiments should be undertaken to verify this aspect that has never been investigated for PNSB.

Despite the several implementations needed, the model can be reasonably used as a tool to simulate and study the dynamic of raceway reactors under several different conditions. Moreover, it could be of support for further experiments in order to investigate and scale up this technology as for the SARASWATI project or other similar researches.

7 References

1. Steffen, W. *et al.* Planetary boundaries: Guiding human development on a changing planet. *Science (80-.).* **347**, (2015).
2. Mo, W. & Zhang, Q. Energy-nutrients-water nexus: Integrated resource recovery in municipal wastewater treatment plants. *J. Environ. Manage.* **127**, 255–267 (2013).
3. Chernicharo, C. A. L., Lier, J. B., Noyola, A. & Ribeiro, T. B. Anaerobic sewage treatment : state of the art , constraints and challenges. *Rev. Environ. Sci. Bio/Technology* **14**, 649–679 (2015).
4. Kleerebezem, R., Joosse, B., Rozendal, R. & Van Loosdrecht, M. C. M. Anaerobic digestion without biogas? *Rev. Environ. Sci. Biotechnol.* **14**, 787–801 (2015).
5. Alloul, A. *et al.* Capture-Ferment-Upgrade: A Three-Step Approach for the Valorization of Sewage Organics as Commodities. *Environ. Sci. Technol.* **52**, 6729–6742 (2018).
6. Ghosh, S., Chowdhury, R. & Bhattacharya, P. A review on single stage integrated dark-photo fermentative biohydrogen production: Insight into salient strategies and scopes. *Int. J. Hydrogen Energy* **43**, 2091–2107 (2018).
7. Hülsen, T. *et al.* Domestic wastewater treatment with purple phototrophic bacteria using a novel continuous photo anaerobic membrane bioreactor. *Water Res.* **100**, 486–495 (2016).
8. Hülsen, T., Hsieh, K., Lu, Y., Tait, S. & Batstone, D. J. Simultaneous treatment and single cell protein production from agri-industrial wastewaters using purple phototrophic bacteria or microalgae – A comparison. *Bioresour. Technol.* **254**, 214–223 (2018).
9. Basak, N. & Das, D. The prospect of purple non-sulfur (PNS) photosynthetic bacteria for hydrogen production: The present state of the art. *World J. Microbiol. Biotechnol.* **23**, 31–42 (2007).
10. Zhou, Q., Zhang, P. & Zhang, G. Biomass and carotenoid production in photosynthetic bacteria wastewater treatment: Effects of light intensity. *Bioresour. Technol.* **171**, 330–335 (2014).
11. Delamare-Deboutteville, J. *et al.* Mixed culture purple phototrophic bacteria is an effective fishmeal replacement in aquaculture. *Water Res. X* **4**, (2019).
12. Tripathi, B. N. & Kumar, D. *Prospects and challenges in algal biotechnology*. *Prospects and Challenges in Algal Biotechnology* (2017). doi:10.1007/978-981-10-1950-0
13. Benemann, J. Microalgae for biofuels and animal feeds. *Energies* **6**, 5869–5886 (2013).
14. Szilveszter, S., Ráduly, B., Ábrahám, B., Lányi, S. & Niculae, D. R. Mathematical models for domestic biological wastewater treatment process. *Environ. Eng. Manag. J.* **9**, 629–636 (2010).
15. Ghosh, S., Dairkee, U. K., Chowdhury, R. & Bhattacharya, P. Hyodrogen from fod processing wastes via photofermentation using Purple Non-sulfur Bacteria (PNSB) – A review. *Energy Convers. Manag.* **141**, 299–314 (2017).
16. Policastro, G., Luongo, V., Frunzo, L. & Fabbricino, M. A comprehensive review of mathematical models of photo fermentation. *Crit. Rev. Biotechnol.* **0**, 1–34 (2021).
17. Puyol, D., Barry, E. M., Hülsen, T. & Batstone, D. J. A mechanistic model for anaerobic phototrophs in domestic wastewater applications: Photo-anaerobic model (PAnM). *Water Res.* **116**, 241–253 (2017).
18. Alloul, A., Cerruti, M., Adamczyka, D., Weissbrodt, D. G. & & Vlaeminck, S. E. Control tools to selectively produce purple bacteria for microbial protein in raceway reactors. *bioRxiv* 1–27 (2020).

19. Lu, H., Zhang, G., Wan, T. & Lu, Y. Influences of light and oxygen conditions on photosynthetic bacteria macromolecule degradation: Different metabolic pathways. *Bioresour. Technol.* **102**, 9503–9508 (2011).

20. Lu, H. *et al.* Natural light-micro aerobic condition for PSB wastewater treatment: a flexible, simple, and effective resource recovery wastewater treatment process. *Environ. Technol. (United Kingdom)* **39**, 74–82 (2018).

21. Capson-tojo, G., Lin, S., Batstone, D. J. & Hülsen, T. Purple phototrophic bacteria are outcompeted by aerobic heterotrophs in the presence of oxygen. *Water Res.* **194**, 116941 (2021).

22. van Niel, C. B. On the morphology and physiology of the purple and green sulphur bacteria. *Arch. Mikrobiol.* **3**, 1–112 (1932).

23. Blankenship, R. E., Madigan, M. T., & Bauer, C. E. *Anoxygenic photosynthetic bacteria (Vol. 2).* (2006).

24. Hansen, T. A. & van Gemerden, H. Sulfide utilization by purple nonsulfur bacteria. *Arch. Mikrobiol.* **86**, 49–56 (1972).

25. Pfennig, N. & Trüper, H. G. Taxonomy of phototrophic green and purple bacteria: A review. *Ann. l'Institut Pasteur Microbiol.* **134**, 9–20 (1983).

26. Hallenbeck, P. C. *Modern topics in the phototrophic prokaryotes: Environmental and applied aspects*. *Modern Topics in the Phototrophic Prokaryotes: Environmental and Applied Aspects* (2017). doi:10.1007/978-3-319-46261-5

27. Hiraishi, A. *et al.* Distribution of phototrophic purple nonsulfur bacteria in massive blooms in coastal and wastewater ditch environments. *Microorganisms* **8**, (2020).

28. Goginyan, V. Eusébio, A. Neves, A. Harutyunyan, B. Hovhannisyan, R. Andreasyan, N. & Marques, I. P. R. Purple non-sulphur photosynthetic bacteria in brewery wastewater during anaerobic digestion. *5th Int. Conf. WASTES Solut. Treat. Oppor.* 87–89 (2019).

29. Kaewsuk, J., Thorasampan, W., Thanuttamavong, M. & Seo, G. T. Kinetic development and evaluation of membrane sequencing batch reactor (MSBR) with mixed cultures photosynthetic bacteria for dairy wastewater treatment. *J. Environ. Manage.* **91**, 1161–1168 (2010).

30. He, J., Zhang, G. & Lu, H. Treatment of soybean wastewater by a wild strain Rhodobacter sphaeroides and to produce protein under natural conditions. *Front. Environ. Sci. Eng. China* **4**, 334–339 (2010).

31. Kornochalert, N., Kantachote, D., Chaiprapat, S. & Techkarnjanaruk, S. Bioaugmentation of latex rubber sheet wastewater treatment with stimulated indigenous purple nonsulfur bacteria by fermented pineapple extract. *Electron. J. Biotechnol.* **17**, 174–182 (2014).

32. Hülsen, T., Batstone, D. J. & Keller, J. Phototrophic bacteria for nutrient recovery from domestic wastewater. *Water Res.* **50**, 18–26 (2014).

33. Koblížek, M. *The Purple Phototrophic Bacteria*. *Photosynthetica* **47**, (2009).

34. Imam, S., Noguera, D. R. & Donohue, T. J. Global insights into energetic and metabolic networks in Rhodobacter sphaeroides Global insights into energetic and metabolic networks in Rhodobacter sphaeroides. (2013).

35. Nowicka, B. & Kruk, J. Powered by light: Phototrophy and photosynthesis in prokaryotes and its evolution. *Microbiol. Res.* **186–187**, 99–118 (2016).

36. Inui, M., Roh, J. H., Momma, K. & Yukawa, H. Studies on CO2 fixation in PNSB : Analysis of CO2 metabolism in purple non-sulfur bacteria. *Stud. Surf. Sci. Catal.* **Vol. 114,** 597–600 (1998).

37. Nakajima, F., Kamiko, N. & Yamamoto, K. Organic wastewater treatment without greenhouse gas emission by photosynthetic bacteria. *Water Sci. Technol.* **35**, 285–291 (1997).

38. Durrens, P., G, L. De, Facults, A. & Talence, F.-. Differences in the control of bacteriochlorophyll formation by light and oxygen. 121–124 (1981).

39. Lu, H., Zhang, G., Wan, T. & Lu, Y. Bioresource Technology Influences of light and oxygen conditions on photosynthetic bacteria macromolecule degradation : Different metabolic pathways. *Bioresour. Technol.* **102**, 9503–9508 (2011).

40. Fernández, I., Acién, F. G., Guzmán, J. L., Berenguel, M. & Mendoza, J. L. Dynamic model of an industrial raceway reactor for microalgae production. *Algal Res.* **17**, 67–78 (2016).

41. Mendoza, J. L. *et al.* Fluid-dynamic characterization of real-scale raceway reactors for microalgae production. *Biomass and Bioenergy* **54**, 267–275 (2013).

42. James, S. C. & Boriah, V. Modeling algae growth in an open-channel raceway. *J. Comput. Biol.* **17**, 895–906 (2010).

43. Kumar, K., Mishra, S. K., Shrivastav, A., Park, M. S. & Yang, J. Recent trends in the mass cultivation of algae in raceway ponds. **51**, 875–885 (2015).

44. Chiaramonti, D. *et al.* Review of energy balance in raceway ponds for microalgae cultivation: Re-thinking a traditional system is possible. *Appl. Energy* **102**, 101–111 (2013).

45. Mendoza, J. L. *et al.* Oxygen transfer and evolution in microalgal culture in open raceways. *Bioresour. Technol.* **137**, 188–195 (2013).

46. Chen, J. *et al.* Photosynthetic bacteria-based technology is a potential alternative to meet sustainable wastewater treatment requirement? *Environ. Int.* **137**, 105417 (2020).

47. Suwan, D., Chitapornpan, S., Honda, R. & Chiemchaisri, C. Conversion of organic carbon in food processing wastewater to photosynthetic biomass in photo-bioreactors using different light sources. *Environ. Eng. Res.* **19**, 293–298 (2014).

48. Zhi, R. *et al.* Effects of light-dark cycles on photosynthetic bacteria wastewater treatment and valuable substances production. *Bioresour. Technol.* **274**, 496–501 (2019).

49. Akkerman, I., Janseen, M., Rocha, J. & Wijffels, R. H. Photobiological hydrogen production: photochemical efficiency and bioreactor design. International journal of hydrogen energy, 27(11-12), 1195-1208. *Int. J. Hydrogen Energy* **27(11–12)**, 1195–1208 (2002).

50. Biel, A. J. & Marrs, B. L. Transcriptional regulation of several genes for bacteriochlorophyll biosynthesis in Rhodopseudomonas capsulata in response to oxygen. *J. Bacteriol.* **156**, 686–694 (1983).

51. Sirianuntapiboon, S. & Srikul, M. Reducing red color intensity of seafood wastewater in facultative pond. *Bioresour. Technol.* **97**, 1612–1617 (2006).

52. Alloul, A., Muys, M., Hertoghs, N., Kerckhof, F. M. & Vlaeminck, S. E. Cocultivating aerobic heterotrophs and purple bacteria for microbial protein in sequential photo- and chemotrophic reactors. *Bioresour. Technol.* **319**, 124192 (2021).

53. Meng, F., Yang, A., Zhang, G. & Wang, H. Effects of dissolved oxygen concentration on photosynthetic bacteria wastewater treatment: Pollutants removal, cell growth and pigments production. *Bioresour. Technol.* **241**, 993–997 (2017).

54. Yang, A. *et al.* A special light-aerobic condition for photosynthetic bacteria-membrane bioreactor technology. *Bioresour. Technol.* **268**, 820–823 (2018).

55. Alloul, A., Wuyts, S., Lebeer, S. & Vlaeminck, S. E. Volatile fatty acids impacting phototrophic

growth kinetics of purple bacteria : Paving the way for protein production on fermented wastewater. *Water Res.* **152**, 138–147 (2020).

56. Fradinho, J. C., Oehmen, A. & Reis, M. A. M. Photosynthetic mixed culture polyhydroxyalkanoate (PHA) production from individual and mixed volatile fatty acids (VFAs): Substrate preferences and co-substrate uptake. *J. Biotechnol.* **185**, 19–27 (2014).

57. Lu, H., Zhang, G., Dai, X. & He, C. Photosynthetic bacteria treatment of synthetic soybean wastewater: Direct degradation of macromolecules. *Bioresour. Technol.* **101**, 7672–7674 (2010).

58. Nagadomi, H., Takahasi, T., Sasaki, K. & Yang, H. C. Simultaneous removal of chemical oxygen demand and nitrate in aerobic treatment of sewage wastewater using an immobilized photosynthetic bacterium of porous ceramic plates. *World J. Microbiol. Biotechnol.* **16**, 57–62 (2000).

59. Yang, A. *et al.* Enhancing protein to extremely high content in photosynthetic bacteria during biogas slurry treatment. *Bioresour. Technol.* **245**, 1277–1281 (2017).

60. Hülsen, T., Barry, E. M., Lu, Y., Puyol, D. & Batstone, D. J. Low temperature treatment of domestic wastewater by purple phototrophic bacteria: Performance, activity, and community. *Water Res.* **100**, 537–545 (2016).

61. Kaftan, D., Bína, D. & Koblížek, M. Temperature dependence of photosynthetic reaction centre activity in Rhodospirillum rubrum. *Photosynth. Res.* **142**, 181–193 (2019).

62. Liu, S., Zhang, G., Zhang, J., Li, X. & Li, J. Performance, carotenoids yield and microbial population dynamics in a photobioreactor system treating acidic wastewater: Effect of hydraulic retention time (HRT) and organic loading rate (OLR). *Bioresour. Technol.* **200**, 245–252 (2016).

63. Cerruti, M., Stevens, B., Ebrahimi, S., Alloul, A., Vlaeminck, S. E., & Weissbrodt, D. G. (2020). Enriching and aggregating purple non-sulfur bacteria in an anaerobic 4 sequencing-batch photobioreactor for nutrient capture from wastewater. *bioRxiv.* 1–13 (2020).

64. Task, E., Participants, A. Q. A., Aqa, U. A. L. & Imic, B. Z. N. D3.2. first-principles based model for open units. 1–29 (2018).

65. Katsuda, T., Fujii, N., Takata, N., Ooshima, H. & Katoh, S. Light attenuation in suspension of the purple bacterium rhodobacter capsulatus and the green alga chlamydomonas reinhardtii. *J. Chem. Eng. Japan* **35**, 428–435 (2002).

66. Arragon, T. Van. Development of an effective process model for algae growth in photobioreactors Tom van Arragon. (2014).

67. Gujer, W., Henze, M., Mino, T. & Van Loosdrecht, M. Errata: Activated sludge model No. 3 (Water Science and Technology (99) 39, 1 (183-193)). *Water Sci. Technol.* **39**, 1999 (1999).

68. Batstone, D. J. *et al.* The IWA Anaerobic Digestion Model No 1 (ADM1). *Water Sci. Technol.* **45**, 65–73 (2002).

69. Kompala, D. S., Ramkrishna, D., Jansen, N. B. & Tsao, G. T. Investigation of bacterial growth on mixed substrates: Experimental evaluation of cybernetic models. *Biotechnol. Bioeng.* **28**, 1044–1055 (1986).

70. Henze, M., Gujer, W., Mino, T. & van Loosedrecht, M. Activated Sludge Models ASM1, ASM2, ASM2d and ASM3. *Water Intell. Online* **5**, 9781780402369–9781780402369 (2015).

71. Ahring, B. K., Sandberg, M. & Angelidaki, I. Volatile fatty acids as indicators of process imbalance in anaerobic digestors. *Appl. Microbiol. Biotechnol.* **43**, 559–565 (1995).

72. Parkin, G. F. & Owen, W. F. Fundamentals of Anaerobic Digestion of Wastewater Sludges. *J. Environ. Eng.* **112**, 867–920 (1986).

73. Tugtas, A. E., Tezel, U. & Pavlostathis, S. G. An extension of the Anaerobic Digestion Model No. 1 to include the effect of nitrate reduction processes. *Water Sci. Technol.* **54**, 41–49 (2006).

74. Envirosim. BioWin Help Manual. 828 (2017).

75. Flickinger, M. C., Heijnen, J. J. & Kleerebezem, R. Bioenergetics of Microbial Growth. *Encycl. Ind. Biotechnol.* 1–24 (2010). doi:10.1002/9780470054581.eib084

76. Solimeno, A. Numerical Modelling of Microalgae Systems for Wastewater Treatment. 291 (2017).

77. El Ouarghi, H., Boumansour, B. E., Dufayt, O., El Hamouri, B. & Vasel, J. L. Hydrodynamics and oxygen balance in a high-rate algal pond. *Water Sci. Technol.* **42**, 349–356 (2000).

78. Kim, J. H. *Effect of Light Intensity on Nutrient Removal and Pigment Production by Purple Non-Sulfur Bacteria*. (2019).

79. Solimeno, A., Samsó, R. & García, J. Parameter sensitivity analysis of a mechanistic model to simulate microalgae growth. *Algal Res.* **15**, 217–223 (2016).

80. Mane, S. S. & Munavalli, G. R. Sequential Batch Reactor – Application to Wastewater – A Review. *Proceeding Internaional Conf. SWRDM* 121–128 (2012).

81. Hosakul, P., Kantachote, D., Saritpongteeraka, K., Phuttaro, C. & Chaiprapat, S. Upgrading industrial effluent for agricultural reuse: effects of digestate concentration and wood vinegar dosage on biosynthesis of plant growth promotor. *Environ. Sci. Pollut. Res.* **27**, 14589–14600 (2020).

82. Mohsin, H., Asif, A. & Rehman, Y. Anoxic growth optimization for metal respiration and photobiological hydrogen production by arsenic-resistant Rhodopseudomonas and Rhodobacter species. *J. Basic Microbiol.* **59**, 1208–1216 (2019).

83. Finneran, K. T., Johnsen, C. V. & Lovley, D. R. Rhodoferax ferrireducens sp. nov., a psychrotolerant, facultatively anaerobic bacterium that oxidizes acetate with the reduction of Fe(III). *Int. J. Syst. Evol. Microbiol.* **53**, 669–673 (2003).

84. Ghosh, S., Dairkee, U. K., Chowdhury, R. & Bhattacharya, P. Hydrogen from food processing wastes via photofermentation using Purple Non-sulfur Bacteria (PNSB) – A review. *Energy Convers. Manag.* **141**, 299–314 (2017).

85. Koku, H., Erolu, I., Gündüz, U., Yücel, M. & Türker, L. Aspects of the metabolism of hydrogen production by Rhodobacter sphaeroides. *Int. J. Hydrogen Energy* **27**, 1315–1329 (2002).

86. Laurinavichene, T. V., Laurinavichius, K. S., Belokopytov, B. F., Laurinavichyute, D. K. & Tsygankov, A. A. Influence of sulfate-reducing bacteria, sulfide and molybdate on hydrogen photoproduction by purple nonsulfur bacteria. *Int. J. Hydrogen Energy* **38**, 5545–5554 (2013).

87. van Lier, J., Mahnoud, N. & Zeeman, G. *Anaerobic wastewater treatment. Biological wastewater treatment: principles, modelling and design*. *Acta Arithmetica* **151**, (2008).

88. Chojnacka, K. & Noworyta, A. Evaluation of Spirulina sp. growth in photoautotrophic, heterotrophic and mixotrophic cultures. *Enzyme Microb. Technol.* **34**, 461–465 (2004).

89. Kompala, D. S. " Microbial Growth on Multiple Substrates ". *Bioprocess Eng. Fundam. Appl.* 750 (2011).

90. Gregor, J. & Klug, G. Regulation of bacterial photosynthesis genes by oxygen and light. *FEMS Microbiol. Lett.* **179**, 1–9 (1999).

91. Cerruti, M. *et al.* Effects of light / dark diel cycles on the photoorganoheterotrophic metabolism of Rhodopseudomonas palustris for differential electron allocation to PHAs and H2. *bioRxiv* (2020). doi:10.1101/2020.08.19.258533

92. Adessi, A., Torzillo, G., Baccetti, E. & De Philippis, R. Sustained outdoor H 2 production with Rhodopseudomonas palustris cultures in a 50 L tubular photobioreactor. *Int. J. Hydrogen Energy* **37**, 8840–8849 (2012).

93. Berberoğlu, H. & Pilon, L. Maximizing the solar to H2 energy conversion efficiency of outdoor photobioreactors using mixed cultures. *Int. J. Hydrogen Energy* **35**, 500–510 (2010).

94. Carlozzi, P., Pushparaj, B., Degl'Innocenti, A. & Capperucci, A. Growth characteristics of Rhodopseudomonas palustris cultured outdoors, in an underwater tubular photobioreactor, and investigation on photosynthetic efficiency. *Appl. Microbiol. Biotechnol.* **73**, 789–795 (2006).

95. Solimeno, A., Parker, L., Lundquist, T. & García, J. Science of the Total Environment Integral microalgae-bacteria model (BIO _ ALGAE): Application to wastewater high rate algal ponds. *Sci. Total Environ.* **601**–**602**, 646–657 (2017).

96. Martínez, C., Mairet, F. & Bernard, O. Theory of turbid microalgae cultures. **456**, 190–200 (2018).

97. Liu, S., Zhang, G., Zhang, J., Li, X. & Li, J. Performance, carotenoids yield and microbial population dynamics in a photobioreactor system treating acidic wastewater: Effect of hydraulic retention time (HRT) and organic loading rate (OLR). *Bioresour. Technol.* **200**, 245–252 (2016).

98. Miron, Y., van Lier, J. B. & Lettinga, G. The role of sludge retention time in the lipids hydrolysis and acidification of lipids, carbohydrates and proteins during digestion of primary sludge CSTR system. *Water Res.* **34**, 1705–1713 (2000).

99. Swinnen, I. A. M., Bernaerts, K., Dens, E. J. J., Geeraerd, A. H. & Van Impe, J. F. Predictive modelling of the microbial lag phase: A review. *Int. J. Food Microbiol.* **94**, 137–159 (2004).

100. Chen, G. E., Canniffe, D. P., Martin, E. C. & Neil Hunter, C. Absence of the cbb3 terminal oxidase reveals an active oxygen-dependent cyclase involved in bacteriochlorophyll biosynthesis in Rhodobacter Sphaeroides. *J. Bacteriol.* **198**, 2056–2063 (2016).

101. Van Bodegom, P. Microbial maintenance: A critical review on its quantification. *Microb. Ecol.* **53**, 513–523 (2007).

102. Batstone, D. J., Puyol, D., Flores-Alsina, X. & Rodríguez, J. Mathematical modelling of anaerobic digestion processes: applications and future needs. *Rev. Environ. Sci. Biotechnol.* **14**, 595–613 (2015).

103. Solimeno, A. *et al.* New mechanistic model to simulate microalgae growth. *Algal Res.* **12**, 350–358 (2015).

104. Hülsen, T., Sander, E. M., Jensen, P. D. & Batstone, D. J. Application of purple phototrophic bacteria in a biofilm photobioreactor for single cell protein production: Biofilm vs suspended growth. *Water Res.* 115909 (2020). doi:10.1016/j.watres.2020.115909

105. Flores-Alsina, X. *et al.* Modelling phosphorus (P), sulfur (S) and iron (Fe) interactions for dynamic simulations of anaerobic digestion processes. *Water Res.* **95**, 370–382 (2016).

106. Solon, K. *et al.* Plant-wide modelling of phosphorus transformations in wastewater treatment systems: Impacts of control and operational strategies. *Water Res.* **113**, 97–110 (2017).

107. Iacopozzi, I., Innocenti, V., Marsili-Libelli, S. & Giusti, E. A modified Activated Sludge Model No.

3 (ASM3) with two-step nitrification-denitrification. *Environ. Model. Softw.* **22**, 847–861 (2007).

108. Rosen, C. & Jeppsson, U. Aspects on ADM1 Implementation within the BSM2 Framework. *Tech. Rep.* 1–37 (2006).

109. Kharcheva, A. V & Zhiltsova, A. A. Studies of green sulphur bacteria using spectral methods: Comparison of fluorescence and absorption characteristics in winter and summer. *WDS'16 Proc. Contrib. Pap. — Phys.* 214–218 (2016).

110. Nybo, S. E., Khan, N. E., Woolston, B. M. & Curtis, W. R. Metabolic engineering in chemolithoautotrophic hosts for the production of fuels and chemicals. *Metab. Eng.* **30**, 105–120 (2015).

111. Khan, N. E., Nybo, S. E., Chappell, J. & Curtis, W. R. Triterpene hydrocarbon production engineered into a metabolically versatile host-Rhodobacter capsulatus. *Biotechnol. Bioeng.* **112**, 1523–1532 (2015).

112. Jupsin, H., Praet, E. & Vasel, J. L. Dynamic mathematical model of high rate algal ponds (HRAP). *Water Sci. Technol.* **48**, 197–204 (2003).

113. Pires, J. C. M., Alvim-Ferraz, M. C. M. & Martins, F. G. Photobioreactor design for microalgae production through computational fluid dynamics: A review. *Renew. Sustain. Energy Rev.* **79**, 248–254 (2017).

Appendix A

Model processes and equations

In this appendix all processes included in the model are reported in this table. The Glossary and the equations discussed in the previous sections should be sufficient to explain all the parameters and constant contained in the table below

Table 9 Summary of all processes implemented in the model

Processes	Process rate [M L^{-3} T^{-1}]
Purple non sulphur bacteria (X_{PB}) processes	
1a. Growth of X_{PB} on S_S (phototrophic)	$\rho_{1a} = \mu_{ph,pb,max} \cdot f(S_S) \cdot \nu_{1,a,pb} \cdot \frac{S_S}{K_S + S_S} \cdot \frac{I}{K_I + I} \cdot \frac{1 - O_2}{K_{O2,ph} + O_2} \cdot X_{PB}$
1b. Growth of X_{PB} on S_{VFA} (phototrophic)	$\rho_{1b} = \mu_{ph,pb,max} \cdot f(S_{VFA}) \cdot \nu_{1,b,pb} \frac{S_{VFA}}{K_{VFA} + S_{VFA}} \cdot \frac{I}{K_I + I} \cdot \frac{1 - O_2}{K_{O2,ph} + O_2} \cdot X_{PB}$
1c Growth of X_{PB} on S_{AC} (phototrophic)	$\rho_{1c} = \mu_{ph,pb,max} \cdot f(S_{AC}) \nu_{1,c,pb} \frac{S_{AC}}{K_{AC} + S_{AC}} \cdot \frac{I}{K_I + I} \cdot \frac{1 - O_2}{K_{O2,ph} + O_2} \cdot X_{PB}$
2a. Growth of X_{PB} on S_S (chemotrophic)	$\rho_{2a} = \mu_{ch,pb,max} \cdot f(S_S) \cdot \nu_{2,a,pb} \cdot \frac{S_S}{K_S + S_S} \cdot \frac{O_2}{K_{O2,ch,PB} + O_2} \cdot X_{PB}$
2b. Growth of X_{PB} on S_{VFA} (chemotrophic)	$\rho_{2b} = \mu_{ch,pb,max} \cdot f(S_{VFA}) \cdot \nu_{2,b,pb} \frac{S_{VFA}}{K_{VFA} + S_{VFA}} \cdot \frac{O_2}{K_{O2,ch,PB} + O_2} \cdot X_{PB}$
2c Growth of X_{PB} on S_{AC} (chemotrophic)	$\rho_{2c} = \mu_{ch,pb,max} \cdot f(S_{AC}) \nu_{2,c,pb} \frac{S_{AC}}{K_{AC} + S_{AC}} \cdot \frac{O_2}{K_{O2,ch,PB} + O_2} \cdot X_{PB}$
3a. Growth of X_{PB} on S_S (chemotrophic)	$\rho_{3a} = \mu_{an,pb,max} \cdot f(S_S) \cdot \nu_{3,a,pb} \cdot \frac{S_S}{K_S + S_S} \cdot \frac{1 - O_2}{K_{O2,ch,PB} + O_2} \cdot X_{PB}$
3b. Growth of X_{PB} on S_{VFA} (chemotrophic)	$\rho_{3b} = \mu_{an,pb,max} \cdot f(S_{VFA}) \cdot \nu_{3,b,pb} \frac{S_{VFA}}{K_{VFA} + S_{VFA}} \cdot \frac{1 - O_2}{K_{O2,ch,PB} + O_2} \cdot X_{PB}$
3c Growth of X_{PB} on S_{AC} (chemotrophic)	$\rho_{3c} = \mu_{an,pb,max} \cdot f(S_{AC}) \nu_{3,c,pb} \frac{S_{AC}}{K_{AC} + S_{AC}} \cdot \frac{1 - O_2}{K_{O2,ch,PB} + O_2} \cdot X_{PB}$
Standard chemotrophic (X_{HET}) (aerobic and anoxic activity)	
4a. Growth of X_{HET} on S_S (aerobic)	$\rho_{4a} = \mu_{ch,HET,max} \cdot f(S_S) \cdot \nu_{4,a,het} \cdot \frac{S_S}{K_S + S_S} \cdot \frac{O_2}{K_{O2,ch,HET} + O_2} \cdot X_{HET}$
4b. Growth of X_{HET} on S_{VFA} (aerobic)	$\rho_{4b} = \mu_{ch,HETmax} \cdot f(S_{VFA}) \cdot \nu_{4,b,het} \frac{S_{VFA}}{K_{VFA} + S_{VFA}} \cdot \frac{O_2}{K_{O2,ch,HET} + O_2} \cdot X_{HET}$
4c Growth of X_{HET} on S_{AC} (aerobic)	$\rho_{4c} = \mu_{ch,HETmax} \cdot f(S_{AC}) \nu_{4,c,het} \frac{S_{AC}}{K_{AC} + S_{AC}} \cdot \frac{O_2}{K_{O2,ch,HET} + O_2} \cdot X_{HET}$
5a. Growth of X_{HET} on S_S (anoxic)	$\rho_{5a} = \mu_{an,HET,max} \cdot f(S_S) \cdot \nu_{5,a,het} \cdot \frac{S_S}{K_S + S_S} \cdot \frac{1 - O_2}{K_{O2,ch,HET} + O_2} \cdot X_{HET}$
5b. Growth of X_{HET} on S_{VFA} S_S (anoxic)	$\rho_{5b} = \mu_{an,max} \cdot f(S_{VFA}) \cdot \nu_{5,b,het} \frac{S_{VFA}}{K_{VFA} + S_{VFA}} \cdot \frac{1 - O_2}{K_{O2,ch,HET} + O_2} \cdot X_{HET}$
5c Growth of X_{HET} on S_{AC} S_S (anoxic)	$\rho_{5c} = \mu_{an,HET,max} \cdot f(S_{AC}) \nu_{5,c,het} \frac{S_{AC}}{K_{AC} + S_{AC}} \cdot \frac{1 - O_2}{K_{O2,ch,HET} + O_2} \cdot X_{HET}$
Fermenting bacteria X_{FR}	

6a. Growth of X_{FR} on S_S (fermenting)	$\rho_{6a} = \mu_{fr,max} \cdot f(S_S) \cdot \nu_{6,a,fr} \cdot \frac{S_S}{K_S + S_S} \cdot X_{FR}$
6b. Growth of X_{HET} on S_{VFA} (fermenting)	$\rho_{6b} = \mu_{fr,max} \cdot f(S_S) \cdot \nu_{6,a,fr} \cdot \frac{S_{VFA}}{K_{VFA} + S_{VFA}} \cdot X_{FR}$
Decay of Bacteria	
7a. Decay of X_{PB}	$\rho_{7a} = k_{dec,PB} \cdot X_{PB}$
7b. Decay of X_{HET}	$\rho_{7a} = k_{dec,HET} \cdot X_{HET}$
7c. Decay of X_{FR}	$\rho_{7a} = k_{dec,FR} \cdot X_{FR}$
Hydrolysis of Bacteria	
8. Hydrolysis of X_S	$\rho_8 = k_{HYD} \cdot X_S$
Gas transfer	
9 Oxygen transfer to the atmosphere	$\rho_{10} = k_{la,O2} \cdot (S_{S,O2} - S_{O2})$
10 Carbon dioxide transfer to the atmosphere	$\rho_{11} = k_{la,CO2} \cdot (S_{S,CO2} - S_{CO2})$
Light attenuation	
11 Lambert-Beer Equation	$I_{avg} = \frac{I_0(1 - e^{-\varepsilon \cdot (X_S + X_{PB} + X_{HET} + X_{FR} + X_I)\, L})}{\varepsilon (X_S + X_{PB} + X_{HET} + X_{FR} + X_I) L}$
Chemical balance	
12 Chemical equilibrium $CO_2 \leftrightarrow HCO_3^-$	$\rho_{12} = k_{eq,1} \cdot (S_{CO2} - S_H S_{HCO3} / K_{eq,1})$

Appendix B

Petersen Matrix

In this table is shown the Petersen Matrix implemented in the model. The terms $v_{i,y}$ stands for the specific values resulting from the chemical and physical reactions where *i* is the column and *y* is the process (Appendix A)

Table 10 Petersen Matrix of the model

		S_S	S_{VFA}	S_{AC}	S_{HCO3}	S_{IN}	S_{IP}	S_{H2}	S_I	X_S	X_{PB}	X_{HET}	X_{FR}	X_I	S_{O2}	S_{CO2}
X_{PNSB}	ρ_{1a}	$v_{1,1a}$			$v_{4,1a}$	$v_{5,1a}$	$v_{6,1a}$				$v_{10,1a}$				$v_{14,1a}$	
	ρ_{1b}		$v_{2,1b}$		$v_{4,1b}$	$v_{5,1b}$	$v_{6,1b}$				$v_{10,1b}$					
	ρ_{1c}			$v_{3,1b}$	$v_{4,1c}$	$v_{5,1c}$	$v_{6,1c}$				$v_{10,1c}$					
	ρ_{2a}	$v_{1,2a}$			$v_{4,2a}$	$v_{5,2a}$	$v_{6,2a}$				$v_{10,2a}$				$v_{14,2a}$	
	ρ_{2b}		$v_{2,2b}$		$v_{4,2b}$	$v_{5,2b}$	$v_{6,2b}$				$v_{10,2b}$				$v_{14,2b}$	
	ρ_{2c}			$v_{3,2c}$	$v_{4,2c}$	$v_{5,2c}$	$v_{6,2c}$				$v_{10,2c}$				$v_{14,2c}$	
	ρ_{3a}	$v_{1,3a}$			$v_{4,3a}$	$v_{5,3a}$	$v_{6,3a}$				$v_{10,3a}$				$v_{14,3a}$	
	ρ_{3b}		$v_{2,3b}$		$v_{4,3b}$	$v_{5,3b}$	$v_{6,3b}$				$v_{10,3b}$				$v_{14,3b}$	
	ρ_{3c}			$v_{3,3c}$	$v_{4,3c}$	$v_{5,3c}$	$v_{6,3c}$				$v_{10,3c}$				$v_{14,3c}$	
X_{HET}	ρ_{4a}	$v_{1,4a}$			$v_{4,4a}$	$v_{5,4a}$	$v_{6,4a}$					$v_{11,4a}$			$v_{14,4a}$	
	ρ_{4b}		$v_{2,4b}$		$v_{4,4b}$	$v_{5,4b}$	$v_{6,4b}$					$v_{11,4b}$			$v_{14,4b}$	
	ρ_{4c}			$v_{3,4c}$	$v_{4,4c}$	$v_{5,4c}$	$v_{6,4c}$					$v_{11,4c}$			$v_{14,4c}$	
	ρ_{5a}	$v_{1,5a}$			$v_{4,5a}$	$v_{5,5a}$	$v_{6,5a}$					$v_{11,5a}$				
	ρ_{5b}		$v_{2,5b}$		$v_{4,5b}$	$v_{5,5b}$	$v_{6,5b}$					$v_{11,5b}$				
	ρ_{5c}			$v_{3,5c}$	$v_{4,5c}$	$v_{6,5c}$	$v_{6,5c}$					$v_{11,5c}$				
X_{FR}	ρ_{6a}	$v_{1,6a}$		$v_{3,6a}$	$v_{4,6a}$	$v_{6,6a}$	$v_{6,6a}$	$v_{7,6a}$					$v_{12,6a}$			
	ρ_{6b}		$v_{2,6b}$	$v_{3,6b}$	$v_{4,6b}$	$v_{6,6b}$	$v_{6,6b}$	$v_{7.6b}$					$v_{12,6b}$			
Decay	$\rho_{7,a}$				$v_{4,7a}$	$v_{5,7a}$	$v_{6,7a}$		$v_{8,16}$	$v_{9,7a}$	$v_{10,7a}$					
	$\rho_{7,b}$				$v_{4,7b}$	$v_{5,7b}$	$v_{6,7b}$			$v_{9,7b}$		$v_{11,7b}$				
	$\rho_{7,c}$				$v_{4,7c}$	$v_{5,7c}$	$v_{6,7c}$			$v_{9,7c}$			$v_{11,7c}$			
Hydrolysis	ρ_8	$v_{1,8}$	$v_{2,8}$	$v_{3,8}$	$v_{4,8}$	$v_{5,8}$	$v_{6,8}$	$v_{7,8}$	$v_{8,8}$	$v_{9,8}$				$v_{12,8}$		
Gas transfer	ρ_9															$v_{15,9}$
	ρ_{10}														$v_{14,10,}$	
Equilibrium HCO_3	ρ_{12}				$v_{4,12}$											$v_{15,12}$

Appendix C

Results of the batch parametrisations

This appendix shows the results of the parametrisation during the batch and sequencing batch reactor experiment focusing on the specific input parameters found to simulate the different scenarios. In this research it was not possible to find a combination input parameters that could simulate sufficiently all the seven experimental conditions. In the end, it was decided to study separately the batch and SBR scenarios, obtaining two diverse set of input parameters. This consideration is acceptable as SBR and batch conditions diverge for several aspects. However, these difference should be emphasized and reasonably explained. These results are were always between the specific boundaries found in the literature (Table 3).

Table 11 Most relevant input parameters found for the batch experiments

Stoichiometry		**Model tuning**	**Values**
$\mathbf{Y_{XPB,PH}}$	Biomass yield phototrophic growth (X_{PB}) [$mgCOD_x/mgCOD_s$]	tuned	0.8
$\mathbf{Y_{XPB,CH}}$	Biomass yield chemotrophic growth (X_{PB}) [$mgCOD_x/mgCOD_s$]	tuned	0.3
$\mathbf{Y_{XPB,AN}}$	Biomass yield anaerobic growth (X_{PB}) [$mgCOD_x/mgCOD_s$]	tuned	0.2
$\mathbf{Y_{XHET,CH}}$	Biomass yield chemotrophic growth (X_{HET}) [$mgCOD_x/mgCOD_s$]	tuned	0.3
$\mathbf{Y_{XHET,AN}}$	Biomass yield anaerobic growth (X_{HET}) [$mgCOD_x/mgCOD_s$]	tuned	0.2
Kinetic		**Model tuning**	**Values**
$\boldsymbol{f(S_i)}$	Substrate preference factor	tuned	0.5
$\mathbf{\mu_{max,ph,XPB}}$	Maximum growth rate phototrophic growth (X_{PB}) [h^{-1}]	tuned	0.08
$\mathbf{\mu_{max,ch,XPB}}$	Maximum growth rate chemotrophic growth (X_{PB}) [h^{-1}]	tuned	0.06
$\mathbf{\mu_{max,an,XPB}}$	Maximum growth rate Anaerobic growth (X_{PB}) [h^{-1}]	tuned	0.006
$\mathbf{\mu_{max,ch,XHET}}$	Maximum growth rate for Chemotrophic growth (X_{HET}) [h^{-1}]	tuned	0.25
$\mathbf{\mu_{max,ch,XAN}}$	Maximum growth rate for Anaerobic growth (X_{HET}) [h^{-1}]	tuned	0.0075
$\mathbf{K_{S,IE}}$	Half velocity constant for Light inhibition [W/m^2]	tuned	10
$\mathbf{K_{S,O2,PH}}$	Half velocity constant for O_2 inhibition phototrophic [mgO_2/L]	tuned	1.0
$\mathbf{K_{S,O2,CH,PB}}$	Half velocity constant O_2 inhibition chemotrophic (X_{PB}) [mgO_2/L]	tuned	0.3
$\mathbf{K_{S,O2,CH,HET}}$	Half velocity constant O_2 inhibition chemotrophic (X_{HET}) [mgO_2/L]	tuned	1.0

Results of the SBR parametrisations

The sequencing batch scenarios were initially run with the input parameters for the batch simulations But then they were adjusted according to the process explained in the previous sections (Figure 14).

Table 12 Most relevant input parameters found for the SBR experiments

Stoichiometry		**Model tuning**	**Values**
$\mathbf{Y_{XPB,PH}}$	Biomass yield phototrophic growth (X_{PB}) [$mgCOD_x/mgCOD_s$]	tuned	1.2
$\mathbf{Y_{XPB,CH}}$	Biomass yield chemotrophic growth (X_{PB}) [$mgCOD_x/mgCOD_s$]	tuned	0.3
$\mathbf{Y_{XHET,AN}}$	Biomass yield Anaerobic growth (X_{PB}) [$mgCOD_x/mgCOD_s$]	tuned	0.2
$\mathbf{Y_{XHET,CH}}$	Biomass yield Chemotrophic growth (X_{HET}) [$mgCOD_x/mgCOD_s$]	tuned	0.4
$\mathbf{Y_{XHET,AN}}$	Biomass yield Anaerobic growth (X_{HET}) [$mgCOD_x/mgCOD_s$]	tuned	0.2
Kinetic		**Model tuning**	**Values**
$\boldsymbol{f(S_i)}$	Subtrate preference factor	tuned	0.5
$\mathbf{\mu_{max,ph,XPB}}$	Maximum growth rate phototrophic growth (X_{PB}) [h^{-1}]	tuned	0.125
$\mathbf{\mu_{max,ch,XPB}}$	Maximum growth rate chemotrophic growth (X_{PB}) [h^{-1}]	tuned	0.06
$\mathbf{\mu_{max,an,XPB}}$	Maximum growth rate Anaerobic growth (X_{PB}) [h^{-1}]	tuned	0.006
$\mathbf{\mu_{max,ch,XHET}}$	Maximum growth rate for chemotrophic growth (X_{HET}) [h^{-1}]	tuned	0.26
$\mathbf{\mu_{max,ch,XAN}}$	Maximum growth rate for Anaerobic growth (X_{HET}) [h^{-1}]	tuned	0.0075
$\mathbf{K_{S,IE}}$	Half velocity constant for Light inhibition [W/m^2]	tuned	10
$\mathbf{K_{S,O2,PH}}$	Half velocity constant for O_2 inhibition phototrophic [mgO_2/L]	tuned	1.0
$\mathbf{K_{S,O2,CH,PB}}$	Half velocity constant O_2 inhibition chemotrophic (X_{PB}) [mgO_2/L]	tuned	0.3
$\mathbf{K_{S,O2,CH,HET}}$	Half velocity constant O_2 inhibition chemotrophic (X_{HET}) [mgO_2/L]	tuned	0.5

Appendix D

Simulation of yearly natural light impact

The following figure reports the effluent PNSB concentration of a yearly simulation with real radiation data for an Indian case scenario. The raceway reactor was run with identical operational conditions to the scenario 2 reported at Table 5. In the figure it is appreciable the higher concentration of PNSB bacteria from April to June, then a relative drop because of the Monsoon period and then a steady decrease, even below 100 mgCOD/L from the end of October.

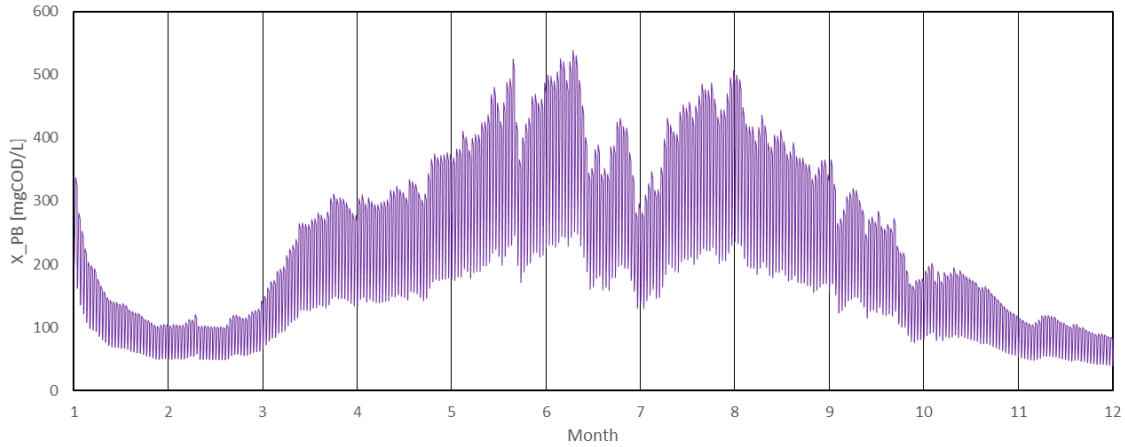

Figure 34 Effluent concentration of PNSB (mgCOD/L) calculated for a yearly simulation. The variations are mainly related to the variation of the natural light during the year. The PNSB concentration increased since the beginning of March (3rd month) until June (6thmonth). From June to August, it was observed a decreased due to the monsoon period and followed by a steady decreased since the month of September (9th month)

Appendix E

Experiments and practical experience at La Trappe Brewery

Experimental project and results

During this project I had the opportunity to work on the field and put in practice the experience acquired in these years of the Master performing some experiments with the raceway reactor. Originally, this master thesis was conceived as a laboratory project which was impossible to accomplish due to COVID-19 and following worldwide pandemic. However, from October to December 2020, I had the opportunity to operate with purple non-sulphur bacteria and raceway reactors at the Koningshoeven Abbey, in Tilburg, where "La Trappe" is produced. The initial objective was to study PNSB dynamics and the robustness of the raceway reactor performance with real wastewater. In the following paragraphs, a short review of the experimental results and the major conclusions will be discussed.

The raceway reactor operated with an HRT and SRT equal to 3 days with a 12h/12h light-dark cycle and one halogen lamp (54 Wm^{-2}) and a 12h/12h paddlewheel rotation. A solution containing macronutrients (6.24 g NH_4Cl/L and 1.01 g KH_2PO_4/L) was created to avoid growth inhibition because of lack of nutrient and tackle evaporation, estimated around 1L per day. One major concern was the influent complexity: different brewing sessions and the cleaning processes can strongly variate the water matrix during the day. The influent was directly pumped out from a buffer tank with a strongly dynamic HRT from 6 – 48h. Moreover, it was usually characterized by a very dark colour, strong odour, and an moderate concentration of suspended solids (0.8-1.2 gTSS/L), possibly indicating the activity of sulphate reducing bacteria. For this reason, it was decided to place previously an IBC tank which was filled and emptied every 3-5 days to let TSS settle and to pump out only the supernatant.

The following pictures show the reactor since the first day of operation for the consecutive 20 days (Figure 35 a-d). The first two figures were taken at the first and fifth days showing that the wastewater had obtained a purplish shade (Figure 35 a-b).The other two pictures (Figure 35 c-d) were taken on the 15^{th} and 20^{th} day and they are visibly characterized by a red-purple wastewater colour and biofilm (e.g. paddlewheel). After one/two week, the reactor system seemed to have reached a stability. Figure 36 and Figure 37 report the hourly variations of the total and soluble COD, nitrogen, and phosphorus in the raceway reactor during the second week of operation.

An overview of the reactor performance is reported at Table 13. The COD removal rate was equal to 466 mgCOD/L/d, the biomass concentration in the effluent was estimated around 799 mgCOD/L and the measured yield resulted 0.38 $mgCOD_x/mgCOD_s$. The total COD removal efficiency was estimated

nearly at 80% and around 50% for nitrogen and phosphorus. The nitrogen and phosphorus uptake was measured respectively around 20 mgN/L/d and 3.63 mgP/L/d. Therefore the system COD:N:P resulted 100:4.5:0.78. Considering biomass composition as 100:7:2 and focusing the balance on the removal and assimilation of phosphate, the measured yield is 0.39 $mgCOD_X/mgCOD_S$, in line with what reported in the table. Despite the slightly different operational conditions compared to the experiments performed by Alloul et al. (2020)[18] (different HRT and SRT), the two COD removal rates are similar (450 mgCOD/L/d). On the other hand, the yield is markedly lower, almost half of the one measured in laboratory conditions (0.65 $mgCOD_x/mgCOD_s$). However, in this case, COD measurements are affected from the influent suspended solids and hydrolysis process which is was properly investigated.

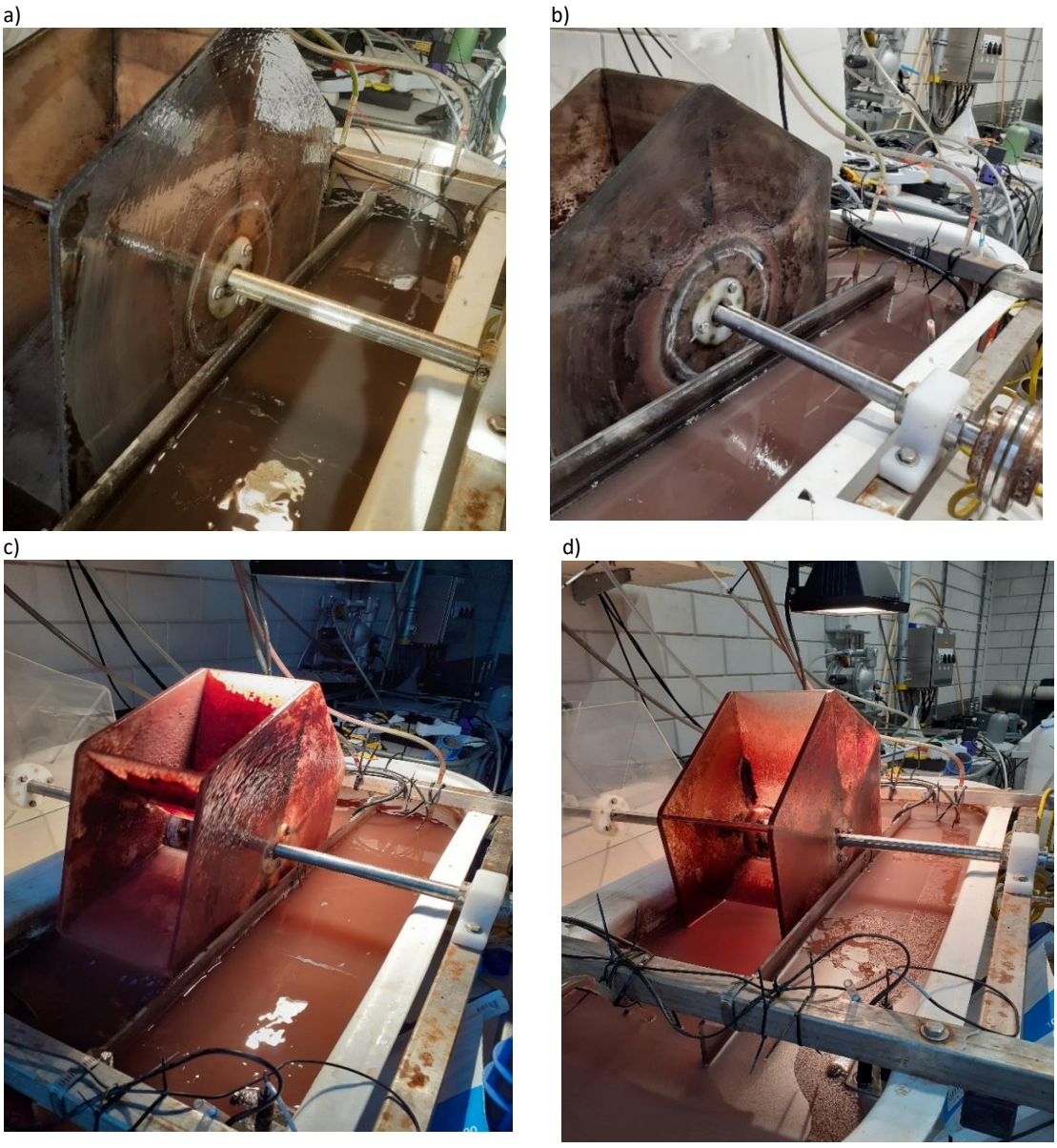

Figure 35 Picture taken from the 1st and 20th (16/10) day of operation: a) 27/10; b) 2/11; c) 11/11; d) 16/11. The images prove that PNSB were properly inoculated and that the reactor remained purple for at least 20 days.

Table 13 Reactor performance during the second week of the experiments. The term "inf" stands for influent; the term "eff" stands for effluent; the term "RR1" stands for the raceway reactor conditions after influent addition. V_r is the volume of the reactor (100 L), Q is the daily influent (32 L/day).

Parameters		Equation	
$r_{s,COD}$ (mgCOD/L/d)	COD Removal rate	$\frac{(TCOD_{inf} - SCOD_{eff})Q}{V_r}$	466 ±21%
$X_{BIO,eff}$ (mgCOD/L)	Effluent biomass	$TCOD_{eff} - SCOD_{eff}$	779 ±23%
$Y_{x/s}$ (mgCOD/mgCOD)	Substrate to biomass yield	$\frac{X_{BIO,eff} - X_{BIO,RR1}}{TCOD_{eff} - SCOD_{RR1}}$	0.38 ±22%
η_s (%)	COD Removal efficiency	$\frac{(TCOD_{inf} - SCOD_{eff}) * 100}{TCOD_{inf}}$	79% ±9%
$r_{s,N}$ (mgN/L/d)	Nitrogen Removal rate	$\frac{(SIN_{RR1} - SIN_{eff}) * 100}{[SIN_{RR1} - SIN_{eff} * \left(1 - \frac{Q}{V}\right)]}$	20.9 ±21%
$r_{s,P}$ (mgP/L/d)	Phosphorus Removal rate	$\frac{(SIP_{RR1} - SIP_{eff}) * 100}{[SIP_{RR1} - SIP_{eff} * \left(1 - \frac{Q}{V}\right)]}$	3.63 ± 36%

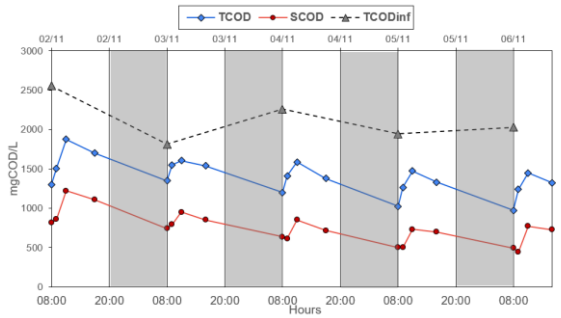

Figure 36 Hourly COD variations in the raceway reactor: total COD (TCOD), soluble COD (SCOD) and total influent COD (TCODinf) during the second week since the beginning of the experiments (2/11 – 6/11)

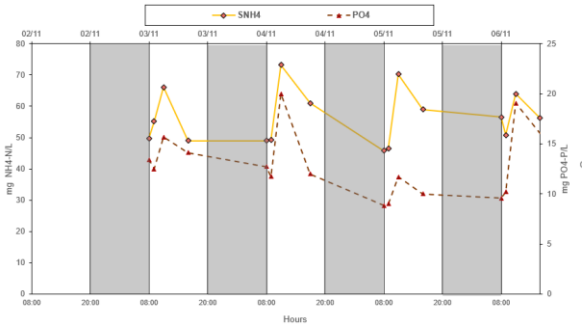

Figure 37 Hourly nitrogen (mgNH_4-N/L) and phosphorus (mgPO_4-/L) variations in the raceway reactor during the second week since the beginning of the experiments (2/11 – 6/11)

Since the 20th day of the experiment, most likely because of a spill of a brewing session, the reactor started to destabilize. In the coming weeks, the influent wastewaters was characterized with a higher concentration of total COD, suspended solids and sulphate which is thought to have negatively affected the PNSB abundance. This change was not only visible as the water was losing the purplish colour, but other signals were also noticed. For instance, the hydrogen sulphide sensor rang several times and, the influent wastewater, despite sedimentation in the IBC tank, measured a high absorbance spectrum. This transformation was also observed through a spectrometer analysis looking at the absorbance peaks between 660-860 nm (Figure 38) in the effluent. Few days after the spill, the effluent was not characterized anymore by peaks around 805-860 nm which are characteristics of PNSB. Therefore, it is thought that, after the spill of the brewing session, PNSB abundance importantly

decreased and they were replaced by other microorganisms, possibly green-sulphur bacteria (GSB). This conclusion can be partially motivated because of the absorbance peaks around 735-780 nm, characteristic of GSB. Figure 39 shows the raceway reactor since the first day of the spill on the 20th day (17/11/2020), proving a rapid transformation on the wastewater colour with brownish and the greenish fades. Finally, the experiment was restarted in another reactor using the same (greenish) wastewater and reinoculating PNSB bacteria with some purple biofilm collected from the paddlewheel. As well, during this new test the influent wastewater showed optimal concentration of COD, TSS and sulphate. After a week, it was observed purple and red biofilm formation in the raceway reactor, possibly indicating that PNSB were recovering and repopulating the system (Figure 40).

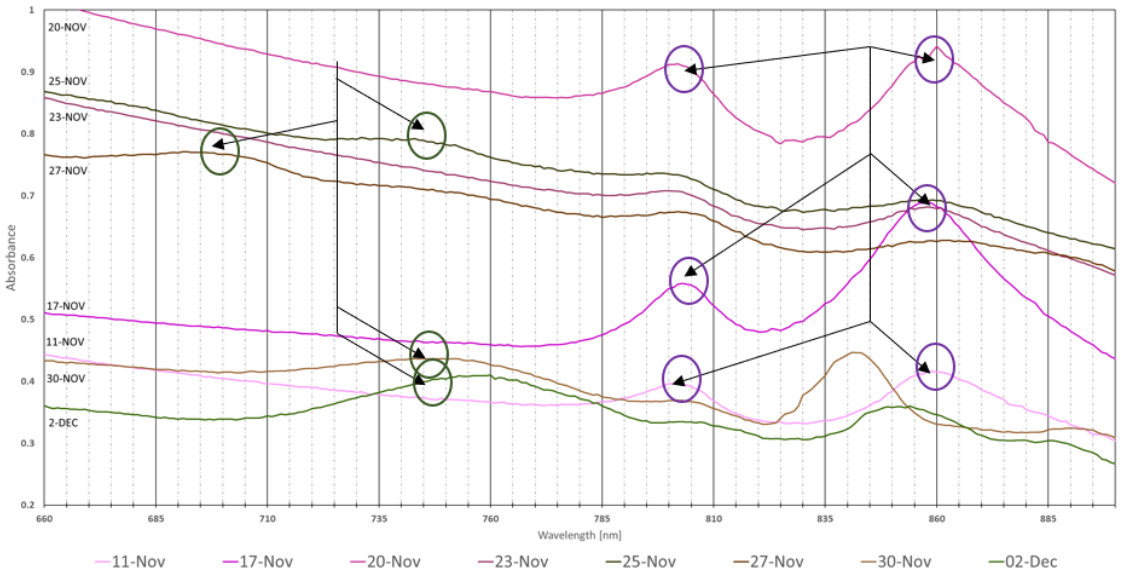

Figure 38 Absorbance measurements of the effluent samples out of the raceway reactor during the month of November (11 Nov. – 2 Dec). The purple circles indicates peaks of bacteriochlorophyll a and b between 805-860 nm which is characteristic of the PNSB bacteria. The green circles indicate peaks between 690 and 740 nm not distinctive of PNSB. After the spill of the brewing session (16th of November) the absorbance generally increased compared to the measurement on the 11th of November. However, the reactor was still abundant of PNSB due to the elevated peaks around 805-860 nm (17th and 20th NOV). Then since the 25th of November peaks around 805-860 nm are smoothers and some peaks between 690 and 740 nm were recorded. These

a) b)

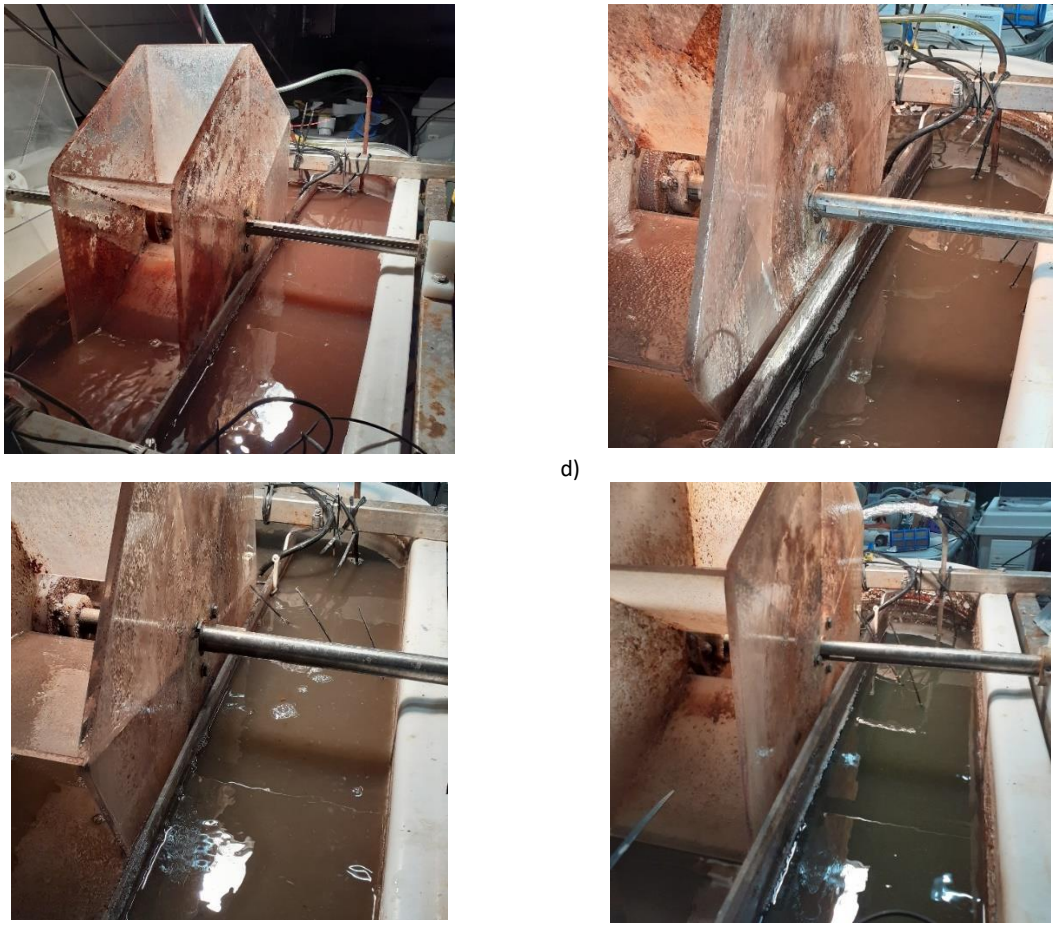

Figure 39 Pictures taken from the 20th and 33rd(16/10) day of operation: a) 17/10; b) 23/11; c) 25/11; d) 30/11. These images prove the rapid change in the microbial community since the begging of the brewery session spill.

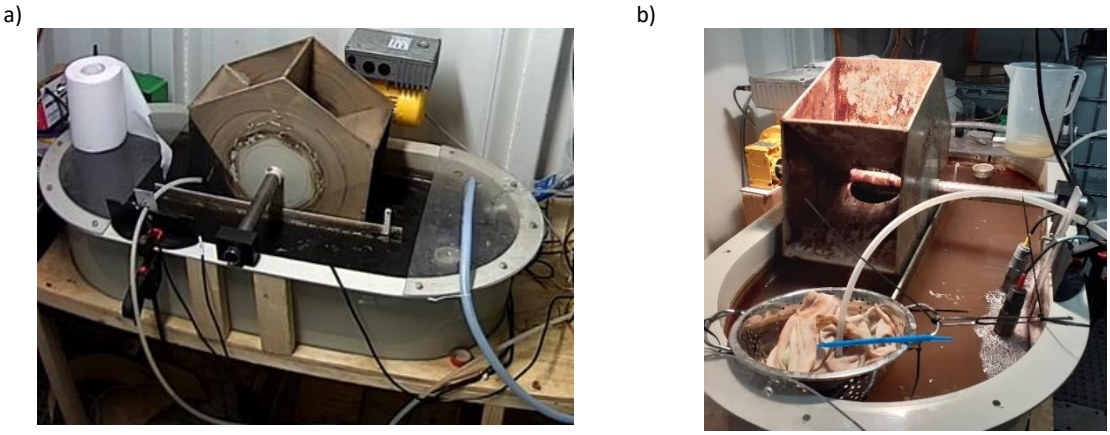

Figure 40 SEMiLLA raceway reactor after the reinoculation with the purple biofilm. The pictures were taken at the begging (a) and after 11 days of operations (b). It can be sad that the reinoculation was successful and the PNSB recovered in the system.

Conclusions of the experimental project

Having the opportunities to manually work with PNSB and raceway reactors was helpful to grasp more clearly the theoretical and modelling knowledge studied during the development of the model. Vice versa the theoretical background can partly motivate the reasons of some events.

For instance, it would be interesting to investigate the reasons of the microbial change after the spill of brewing session. With the experimental data, it was measured a three time increase of TSS in the influent wastewater from an average of 0.100 gTSS/L to 0.300 gTSS/L. In the model, this aspect was considered and some scenarios simulated the negative effects of influent suspended solids (page 55, 58). Nevertheless, the reasons of such drastic change in the microbial community might be due to the other compounds as greater presence of sulphate, either a greater pressure in the biotic competition or a combinations of these events.

This example was just one of the possible events that might negatively influence the abundance of PNSB in the raceway reactor. To proper inoculate and maintain stable PNSB in raceway reactors, it should work toward a tight collaboration between experiments and mathematical modelling. Moreover, because of the intrinsic problems controlling external conditions for raceway reactors (e.g. temperature, light), mathematical modelling it is highly recommended to predict critical conditions, instead of counteract once already happed. This aspect introduces another aspect of the wastewater treatment sector related to the monitoring and control of the raceway reactor which is still at a basic stage for PNSB, but some useful methods can be derived from microalgae technology in raceway reactors.

Appendix F

Batch experiments from Alloul et al. (2020)

The initial conditions of batch experiments are summarized at Table 14 showing some slightly variations from the theoretical values reported at Table 4. Especially in scenarios 3 and 4, the initial biomass (X_{in}) is much higher than expected, and, in addition, in contrast with the linear correlation of the optical density, expressed at Eq. 22. Moreover, in scenario 3, the initial substrate concentration was measured around 2500 mgCOD/L (Figure 41), in contrast with what reported at Table 14 (1276 mgCOD/L). Additional results are shown at Table 15 reporting yield ($Y_{x/s}$), the final biomass ($X_{end,m}$ $X_{end,e}$), the reaction time, different growth rates. (μ_{mean}, μ_{light}, μ_{dark}) and the PNSB abundance (%PNSB). It is important to underline the main difference between the two biomass parameters ($X_{end,m}$ $X_{end,e}$): the first one was calculated as difference of the TCOD and SCOD chemical measurements, the second trough OD_{660} measurements and estimated with Eq. 22. Lastly, Table 16 shows the growth rate for specific time-steps calculated with Eq. 21. Figure 41 shows the growth of the biomass expressed through the optical density measurements and the consumption of the organic substrate. In the figure, especially for the SCOD measurements, it is appreciable an alternate curve representing the switch of the dark and light phase.

Table 14 Initial and final conditions of batch experiments: initial total COD, biomass and optical density ($TCOD_{in}$, X_{in}, $OD_{660,in}$) and final substrate, biomass and optical density ($SCOD_{end}$, X_{end}, OD_{end}).

Scenario	$TCOD_{in}$ [mgCOD/L]	X_{in} [mgCOD/L]	$OD_{660\ in}$ [Abs]	$SCOD_{end}$ [mgCOD/L]	X_{end} [mgCOD/L]	$OD_{660\ end}$ [Abs]
BATCH 1	2784	18	0.078	87	792	1.983
BATCH 2	2718	33	0.089	112	1032	2.331
BATCH 3	1276	356	0.062	302	698	2.004
BATCH 4	2324	784	0.064	334	418	1.182

Table 15 Batches' experimental results: yield ($Y_{x/s}$), final biomass measured ($X_{end,m}$) and estimated ($X_{end,e}$), duration of the experiment (time), average, light and dark growth rate and relative abundance of PNSB.

Scenario	$Y_{x/s}$ [mgCOD/mgCOD]	$X_{end,m}$ [mgCOD/L]	$X_{end,e}$ [mgCOD/L]	Time [h]	μ_{mean} [h^{-1}]	μ_{light} [h^{-1}]	μ_{dark} [h^{-1}]	%PNSB
BATCH 1	0.33	792	911	153	0.034	0.037	0.025	8%
BATCH 2	0.41	1032	1071	96	0.040	0.043	0.043	31%
BATCH 3	0.70	698	921	156	0.034	0.051	0.002	20%
BATCH 4	0.20	418	540	80	0.0474	0.047	0.036	[-]?

Table 16 Batches experimental results: growth rate at different time steps since the beginning of the experimentsestimated as in Eq. 21

Scenario	μ_{48h} $[h^{-1}]$	μ_{72h} $[h^{-1}]$	μ_{96h} $[h^{-1}]$	μ_{120h} $[h^{-1}]$	μ_{150h} $[h^{-1}]$
BATCH 1	0.037	0.036	0.31	0.29	0.25
BATCH 2	0.062	0.043	0.037	0.0339	0.0302
BATCH 3	0.053	0.050	0.045	0.0385	0.034
BATCH 4	0.049	0.040	[-]	[-]	[-]

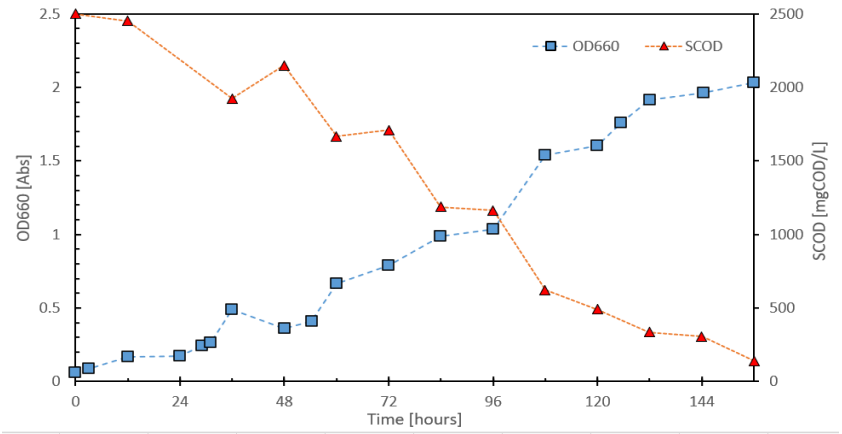

Figure 41 Optical density (blue line) and SCOD (orange-line) variations for the batch scenarios as expressed at Table 4.

The interpretation of the experimental results are of primary importance in order to correctly parametrize the model. For this reason, the consistency of the same variable should be looked with particularly regard. In Table 15, scenarios 3 and 4 show a significant difference between the two biomass calculations ($X_{end,m}$ $X_{end,e}$). In conclusion, only one of the two measurements should be taken into account for the model parametrization. In this case, it was opted for the the optical density measurements ($X_{end,e}$), whereas COD measurements were considered not applicable ($X_{end,m}$). As consequence, it is also likely that the yield measurements for scenarios 3 and 4 would show a high error because they were estimated using $X_{end,m}$. More precisely, for scenarios 1 and 2 the initial biomass conditions corresponded at the chemical oxygen demand measurements (TCOD-SCOD), while for scenarios 3 and 4, the optical density measurements data were used (Eq. 22). The initial substrate concentration was set equal to the one measured from the COD analysis.